NUMERICAL SIMULATION OF
INCOMPRESSIBLE AND COMPRESSIBLE FLOW

BY

ZHIYIN YANG

THESIS SUBMITTED TO THE
UNIVERSITY OF SHEFFIELD FOR THE DEGREE OF
DOCTOR OF PHILOSOPHY

DEPARTMENT OF MECHANICAL AND PROCESS ENGINEERING
UNIVERSITY OF SHEFFIELD

FEBRUARY, 1989

SUMMARY

This thesis describes the development of a numerical solution procedure which is valid for both incompressible flow and compressible flow at any Mach number. Most of the available numerical methods are for incompressible flow or compressible flow only and density is usually chosen as a main dependent variable by almost all the methods developed for compressible flow. This practice limits the range of the applicability of these methods since density changes can be very small when Mach number is low. Even for high Mach number flows the existing time-dependent methods may be inefficient and costly when only the finial steady-state is of concern. The presently developed numerical solution procedure, which is based on the SIMPLE algorithm, solves the steady-state form of the Navier-stokes equations, and pressure is chosen as a main dependent variable since the pressure changes are always relatively larger than the density changes. This choice makes it possible that the same set of variables can be used for both incompressible and compressible flows.

It is believed that Reynolds stress models would give better performance in some cases such as recirculating flow, highly swirling flow and so on where the widely used two equation k-ϵ model performs poorly. Hence, a comparative study of a Reynolds stress model and the k-ϵ model has been undertaken to assess their performance in the case of highly swirling flows in vortex throttles. At the same time the relative performance of different wall treatments is also presented.

It is generally accepted that no boundary conditions should be specified at the outflow boundary when the outflow is supersonic, and all the variables can

be obtained by extrapolation. However, it has been found that this established principle on the outflow boundary conditions is misleading, and at least one variable should be specified at the outflow boundary. It is also shown that the central differencing scheme should be used for the pressure gradient no matter whether it is subsonic or supersonic flow.

ACKNOWLEDGEMENTS

I would like to express my sincere thanks to Prof. J. Swithenbank for his supervision, encouragement and many helpful suggestions during the study.

I am also grateful to many academic and technical staff, and to my colleagues in the department for their advice and assistance, especially to Dr. F. Boysan who gave me great help at the initial stage of the work.

The author is also indebeted to the Chinese Government and the British Council for their financial sponsorship.

Contents

NOMENCLATURE

a_P, a_W, a_E, a_N, a_S	Coefficients in the discretization equations
a	Local sound velocity
A_P, A_W, A_E, A_N, A_S	Area of cell boundaries
A	Cross section area of nozzles
A^*	Throat area of nozzles
$C_1, C_2, C_D, C_s, C_\epsilon,$	
$C_T, C_\mu, C_{\epsilon 1}, C_{\epsilon 2}$	Turbulence model constants
C_l	$\kappa / C_\mu^{3/4}$
C_p	Specific heat at constant pressure
C_v	Specific heat at constant Volume
D_P^U	A_P^U / a_P^U
D_{ij}	Diffusion tensor
e	Internal energy
E, E^{**}, b, s, m	Constants and parameters used in wall functions
f	Body force
g	Heat transfer by conduction
h	Enthalpy
K	1/RT
k	Turbulent kinetic energy
k	Thermal conductivity
l	Mixing length
M	Mach number

p	Fluctuating pressure
P	Mean pressure
P^*	Stagnation pressure
P	Production term in the k-equation
Pe	Peclet number
P_{ij}	Production tensor
Pr	Prandtl number
Pr_k	Prandtl number for turbulent kinetic energy
Pr_ϵ	Prandtl number for dissipation rate
Q	Heat generation
r	Radial coordinate
R	Gas constant
Re	Reynolds number
R_{ij}	Reynolds stress tensor
S	Source term
t	Time
T	Temperature
T^*	Stagnation temperature
$\rho\overline{u_i u_j}$	Reynolds stress tensor
u, v, w	Fluctuating velocities
U, V, W	Mean velocities
x, y, z	Cartesian coordinates
v_t	characteristic velocity of turbulence

GreekSymbols

α	The Reynolds stress model constant
ρ	Density
ρ^*	Stagnation density
τ	Shear stress
τ_w	Wall shear stress
τ_{ij}	Viscous stress tensor
ν	Kinematic viscosity
μ	Viscosity
μ_{tur}	Turbulent Viscosity
μ_{eff}	Effective Viscosity, $\mu_{tur} + \mu$
κ	Von Karman constant
κ^*	$\kappa C_\mu^{1/4}$
Φ	Dissipation function
Φ_{ij}	Pressure-strain tensor
γ	Ratio of specific heats
Γ	$C_T k^2/\epsilon$
Γ_ϵ	$C_\epsilon k^2/\epsilon$
δ_{ij}	Kronecker delta function
ϵ	Turbulent kinetic energy dissipation rate
ω	Time-averaged square of the vorticity fluctuation

Subscripts

e	Denotes edge of inertial sub-layer

nb	Denotes neighbouring points
P	Central point of control volume
v	Denotes edge of viscous sub-layer
W, E, N, S	Neighbouring points
w, e, n, s	Neighbouring points at control volume boundaries

Superscripts

U	Related to axial direction
V	Related to radial direction
—	Averaged value
′	Fluctuating value, or correction value
*	Intermediate value, or stagnation value

Chapter 1

INTRODUCTION

1.1 Numerical Flow Simulations

In the last decade, advances in computer technology and data communication have speeded up numerical flow simulations enormously. The availability of modern supercomputers and the ingenuity of computational fluid dynamics researchers have resulted in new methods for solving historically intractable nonlinear flow field problems. Advances in data communication have facilitated remote access to those computing engines, and advances in computer technology incorporated in mini- and midicomputers now provide sophisticated interactive graphics and data manipulation capability. All of these have brought about profound effects on the engineering design process (1).

It is generally accepted that fluid dynamics can be divided into theoretical, experimental and computational branches (2). Analytical methods provide quick, closed-form solutions, but they require unduly restrictive assumptions, can handle

only very simple configurations, and capture only the idealized fluid dynamics. Through experimentation, representative or actual configurations can be tested and representative or completely experimental data can be obtained. However, experimentation is costly both in terms of model and actual test time. In addition, the limited conditions that can be attained by experimental facilities restrict the scope of experimental programs. By comparison, computational procedures require few restrictive assumptions and can be used to treat complicated configurations. Moreover, they have few Mach number or Reynolds number limitations, they have complete control over fluid properties such as density, viscosity etc., they have enormous flexibility in the choice of flow parameters, in particular, they can do what neither analytical methods nor experimental methods can do - to test the sensitivity of phenomena to independent theoretical approximations such as constant viscosity coefficient, neglect of buoyancy forces, unit Prandtl number etc., and most important, they are far more cost effective than experiments. Thus, the desirability of numerical flow simulations is enhanced when one considers that the cost of experiments is continually increasing because of model, labour, and energy overhead, whereas the cost of computer simulations is continually decreasing as a result of improved numerical procedures and advances in computer technology (3).

In spite of the advantages and the rapid development of numerical flow simulations, it is not expected that computational methods will completely replace experimental testing in the foreseeable future. Their roles instead are complementary. The inadequacies in computational simulations are primarily associated

with poor resolution of physical phenomena, and this is the direct result of insufficient computer power. If one accepts the unsteady Navier-Stokes equations as an adequate system to describe fluid flows, then physical phenomena of interest could be accurately simulated with sufficient computer power. However, current computer power is inadequate to permit numerical solution of these equations with suitable resolution of the wide range of length scales active in high Reynolds number turbulent flows. As a result of this, the averaged Navier-Stokes equations have to be used at present. Computations require an adequate turbulence model to correctly simulate viscous dominated flows (4).

It is such a comparative weighing of all the advantages and disadvantages that underlies the growth of computational fluid dynamics and, especially, its increasing role in design of new flight vehicles. Many numerical methods have been developed but most of these methods are specific for either incompressible or compressible flows; for either unsteady or steady flows. In the next two sections, some general features of incompressible and compressible flows will be given, which result in different numerical methods.

1.2 Incompressible Flows

The very obvious point is that density does not vary with the change of pressure for incompressible flows. In other words, density is totally decoupled from pressure and can be assumed constant. As a result, the time derivative term in the continuity equation vanishes and density can be dropped from the continuity

equation. Therefore, neither density nor pressure can be directly associated with the incompressible continuity equation. The continuity equation, in this case, assumes only the role of a compatibility condition on the velocity field. This is very important to the choice of the main dependent variables in the calculation procedures.

It is apparent from what is mentioned above that density cannot be chosen as a main dependent variable. Thus, there must be a way of calculating pressure in order to solve the momentum equations. For two dimensional flows the vorticity-stream function approach has been used very successfully instead of solving the 'primitive' equations. However, for three dimensional flows the stream function as such does not exist, i.e., there is not a function such that its isoline is the streamline. Nevertheless, a vorticity -stream function like system has been formulated (2) to compute three dimensional incompressible flows in order to avoid calculating pressure directly. Unfortunately, those methods require more computer time and storage, and there may be some difficulties in specifying boundary conditions.

The main obstacle arising from the choice of pressure as a main dependent variable is that the original set of equations does not contain an equation for pressure. Although a Poisson equation can be derived from the momentum equations this method has not been widely used. An effective method to solve the 'primitive' equations had not been really developed until a mechanism was developed by which the continuity and the momentum equations could be linked together to produce a so called pressure correction equation for calculating pressure. It can

be said with confidence now that there is usually no difficulty in obtaining a good numerical solution for incompressible flows. The current research in this field is to refine the solution methods and to make them converge faster and perform more effectively.

1.3 Compressible Flows

It is customary to calculate density directly from the continuity equation in the case of compressible flows, and then pressure is obtained from the equation of state. A great number of numerical methods with density as a main dependent variable have been developed for unsteady flow problems and quite satisfactory results have been obtained. But when only steady-state is concerned it usually comes as a surprise to find that most (through not all) of the successful numerical studies of steady-state flow problems are based on the time-dependent equations, the steady-state solution being obtained, if it exists, as the asymptotic time limit of the unsteady equations. The problem with density as a main dependent variable is that pressure and density become weakly related and the variation of density is almost negligible at low Mach numbers. Thus such an approach with density as a main dependent variable is not viable. Even for supersonic flows in some complicated configurations there exist some subsonic regimes where Mach number can be very low. Furthermore, there are few methods developed for solving the steady-state form of the compressible Navier-Stokes equations. It is apparent that there is still considerable scope for further development and

improvements in this area.

1.4 Turbulence

Turbulence is one of the remaining unsolved problems in the area of physical science. It is believed that the solution of the time-dependent three dimensional Navier-Stokes equations and the conservation equations for mass and energy can describe turbulent flows. However, the fastest and largest computers at present are neither fast nor large enough to solve the equations directly for the required range of length and time scale, even for simple flows. Many industrially important flows, such as the flow in a scramjet engine, are quite complex. The basic problem in computations arises from the vast disparity in time and space scales among the fundamental physical processes. Therefore, it is of practical importance to describe turbulent flows in terms of time averaged quantities rather than instantaneous. This kind of description leads to the well known turbulence closure problem. The time-average processing of the Navier-Stokes equations brings more unknowns, so called Reynolds stresses, which increase the number of unknowns above the number of equations. The problem is then to supply the information missing from the time-averaged equations by formulating a model to describe some or all of the six independent Reynolds stresses.

Most turbulence models developed and tested so far are only for incompressible flows. Some models give good predictions for certain flow configurations but fail to give successful results in other cases (4). For flows with strong streamline

curvature such as highly swirling flows, it is expected that Reynolds stress models which solve six partial differential equations for the six Reynolds stresses would perform better. However, they have not been thoroughly tested for recirculating and swirling flows. Turbulence modelling is still a great challenge even for incompressible flows.

The literature on turbulence modelling for compressible flows is much more scarce. It is not expected that turbulence models developed for incompressible flows can be applied successfully to compressible flows without any modifications. When the mass density is constant, as it is in all the turbulence models for incompressible flows, all of the effects potentially depending on the vorticity source term are absent. In chemically reactive flows the expansion due to heat release influences turbulent mixing by providing the density gradient which leads to vorticity generation (5). Even in non-reactive flows density gradients exist for some cases. Furthermore, density fluctuations cannot be neglected when Mach number is high. A successful turbulence model for compressible flows should incorporate the factors mentioned above. Unfortunately, such a model would be very complicated and one has not been developed so far. Turbulence modelling for compressible flows is still at an early stage, and many numerical simulations for supersonic and hypersonic flows have been performed with very simple turbulence models which contain many empirical factors. The big gap between the "real world" and the models requires to be narrowed and a great deal of research work in this area needs to be done.

1.5 The Objectives of The Present Study

The objectives of the present work are as follows:

1). Numerical methods for compressible flows have been highly developed but they cannot be applied to low Mach number subsonic or incompressible flows since density is used as a main dependent variable. Even for high Mach number flows the existing time-dependent methods may not be very efficient when only the final steady state is required. One of the main objectives of the present study is to develop a prediction procedure which is valid for both incompressible and compressible flows. The scheme, which is based on the SIMPLE (Semi-Implicit Method for Pressure Linked Equations) method (6,7), solves the steady-state form of the Navier-Stokes equations. Pressure is selected as a main dependent variable since the pressure changes are always larger than the density changes which become very small at low Mach numbers. This choice allows the same set of variables to be used for both incompressible and compressible flows at any Mach number.

2). Turbulence is still a remaining unsolved problem in the area of physics as stated above. A number of turbulence models have been developed for incompressible flows. Among those, the two equation k-ϵ model (8) is the one most widely used, and it provides an efficient way of calculating engineering flows. But the performance of the standard k-ϵ model becomes poor for some recirculating flows, swirling flows and so on. It is believed that Reynolds stresses models would give better performance but they have not well tested for some cases such

as highly swirling flows, One facet of the present work is to apply a Reynolds stress model to the case of strongly swirling flows in vortex throttles and compare the performance of the Reynolds stress model with that of the two equation model. At the same time the relative performance of different wall treatments is to be assessed.

1.6 Outline of The Thesis

In chapter two, a literature survey on numerical methods for both incompressible and compressible flows is presented. As computational techniques have progressed dramatically and rapidly there are a great number of methods available. Therefore, it is impossible to give a detailed survey within the scope of this thesis since it is not the intention of the thesis to cover all aspects of numerical simulations of fluid flows. Bearing this in mind only the relevant finite-difference methods for solving the 'primitive' equations will be given in the survey.

In chapter three, the governing equations which describe the flows of a Newtonian fluid are presented. The time-average processing which introduces more unknowns is discussed. A general survey on turbulence models and some assumptions used in the process of modelling are presented.

Chapter four is devoted to the details of the prediction procedure. The coupling between the continuity and the momentum equations together with the discussion on the finite-difference scheme for the pressure gradient term in the case of supersonic flows etc. are described.

In chapter five, applications of the prediction procedure to the incompressible strongly swirling flows in vortex throttles are presented. The main point is to test a Reynolds stress model in a case where the widely used two equation k-ϵ model gives poor performance. Several wall treatments will be used to assess their performance in modelling the near wall regions.

The prediction procedure is tested in chapter six for some compressible flows. Quasi-one dimensional convergent and divergent nozzle flows are selected to check the accuracy of the developed prediction procedure since in this case the analytical results are available. The prediction procedure is also applied to other cases to demonstrate the general validity of the procedure.

In chapter seven, concluding remarks and suggestions for future work are given.

Chapter 2

LITERATURE SURVEY

As computational techniques have developed very rapidly, numerous numerical methods are available now to simulate fluid flows. It is beyond the scope of this thesis to cover the whole area and only the relevant numerical methods for solving the 'primitive' equations directly are presented.

2.1 Methods for Incompressible Flows

As pointed out in chapter one, density cannot be chosen as a main dependent variable for incompressible flows. The problem with the 'primitive' equations is then how to calculate pressure since the solution of the momentum equations requires knowledge of the pressure gradient term. The solutions available to the pressure-velocity coupling problem can be classified into the following groups:

1). Derive and solve a Poisson equation for pressure.

2). Use the artificial compressibility method of Chorin (9).

3). Pressure correction methods.

2.1.1 The Poisson Equation Method

A Poisson equation for the static pressure can be derived from the momentum equations by differentiating the momentum equations first and then adding them together. Details about the derivation and the final form of the equation are given in (2). This equation can be solved with iterative solution methods.

Harlow and Welch (10) developed a computational method to get pressure from a Poisson equation for time-dependent incompressible viscous flow in two dimensional Cartesian coordinates. A staggered grid arrangement was used in their calculation to avoid an unrealistic solution and "marked particles" were introduced to make the flow visible. It was stated that their computational method had some advantages over the vorticity-stream function approach in this case.

Donovan (11) used a similar method to compute two dimensional flow in a square cavity. The fluid in the cavity was initially at rest. The Poisson equation derived from the momentum equations, with a source term as a function of velocities, was solved iteratively at each time step using the successive over-relaxation (SOR) method. With pressure known, the Navier-Stokes equations were solved explicitly for velocities. The terminal position of the calculated vortex center was in agreement with the experimentally determined steady vortex center. The predicted velocity and pressure distributions at large times agreed with previous solutions of the steady Navier-Stokes equations indicating that the unsteady

solution could give the correct steady results.

More recently, Lawal and Mujumdar (12) developed a numerical method to handle three dimensional steady laminar flow and heat transfer of non- Newtonian fluid in ducts. The Poisson equation for the static pressure was solved by the successive over-relaxation method. For the purpose of testing the algorithm and their computer code, the well known case of a Newtonian fluid in a square duct was computed and very good agreement with available experimental results was shown.

The main disadvantage of such a method is that a great of computer time is needed. Another shortcoming of this method lies in its treatment of the boundary conditions. However, this method has not been widely used mainly due to the fact that a more efficient scheme which combines the continuity and the momentum equations to derive a so called pressure correction equation has been developed. Connell (13) found that the Poisson equation method took over 70% more CPU time than using the popular SIMPLE algorithm.

2.1.2 Artificial Compressibility Method

Another technique to handle 'primitive' equations was developed by Chorin (9) to calculate thermal convection problems in both two and three dimensional cases. The basic principle of the method lies in the introduction of an artificial compressibility into the equations, in such a way that the final results do not depend on the artificial compressibility. This is done by introducing an explicit time derivative of artificial density into the continuity equation. In addition,

an artificial equation of state is introduced to couple pressure and the artificial density. This set of governing equations is then comparable with the governing equations of motion for compressible flows, which can be solved using a time-marching technique. Connell and Stow (14) presented another so called density correction algorithm to solve such a set of equations. The basic idea of their algorithm was based on pressure correction methods which will be discussed next. The first step consists of solving the momentum equations for the velocity field. As the velocity field will, in general, not satisfy the continuity equation, the artificial density is then corrected using the continuity equation and pressure is obtained through the use of the artificial equation of state. The results for a driven cavity test example were published, and it was concluded that this algorithm took more CPU time than one of the pressure correction methods such as the SIMPLE method (6,7). The artificial compressibility method is only applicable to steady flows in order to make the final solution independent of the artificial compressibility. In other words, the solution is meaningful only if a steady state is attained and the time derivative of the artificial density vanishes. As a result the method has not been widely used.

2.1.3 Pressure Correction Methods

In 1972, Patankar and Spalding (6) proposed a new approach to calculate pressure in their calculation procedure for three dimensional parabolic flows. More details about this approach were given by Patankar in (7). The basic idea is to first guess the pressure field, get an approximation to the velocity field, and then

make corrections to the pressure field in such a sense as to bring the velocity field into conformity with the continuity equation. This is the fundamental principle of pressure correction methods. The central part of these methods is a so called pressure correction equation which is generally derived from the finite-difference form of the momentum and the continuity equations. Pressure correction methods have found wide applications since their original development.

One of the most frequently used pressure correction method is the SIMPLE algorithm (6,7). This algorithm has been used very successfully for a wide variety of cases (6,13,14,15,16,17,18). There is no doubt about the creditability of this algorithm. Various modifications introduced so far have merely served the purpose of making the original one perform more efficiently. Among those, Patankar (7,19) introduced a modified version called SIMPLER (which stands for SIMPLE-Revised). The main difference is that SIMPLER uses a pressure correction equation to adjust the velocity field just as the SIMPLE algorithm does but employs a separate pressure equation to predict the pressure field. Furthermore, no approximations are used for the pressure equation in the development of the SIMPLER method. The pressure field is a direct consequence of the given velocity field. Hence, if the correct velocity field is obtained then the pressure equation would produce the correct pressure field. However, both a pressure correction equation and a pressure equation must be solved at each iteration so that much more CPU time is needed.

Relevant experiences with the SIMPLE and the SIMPLER methods have been reported by Raithby and Schneider (20) who investigated some of the SIMPLE

variants. They also introduced CTS SIMPLE (Consistent Time Step SIMPLE). Several alternative methods of updating pressure were examined. The PUMPIN (Pressure Update from Multiple Path Integration) method which updates pressure without the need to solve a separate Poisson equation was presented. A set of methods PLUS- (Pressure Update from Least-Square Residual Minimization) were derived. A pressure distribution that agrees with the results in some "best" sense can be obtained by each of those methods. Unfortunately, an evaluation of the relative performance of each method cannot be made since only the decrease in error as a function of the iteration count was determined.

VanDoormaal and Raithby (21) provided several suggestions for the enhancement of the SIMPLE method. The enhancements included the application of boundary conditions, equation solution techniques, convergence criteria, and a new variant SIMPLEC (SIMPLE Consistent). The SIMPLEC method recasts the pressure correction equation such that relaxation is not necessary for pressure. The relative performance of the SIMPLE, SIMPLER, and SIMPLEC methods was compared.

Latimer and Pollard (22) introduced a new solution algorithm called FIMOSE (Fully Implicit Method for Operator-Split Equations). The assumptions in the derivation of the pressure correction equation that cause the other methods to be Semi-Implicit was removed. The basis of the FIMOSE algorithm is to split the operators in the governing equations to decouple the pressure-velocity link so that only one variable is dealt with at any time. Moreover, two integral equations were introduced to maintain a global conservation balance. The FIMOSE algo-

rithm is fully implicit because it uses a true predictor-corrector method in which the governing equations are solved again by using updated sources to update the velocity field, rather than using velocity-correction formulas. The interaction of the governing equations are decoupled by splitting the operations on velocity and pressure. Each equation is solved separately but tight coupling is maintained between the equations by using the updated velocity and pressure field when recalculating the source terms before each equation is solved. In addition, they compared several different versions of pressure correction methods, and the results for three laminar, incompressible, steady-state, uniform property fluid flow problems were presented using four pressure-velocity coupling solution algorithms - SIMPLER, CTS SIMPLE, SIMPLEC, and FIMOSE. All equations were solved by the same routine. Their relative performance was estimated by calculating the percentage difference in execution times. None of the methods showed general advantages over other methods in three cases. The SIMPLEC algorithm was faster than the SIMPLER and FIMOSE methods for a axisymmetrical sudden expansion problem. However, the FIMOSE method was much faster in the case of a porous wall in a plane duct while the SIMPLER algorithm provided quite poor results.

From the discussions above it can be seen that a class of the SIMPLE methods has been developed and used successfully instead of the Poisson equation and the artificial compressibility methods. Unfortunately, in spite of many of the SIMPLE variants, the relative performance of each method has not been systematically tested. There appears to be no consensus of opinion as to which is

the best method for general engineering flow problems. The SIMPLE method, generally speaking, requires notably more iterations for convergence than the other methods evaluated but it is possible that the SIMPLE method may appear more competitive when the actual computation time rather than the number of iterations is taken as the measure of merit. Therefore, the SIMPLE method is still widely used and is employed in the present work for the strongly swirling incompressible flows in vortex throttles.

2.2 Methods for Compressible Flows

Most of the computational methods developed so far are for unsteady flows as density can be calculated from the continuity equation directly, and then pressure is evaluated from the equation of state. Even for steady flow problems the unsteady governing equations are integrated in time until a steady state is reached. For totally supersonic flow regimes, it is believed that space-marching methods may be effective for solving steady-state equations of parabolic type with respect to a spatial coordinate. Therefore, the numerical methods developed for unsteady flows can be adapted to steady overall supersonic flows by eliminating the time derivative and integrating the derivative in the flow direction as if it were a time derivative. However, many engineering complicated flows contain some subsonic regions, recirculating regions etc. instead of purely supersonic flows and they can only be fully described by the Navier-Stokes equations. Unfortunately, the methods available for solving the steady-state Navier-Stokes equations are very few

and involve an extension of the SIMPLE algorithm (6,7) to compressible flows. On the other hand, the literature on the solution of the Euler equations is very vast and schemes for viscous flows are also applicable to the Euler equations. Thus, discussions below will be focused on numerical methods for solving the Navier-Stokes equations.

2.2.1 Unsteady Methods

The methods for unsteady flows can be classified into explicit and implicit methods according to the time differencing method. In an explicit technique the unknown variables are expressed at the advanced time level entirely in terms of the known values at the current time level hence the finite-difference equations can be solved directly. In an implicit procedure the finite-difference equations introduce unknown variables at both the current and the advanced time level. Generally speaking, a procedure of this type necessitates the solution of a set of simultaneous equations, which usually results in a complex and time consuming procedure on a per grid point per time step basis. However, the explicit schemes tend to be conditionally stable and suffer from the limitation of the time step while the implicit methods are usually stable for large time steps (although not necessarily unconditionally stable). Some methods split the equations and use the explicit or implicit differencing schemes depending on the fractional step considered. A more detailed survey can be found in (2,23 24,25).

Explicit Methods

The basic algorithm that has been used widely and successfully is the MacCormack predictor-corrector method (26). It is a second order accurate method and can be programmed quickly. In the predictor step, forward difference operators are used, while backward difference operators are used in the corrector step. Since it is easily applied to complex flow fields and is very robust this method is still widely used today.

Baldwin and MacCormack (27) developed the explicit predictor-corrector method further by splitting the set of two dimensional equations into two sets of one dimensional equations while retaining second order accuracy, which makes the solution more straightforward. The modified method is called the time-splitting explicit numerical scheme. This scheme was used by Shang and Hankery (28) to calculate supersonic turbulent flows for a series of compression corner configurations. Good agreement between the experimental and calculated density profiles in the viscous- inviscid interaction region was presented.

Knight (29) used the explicit predictor-corrector algorithm to solve two dimensional Navier-Stokes equations in conservation form. Predictions compared favourably with experimental data for two different supersonic inlet designs. The qualitative behaviour of shock wave/boundary layer interactions was predicted as well.

Drummond (30) developed a computer program to model the turbulent reacting flowfield in an axisymmetrical ramjet dump combustor. The governing equations were integrated using the explicit predictor- corrector method until a

steady-state solution was reached. Comparison between the nonreacting experimental data and the predictions was presented and fair agreement overall was observed.

Some other applications of MacCormack's explicit predictor-corrector method can be found in (31,32,33). There are some other explicit schemes which are given in (2,25). However, the stability limits of the explicit schemes can be very restrictive in certain cases such as reacting flows, high Reynolds number flows and so on. As a result of this, most methods currently used for the compressible Navier-Stokes equations are of the implicit or hybrid type.

Implicit Methods

Implicit schemes are not subject to severe stability restrictions on the size of time step and, therefore, may achieve a convergence rate increase of one to two orders of magnitude compared to explicit methods. However, the solution procedure typically involves inversion of block tridiagonal matrices, and is more difficulty to program. The pioneering work on implicit schemes for the finite-difference solution of the fluid dynamics equations of motion was performed by Briley and McDonald (34); Beam and Warming (35).

Beam and Warming (35) developed an implicit scheme for the numerical solution of the compressible Navier-Stokes equations in conservative form. The scheme is second-order-time accurate, noniterative and unconditionally stable. The ADI method is employed and the unknowns of the block-tridiagonal linear system are conserved variables (density, momentum, total energy). Numerical

predictions for a two dimensional shock boundary layer interaction problem were presented.

Visbal and Knight (36,37) developed a computer code using Beam and Warming's implicit scheme. The developed computer code was well tested (36) and very good results were obtained for several test cases including inviscid shocked flows, laminar and turbulent boundary layer flows, and laminar shock/boundary-layer interactions. Some other applications of this scheme can be found in (38,39,40).

The method developed by Briley and McDonald (34) is more or less the same as that of Beam and Warming. The major difference is that the primitive variables (density, velocity, temperature) appeared as unknowns in the block-tridiagonal linear system rather than the conserved variables. The applications of this method are mainly to internal flows (41,42).

MacCormack (43) described a hybrid explicit-implicit scheme which is based on his explicit predictor-corrector method (26). The scheme consists of two stages. The explicit predictor-corrector method is used in the first stage, which is subject to the explicit stability restrictions. The second stage removes those stability restrictions by transforming the equations of the first stage into an implicit form. The method requires no block or scalar tridiagonal inversions as the matrix equations to be solved are block bidiagonal. As a result, the method is simple and straightforward to program and should be more efficient than other methods. In fact the new method was compared with the original explicit method for a series of shock interaction problems, and it was shown that the new method was very efficient as it took much less computer time. However, when compared with the

hybrid explicit-implicit characteristic method which was also developed by MacCormack (44), it was only slightly more efficient (43). Applications of this hybrid explicit-implicit method are also given in (45,46,47).

Knight (48) extended his previously developed technique (49,50,51) for the two dimensional Navier-Stokes equations to a three dimensional algorithm. The algorithm combines MacCormack's explicit method with an implicit scheme for the viscous sublayer and transition wall region of the turbulent boundary layer. The algorithm was employed to integrate the Navier-Stokes equations in time until a steady-state flowfield was obtained for the interaction of an oblique shock wave with a turbulent boundary layer in three dimensions. It was shown that the predictions were generally in close agreement with the experimental data.

All the methods discussed so far for unsteady compressible flows use density as one main dependent variable since density can be obtained from the continuity equation directly. Pressure is then calculated from the equation of state. However, as pointed out before, the methods with density as a main dependent variable are not applicable to low Mach number flows since density changes become very small while the pressure changes are always finite. For incompressible flows it is impossible to solve the governing equations anymore with density as a main dependent variable. Furthermore, when only the final steady-state solution is of concern, it may be not economical to still use unsteady methods.

2.2.2 Steady Methods

When supersonic flows are considered, shock waves appear necessarily in certain flow configurations. The conservation equations in integral form are valid for all flows, including the ones with finite jumps. By applying Green's formulas, the same equations can be recast into partial differential form (known as the "divergence form"). However, partial differential equations have a more restricted range of validity. In fact, partial differential equations cease to be valid wherever the functions can not be differentiated. Therefore, they can describe regions of continuous flows but not shock waves. Nevertheless, if the concept of the derivative is generalized in the spirit of distribution theory, it has been shown (52) that the equations in divergence form admit "weak" solutions (that is, solutions containing a jump), and that such jumps appear in the right places. However, the same cannot be said if the equations of motion are recast in any other form.

Two numerical techniques have emerged for the analysis of flows with shocks. The first, known as "shock capturing", relies on the proven mathematical legitimacy of weak solutions, which requires no special treatment to deal with discontinuities. All types of flows, including flows with shocks, can be computed by using the same discretization of the governing equations in divergence form at all nodes. The unsteady methods discussed before can be classified into this category. The second, known as "shock fitting", makes provisions for explicitly computing the discontinuities. Basically, it locates the discontinuities and treats them as boundaries between regions where a regular solution is valid. In this case, there is no need for maintaining the equations of motion in divergence form. Although

shock capturing methods give a poor interpretation of physical phenomena and are an uneconomical way of computing, as concluded by Moretti (53), they are far more popular for several reasons. First, it would be very convenient to have a computer code that can describe any flows, no matter how complicated, by repeating the same set of operations at all nodes without having to set up special logic to detect and track down discontinuities. In addition, it is possible to discuss the mathematical properties of such a code by a local analysis, and general conclusions can be drawn about the order of accuracy, stability, and convergence. In the shock fitting methods, the interaction between the discretized codes and the original algebraic codes is much harder to analyze formally. Furthermore, for problems of three or more independent variables, the partitioning of a flowfield into regions where a regular solution is valid can create some difficult topological problems (54). However, Moretti (53) presented a technique called "floating shock fitting", which does not necessarily require discontinuities as boundaries of flows. This procedure therefore eliminates the problems associated with partitioning the flowfield. Nevertheless, no studies will be made of this procedure since shock fitting techniques are not within the scope of this thesis. More details about shock fitting can be found in (53,54,55,56,57).

It is also necessary at this point to mention that instabilities may occur due to large pressure gradients when shocks are present. Actually, in real flow computations, instabilities may occur due not only to shocks but also to some other sources such as non-linear effects, presence of walls or other boundaries of the computational domain and so on. The computations do not necessarily diverge

but often oscillations occur and remain of finite amplitude as a result of instabilities. The use of central differencing for convective terms can also result in spatial oscillations at high Reynolds numbers even for incompressible flows. These oscillations can be suppressed by adding artificial viscosity, which can be done in two ways. The first is to explicitly add an artificial damping term into the equations. This has been used widely for supersonic flows. The other is to use certain finite-difference schemes such as upwind differencing which will introduce the artificial viscosity automatically.

The literature on the solution of the steady-state form of the compressible Navier-Stokes equations is very scarce despite the fact that quite a few methods have been developed for solving the steady-state Euler equations (58,59,60). Several parabolic Navier-Stokes solvers were reviewed by Drummond et al (61) for solving steady supersonic flows, but they are not applicable to complicated engineering flows such as flows with recirculating regions, supersonic flows with embedded subsonic regions and so on. These flows can only be fully described by solving the compressible Navier-Stokes equations with pressure as a main dependent variable. It appears that only a few schemes (62,63,64) have been developed for solving the steady-state form of the compressible Navier-Stokes equations, which are extensions of the SIMPLE or the SIMPLER (6,7) methods for compressible flows.

Issa and Lockwood (62) introduced some modifications in order to properly model the hyperbolic nature of supersonic flows. The basic idea is to cut off downstream influences as theory tells us that any small disturbances downstream

cannot be felt upstream in supersonic flows, and furthermore, the disturbances can only propagate downstream within certain regions. This is the hyperbolic character which only the supersonic flows have. To put this into practice, the pressure gradient term in the momentum equations is upwind differenced so that downstream pressure will not influence upstream velocity. Convective terms are also automatically upwind differenced due to the use of the hybrid differencing scheme which switches to upwind differencing when the control volume Reynolds number is above certain value. Furthermore, the supersonic mass fluxes are calculated using upstream densities . This modified procedure (62) was applied to compute near-wall supersonic flows. It was concluded that the modified procedure performed tolerably well and was definitely superior to the existing parabolic prediction methods which could not simulate the significant elliptic effects due to the existence of the subsonic layer. However, the abrupt switch of the difference scheme for the pressure gradient term, as the flow changes from the subsonic to supersonic, may cause computational difficulties in the case of supersonic flows with recirculating subsonic regions and transonic flow regimes. Also, the switch from central differencing to upwind differencing for the pressure gradient term may violate the conservation of mass. This will be discussed in more detail in chapter four.

Hah (63) presented a procedure to compute turbulent flows in various turbomachinery components. The scheme was developed for non-orthogonal grids. However, it was pointed out by Karki (64) that this method had several serious shortcomings and the general validity was doubtful.

Karki (64) developed a calculation procedure for flows at all speeds, and it was shown clearly that only when pressure was chosen as a main dependent variable could such a calculation procedure be valid for flows at all speeds. The calculation procedure is a extension of the SIMPLER algorithm (7,19) to compressible flows. In the original version of the SIMPLER method, the pressure field was obtained by solving a pressure equation which is derived from the finite-difference form of the full momentum equations and the continuity equation. Moreover, a pressure correction equation was also employed to update the velocity fields. However, the modified procedure uses two pressure correction equations to update the velocity fields and the pressure field respectively. The pressure correction equation for updating the pressure field is very similar to an alternative pressure correction equation apart from the fact that the full momentum equations are used instead of their truncated form. Furthermore, the central differencing scheme is used for the pressure gradient term no matter whether it is subsonic or supersonic flow in the modified procedure. In addition, the artificial viscosity could be introduced by using upwind biased density when the Mach number is over one instead of adding it explicitly. However, Karki argued that the use of two differencing schemes for density might cause computational problems near the switch-over point, therefore, the density was always upwinded, i.e., the density at a control-volume face was taken to be the value prevailing at the grid point upstream of it no matter what the Mach number was. This practise seems to lack a sound theoretical basis although the author stated that it led to a well-behaved pressure equation. Nevertheless, the predictions showed that for quasi-one-dimensional inviscid and

two dimensional laminar flows the modified prediction procedure performed quite well. Unfortunately, the calculation procedure was not put through more severe tests such as recirculating flows where both supersonic and subsonic regions may coexist. Thus, the general validity of the procedure remains questionable.

From the forgoing survey of the available numerical schemes, it is obvious that there is considerable scope for further developments and improvements. The computational techniques for compressible flows are highly developed but they cannot be applied to low Mach number subsonic or incompressible flows due to the choice of density as a main dependent variable. Even for high Mach number flows, however, the existing time-dependent methods may not be very efficient when only the final steady state is required. Few calculation procedures have been developed to solve the steady- state form of the compressible Navier-Stokes equations with pressure as a main dependent variable. These procedures are supposed to be valid for flows at all speeds but they have not been well tested, especially in some severe situations such as supersonic flow with recirculating subsonic regions. Furthermore, turbulence modelling is still a great challenge and it is believed that it is almost impossible to develop a universal turbulence model (other than the Navier-Stokes equations themselves).

Chapter 3

GOVERNING EQUATIONS AND TURBULENCE MODELLING

In this chapter, the governing equations of fluid dynamics are presented, followed by a description of the time-averaging procedure as proposed first by Osborne Reynolds (65) giving rise to terms which have subsequently become known as the Reynolds stresses. A brief introduction to turbulence modelling is also given.

The governing equations in this chapter are written in the Cartesian coordinate system for the sake of simplicity. The equations in other coordinate systems can be found in numerous textbooks, articles etc.

3.1 Basic Equations

The governing equations of fluid dynamics are based on the following universal laws of conservation:

1). Conservation of Mass

2). Conservation of Momentum

3). Conservation of Energy

3.1.1 Continuity Equation

The continuity equation is obtained by applying the Conservation of Mass Law to an infinitesimal, fixed control volume.

$$\frac{\partial \rho}{\partial t} + \frac{\partial}{\partial x}(\rho u) + \frac{\partial}{\partial y}(\rho v) + \frac{\partial}{\partial z}(\rho w) = 0 \tag{3.1}$$

where ρ is density, u, v, w represent the x, y, z components of the velocity vector. When incompressible flows are considered, i.e., density is constant. The above equation reduces to:

$$\frac{\partial u}{\partial x} + \frac{\partial v}{\partial y} + \frac{\partial w}{\partial z} = 0 \tag{3.2}$$

3.1.2 Momentum Equations

The Conservation of Momentum Law is nothing but Newton's second law. Applying this law to a fluid passing through an infinitesimal, fixed control volume yields the following momentum equations written in conservation law form (also called "divergence" form):

$$\frac{\partial}{\partial t}(\rho u) + \frac{\partial}{\partial x}(\rho u^2 + p - \tau_{xx}) + \frac{\partial}{\partial y}(\rho uv - \tau_{xy}) + \frac{\partial}{\partial z}(\rho uw - \tau_{xz}) = \rho f_x \tag{3.3}$$

$$\frac{\partial}{\partial t}(\rho v) + \frac{\partial}{\partial x}(\rho uv - \tau_{xy}) + \frac{\partial}{\partial y}(\rho v^2 + p - \tau_{yy}) + \frac{\partial}{\partial z}(\rho vw - \tau_{yz}) = \rho f_y \quad (3.4)$$

$$\frac{\partial}{\partial t}(\rho w) + \frac{\partial}{\partial x}(\rho uw - \tau_{xz}) + \frac{\partial}{\partial y}(\rho vw - \tau_{yz}) + \frac{\partial}{\partial z}(\rho w^2 + p - \tau_{zz}) = \rho f_z \quad (3.5)$$

where f is the body force per unit volume and the most common body force is the gravitational force. The components of the viscous stress tensor τ_{ij} are given by

$$\tau_{xx} = 2\mu\frac{\partial u}{\partial x} - \frac{2}{3}\mu\left(\frac{\partial u}{\partial x} + \frac{\partial v}{\partial y} + \frac{\partial w}{\partial z}\right) \quad (3.6)$$

$$\tau_{yy} = 2\mu\frac{\partial v}{\partial y} - \frac{2}{3}\mu\left(\frac{\partial u}{\partial x} + \frac{\partial v}{\partial y} + \frac{\partial w}{\partial z}\right) \quad (3.7)$$

$$\tau_{zz} = 2\mu\frac{\partial w}{\partial z} - \frac{2}{3}\mu\left(\frac{\partial u}{\partial x} + \frac{\partial v}{\partial y} + \frac{\partial w}{\partial z}\right) \quad (3.8)$$

$$\tau_{xy} = \mu\left(\frac{\partial u}{\partial y} + \frac{\partial v}{\partial x}\right) = \tau_{yx} \quad (3.9)$$

$$\tau_{xz} = \mu\left(\frac{\partial u}{\partial z} + \frac{\partial w}{\partial x}\right) = \tau_{zx} \quad (3.10)$$

$$\tau_{yz} = \mu\left(\frac{\partial v}{\partial z} + \frac{\partial w}{\partial y}\right) = \tau_{zy} \quad (3.11)$$

substituting the expressions for the viscous stress tensor into the above momentum equations the so called Navier-Stokes equations are obtained which can be written in tensor form as:

$$\frac{\partial}{\partial t}(\rho u_i) + \frac{\partial}{\partial x_j}(\rho u_i u_j) = -\frac{\partial p}{\partial x_i} + \frac{\partial}{\partial x_j}\left(\mu\frac{\partial u_i}{\partial x_j}\right) + \frac{1}{3}\frac{\partial}{\partial x_i}\left(\mu\frac{\partial u_k}{\partial x_k}\right) \quad (3.12)$$

the body force is neglected in the above equation. The Navier-Stokes equations form the basis upon which the entire science of viscous flow theory has been developed.

If the flow is assumed incompressible and steady the above equation will reduce to the following simpler form:

$$\frac{\partial}{\partial x_j}(\rho u_i u_j) = -\frac{\partial p}{\partial x_i} + \frac{\partial}{\partial x_j}\left(\mu\frac{\partial u_i}{\partial x_j}\right) \quad (3.13)$$

3.1.3 Energy Equation

The Conservation of Energy Law is identical to the First Law of Thermodynamics. Applying this law to a fluid passing through an infinitesimal, fixed control volume yields the following energy equation:

$$\rho\frac{De}{Dt} + p(\nabla \bullet V) = \frac{\partial Q}{\partial t} - \nabla \bullet q + \Phi \tag{3.14}$$

where e is the internal energy per unit mass, Q is the heat generation per unit volume due to some chemical process such as combustion etc. The heat transfer q by conduction can be expressed according to Fourier's Law as:

$$q = -k\nabla T \tag{3.15}$$

where k is the coefficient of thermal conductivity and T is temperature. Φ is called the dissipation function which represents the rate of mechanical energy dissipated into heat in the process of deformation of the fluid due to viscosity. In a Cartesian coordinate system it has the following form:

$$\Phi = \mu\left[\frac{1}{2}\left(\frac{\partial u_i}{\partial x_j} + \frac{\partial u_j}{\partial x_i}\right)^2 - \frac{2}{3}\left(\frac{\partial u_k}{\partial x_k}\right)^2\right] \tag{3.16}$$

If the flow is assumed to be incompressible, heat generation is neglected (no combustion etc.) and the coefficient of thermal conductivity is assumed constant, Eq. (3.14) reduces to the following form:

$$\rho\frac{De}{Dt} = k\nabla^2 T + \Phi \tag{3.17}$$

and the dissipation function is as follows:

$$\Phi = \frac{1}{2}\mu\left(\frac{\partial u_i}{\partial x_j} + \frac{\partial u_j}{\partial x_i}\right)^2 \tag{3.18}$$

3.1.4 Equation of State

The equations presented above cannot be solved as the number of unknowns is greater than the number of equations. In order to close the system of fluid dynamics equations it is necessary to estab lish relationships between the thermodynamic variables (p, ρ, T, e, h) as well as to relate the transport properties (μ, k) to the thermodynamic variables. Usually, a perfect gas is assumed and the equation of state, in this case, takes the following form:

$$p = \rho RT \tag{3.19}$$

where R is the gas constant. Also for a perfect gas, the following relationships exist:

$$e = C_v T \tag{3.20}$$

$$h = C_p T \tag{3.21}$$

$$\gamma = \frac{C_p}{C_v} \tag{3.22}$$

$$R = C_p - C_v \tag{3.23}$$

where C_v is the specific heat at constant volume, h is enthaply, C_p is the specific heat at constant pressure and γ is the ratio of specific heats. For air at standard condition, $R = 287 m^2/s^2 K$ and $\gamma = 1.4$. Furthermore, the Prandtl number

$$Pr = \frac{C_p \mu}{k} \tag{3.24}$$

is often used to determine the coefficient of thermal conductivity k once μ is known as the ratio (C_p/Pr) is approximately constant for most gases. For air at standard condition $Pr = 0.72$.

3.2 Time-Averaging Procedure

The time-averaging procedure, following Reynolds, involves the decomposition of instantaneous dependent variables into a time-averaged component plus a fluctuating component about the average, i.e.

$$\Phi = \overline{\Phi} + \Phi' \tag{3.25}$$

where Φ stands for u, v, w, p, ρ, T. For convenience, the mean value will be denoted with capital letters and the fluctuating component will be denoted with small letters hereafter. For example, U is the mean value of the velocity component in the x-coordinate direction while u is the corresponding fluctuating part. Substitute the above relation into the continuity and momentum equations and then the entire equations are time averaged yields the following averaged equations in tensor form as:

$$\frac{\partial \overline{\rho}}{\partial t} + \frac{\partial}{\partial x_i}(\overline{\rho} U_i + \overline{\rho' u_i}) = 0 \tag{3.26}$$

$$\frac{\partial}{\partial t}(\overline{\rho} U_i + \overline{\rho' u_i}) + \frac{\partial}{\partial x_j}(\overline{\rho} U_i U_j + U_i \overline{\rho' u_j}) = -\frac{\partial P}{\partial x_i} + \frac{\partial}{\partial x_j}(\overline{\tau_{ij}} - U_j \overline{\rho' u_i} - \overline{\rho u_i u_j} - \overline{\rho' u_i u_j}) \tag{3.27}$$

where the stress tensor is

$$\overline{\tau_{ij}} = \mu \left[\left(\frac{\partial U_i}{\partial x_j} + \frac{\partial U_j}{\partial x_i} \right) - \frac{2}{3} \delta_{ij} \frac{\partial U_k}{\partial x_k} \right] \tag{3.28}$$

where δ_{ij} is the Kronecker delta function ($\delta_{ij} = 1$ if i=j and $\delta_{ij} = 0$ if $i \neq j$). For incompressible flows the above equations reduce to:

$$\frac{\partial}{\partial x_i}(\rho U_i) = 0 \tag{3.29}$$

$$\frac{\partial}{\partial t}(\rho U_i) + \frac{\partial}{\partial x_j}(\rho U_i U_j) = -\frac{\partial P}{\partial x_i} + \frac{\partial}{\partial x_j}(\overline{\tau_{ij}} - \rho\overline{u_i u_j}) \tag{3.30}$$

where $\rho\overline{u_i u_j}$ is the so called Reynolds stress and $\overline{\tau_{ij}}$ takes the following simpler form:

$$\overline{\tau_{ij}} = \mu\left(\frac{\partial U_i}{\partial x_j} + \frac{\partial U_j}{\partial x_i}\right) \tag{3.31}$$

Apart from simple time-averaging, there is another approach to averaging the equations which is called mass-weighted averaging. For the treatment of compressible flows and mixtures of gases in particular, mass-weighted averaging is convenient as the averaged equations take a simpler form than the time-averaged equations. More details about mass-weighted averaging can be found in (25,66,67,68).

3.3 Turbulence Modelling

The need for turbulence modelling was pointed out in chapter one. In order to predict turbulent flows by solving the time-averaged equations it is necessary to make closure assumptions for the unknowns which appear in the equations due to the averaging procedure. Most of the turbulence models developed so far are for incompressible flows, i.e., density is constant. In this case, the unknowns in the averaged momentumequations are the six Reynolds stresses. The discussions here will focus on the modelling of the Reynolds stresses and some other approaches to turbulence modelling will be also briefly introduced.

Boussinesq (69) proposed that the apparent turbulent stresses might be related to the rate of mean strain through an apparent scalar turbulent or "eddy"

viscosity. Although this concept was proposed more than one hundred years ago it is still widely used in turbulence models today. For incompressible flows, the Reynolds stresses can be expressed using the Boussinesq assumption as:

$$-\rho\overline{u_i u_j} = \mu_t \left(\frac{\partial u_i}{\partial x_j} + \frac{\partial u_j}{\partial x_i} \right) - \frac{2}{3}\delta_{ij}\rho k \tag{3.32}$$

where μ_t is the turbulent viscosity and k is the averaged kinetic energy of turbulence, $k = \overline{u_i u_i}/2$. The problem is how to find μ_t when the above relation is employed.

There are several ways of classifying turbulence models. One way is to divide them into two categories according to whether the Boussinesq assumption is used or not. Models using the Boussinesq assumption will be classified into category one or called turbulent viscosity models. Most models currently used in engineering caculations are of this type and experimental evidence indicates that the turbulent viscosity hypothesis is valid in many flow situations. There are exceptions, however, and there is no physical basis that it holds. Other models which obtain the Reynolds stresses from the transport equations without the Boussinesq assumption are referred to as category two, including those known as Reynolds stress or, more generally, stress-equation models.

Another common classification of turbulence models is according to the number of partial differential transport equations solved in addition to the mean flow equations. It is easier to follow the discussion in this way. According to this classification turbulence models can be grouped into the following four classes (4, 70)

1). Zero equation models

2). One equation models

3). Two equation models

4). Stress equation models

Models in classes 1)—3) also belong to category one according to the previous classification which use the Boussinesq assumpton while stress equation models in class 4) fall into category two.

The zero equation model, which does not need any transport equations for turbulence quantities, is also called "mean field" closure (71) while classes 2)—4) are called "transport equation" closure.

A brief introduction to turbulence modelling will be given in the following part of this chapter although detailed consideration of modelling of turbulent flows is beyond the scope of this thesis. A general review of turbulence models and their applications can be found in (4, 25, 71, 72, 73, 74). Bradshaw (75) describes the interplay between the development of models and the experiments. Launder and Spalding (76) give the mathematical concepts of turbulence models. Bradshaw and Cebeci (77) present calculation methods for various classes of turbulent flows. Lumley (78, 79) and Launder (80) discuss the prospects for high order closure models. Turbulence models available for the prediction of three-dimensional flows with curvature, rotation and flow separation are reviewed by Lekshminarayana (81). An exhaustive review of turbulence models for near-wall and low Reynolds number flows is given by Patel et al (82).

3.3.1 Zero Equation Models

Zero equation models (also called algebraic models) utilize the Boussinesq assumption invariably. The first and most successful turbulence model of this type proposed by Prandtl is still among the most widely used models. For thin shear layers the Boussinesq assumption is applied to yield:

$$-\rho\overline{uv} = \mu_t \frac{\partial U}{\partial y} \tag{3.33}$$

where μ_t is the turbulent viscosity which is related to the mean velocity by the Prandtl mixing length hypothesis as follows:

$$\mu_t = \rho C_\mu l^2 \mid \frac{\partial U}{\partial y} \mid \tag{3.34}$$

where C_μ is a constant and l is the so called "mixing length" that can be thought of the distance over which particles maintain their original momentum. The product $l \mid \frac{\partial U}{\partial y} \mid$ can be interpreted as the characteristic velocity of turbulence v_t by which the above relation can be rewritten in a more general form as:

$$\mu_t = \rho C_\mu v_t l \tag{3.35}$$

The mixing length has to be known before performing calculations but there is no exact method for its prediction, hence it has to be prescribed with the aid of empirical information. Nevertheless, the mixing length model has been used for free shear and boundary layers very successfully. However, the evaluation of l in the mixing length model changes according to the type of flows being considered and it becomes extremely difficult to evaluate l for recirculating flows, three-dimensional flows etc. The incorporation of the effects of curvature, buoyancy

and rotation in the model is also entirely empirical. In addition,the transport and history effects of turbulence are not accounted for. In particular, the mixing length model may give totally wrong answer in some cases, for example, when two dimensional or axisymmetrical internal channel flows are considered, $\frac{\partial U}{\partial y} = 0$ in the centre, then μ_t will become zero by Eq.(3.34) whereas experimental evidence indicates that this is not true.

One major motivation for developing more complex models is the observation that the algebraic models evaluate the turbulent viscosity in terms of only local flow parameters, yet it is generally accepted that a turbulence model should be able to provide a mechanism by which effects upstream can influence the turbulence structure (and viscosity) downstream. In addition, with the simplest models ad hoc additions and corrections are frequently required to handle specific effects, and constants need to be adjusted to deal with different classes of flows.

If the general form for the turbulent viscosity, $\mu_t = \rho C_\mu v_t l$, is accepted, then a logical way to extend the generality of turbulent viscosity models is to construct a more complex and general function of the flow for v_t and perhaps l, which can account for the transport and history effects of turbulence. Specific modifications to the constants are not then required for different classes of flows.

3.3.2 One Equation Models

In order to extend the generality of the algebraic models Prandtl and Kolmogorov suggested in the 1940s that v_t be proportional to the square root of the turbulent kinetic energy, $k = \overline{u_i u_i}/2$. As a result, the turbulent viscosity can be expressed

as:

$$\mu_t = \rho C_\mu l k^{1/2} \tag{3.36}$$

and μ_t will not be zero when $\frac{\partial U}{\partial y} = 0$. Turbulent kinetic energy is a measurable quantity and its physical meaning is quite clear, but the problem is how to predict it.

A transport partial differential equation for k can be derived from the Navier-Stokes equations after some manipulations. However, there are some unknowns in the exact transport equation which need to be approximated by modelling assumptions. For instance, when two dimensional incompressible thin-shear-layer flows are considered, the exact transport equation for k takes the following form:

$$\rho\frac{Dk}{Dt} = \mu\frac{\partial^2 k}{\partial y^2} - \frac{\partial}{\partial y}\left(\rho\overline{vk'} + \overline{vp}\right) - \rho\overline{uv}\frac{\partial U}{\partial y} - \mu\left[\overline{\left(\frac{\partial u}{\partial y}\right)^2} + \overline{\left(\frac{\partial v}{\partial y}\right)^2}\right] \tag{3.37}$$

The first term on the right hand side represents diffusion due to viscous action while the second term represents diffusion due to turbulence. The third and fourth terms represent the generation and dissipation of turbulent kinetic energy respectively. The turbulent diffusion term is usually modelled similarly to the Reynolds stresses expressed in Eq.(3.32)

$$-\rho\overline{vk'} = \frac{\mu_t}{Pr_k}\frac{\partial k}{\partial y} \tag{3.38}$$

where Pr_k is the Prandtl number for turbulent kinetic energy (≈ 1.0). The correlation of velocity and pressure fluctuation term $\frac{\partial}{\partial y}(\overline{vp})$ is usually neglected. The dissipation term is modelled using turbulent kinetic energy and a length scale in this case. The modelled equation is as follows (25):

$$\rho\frac{Dk}{Dt} = \frac{\partial}{\partial y}\left[\left(\mu + \frac{\mu_t}{Pr_k}\right)\frac{\partial k}{\partial y}\right] + \mu_t\left(\frac{\partial U}{\partial y}\right)^2 - \frac{C_D\rho k^{3/2}}{l} \tag{3.39}$$

the physical interpreation of various terms on the right hand side is quite clear, i.e., they are the diffusion, generation and dissipation terms respectively. However, the length scale l needs to be specified algebraically. $C_D \approx 0.164$ if l is taken as the ordinary mixing length (25).

In one equation models, the length scale has to be specified algebraically as in zero equation models, and hence is also flow dependent. Moreover, it is difficult to incorporate the length scale empirically for complicated flows such as recirculating flows, flows with separation, streamline curvature etc. Therefore, most one equation models do not show much improvement over zero equation models and hence they are not very popular.

3.3.3 Two Equation Models

In order to eliminate the need for specifying the length scale based on empirical information, the two equation models employ another transport partial differential equation to predict l.

A transport equation for l can be derived, in principle, from the Navier-Stokes equations but the unknows introduced in the transport equation cannot be easily modelled. As a matter of fact, the introduction of several drastic modelling approximations produce a rather empirical equation for l. However, successful experience has indicated that it is better to solve a transport partial differential equation for a length scale related parameter rather than for the length scale itself. Such a parameter is generally a combination of k and l, $Z = k^{\alpha} l^{\beta}$.

Quite a few two equation models have been developed using different com-

binations of k and l. The Imperial College group led by Professor Spalding has experimented with three different kinds of two equation models (74): k-kl; k-ω; k-ϵ. Here l is a length representing the macroscale of turbulence which may be defined in terms of k, ϵ and a constant as:

$$l = \frac{C_D k^{3/2}}{\epsilon} \tag{3.40}$$

ω can be interpreted physically as the time-averaged square of the vorticity fluctuations and is related to k, ϵ, and C_D through the following relation

$$\omega = \frac{\epsilon^2}{(C_D k)^2} \tag{3.41}$$

where ϵ represents the dissipation rate of turbulent kinetic energy which is defined as:

$$\epsilon = \nu \overline{\frac{\partial u_i \partial u_i}{\partial x_k \partial x_k}} \tag{3.42}$$

the following relations can be obtained from the above definitions:

$$\frac{d(kl)}{kl} = \frac{5}{2}\frac{dk}{k} - \frac{d\epsilon}{\epsilon} \tag{3.43}$$

$$\frac{d\omega}{\omega} = -2\frac{dk}{k} + 2\frac{d\epsilon}{\epsilon} \tag{3.44}$$

with the aid of these equations it is possible to transform one pair of equations into another (74). Therefore, the three models are closely related to one another although the form of diffusion and near wall terms are different. Among these two equation models, the k-ϵ model is the one most frequently used due to several reasons: Firstly, the ϵ-equation does not require any extra terms near walls; Secondly, the ϵ-equation requires no secondary source term which appears in some

other models. Moreover, ϵ itself appears in the k-equation, which is convenient as less modelling work is needed for the k-equation.

An exact transport equation for ϵ can be derived from the Navier-Stokes equations (84, 85) and can be modelled by analogy with that of the k-equation. The modelled transport equations for k and ϵ with viscous diffusion presumed negligible are given below (74):

$$\rho\frac{Dk}{Dt} = \frac{\partial}{\partial x_k}\left[\left(\frac{\mu_t}{Pr_k}\right)\frac{\partial k}{\partial x_k}\right] + \mu_t\left(\frac{\partial U_i}{\partial x_k} + \frac{\partial U_k}{\partial x_i}\right)\frac{\partial U_i}{\partial x_k} - \rho\epsilon \tag{3.45}$$

$$\rho\frac{D\epsilon}{Dt} = \frac{\partial}{\partial x_k}\left[\left(\frac{\mu_t}{Pr_\epsilon}\right)\frac{\partial \epsilon}{\partial x_k}\right] + C_1\mu_t\frac{\epsilon}{k}\left(\frac{\partial U_i}{\partial x_k} + \frac{\partial U_k}{\partial x_i}\right)\frac{\partial U_i}{\partial x_k} - C_2\rho\frac{\epsilon^2}{k} \tag{3.46}$$

and the turbulent (eddy) viscosity is related to k and ϵ as follows:

$$\mu_t = C_\mu\rho\frac{k^2}{\epsilon} \tag{3.47}$$

the constants in these equations take the following values (74)

$$C_\mu = 0.09 \qquad C_1 = 1.44 \qquad C_2 = 1.92 \qquad Pr_k = 1.0 \qquad Pr_\epsilon = 1.3$$

These constants are not changed, generally speaking, in any calculations. Nevertheless, they need to be adjusted in order to account for effects such as streamline curvature, low Reynolds number etc.

It is necessary to point out at this stage that the above transport equations for k and ϵ are not appropriate for the near wall region, i.e., in the viscous sublayer where the Reynolds number is very low and molecular transport becomes more important. Thus, most applications of the k-ϵ model (and other models) have made use of wall functions which will be presented in chapter five. Alternatively, additional terms can be put into the k and ϵ equations to extend their applicability to the viscous sublayer (86).

At present, the two equation k-ϵ model is the most popular one for engineering calculations. However, this model (and all other two equation models as well) have several limitations. Firstly, all two equation models are turbulent viscosity models which assume that the Boussinesq assumption holds. The two equation models fail if the Boussinesq assumption fails. Nevertheless, in many flow situations the assumption gives results accurate enough for engineering calcualtions. Another practical limitation is the assumption of isotropic eddy viscosity, i.e., the same values of μ_t are taken for different $\overline{u_i u_j}$ terms as can be seen from Eq.(3.32) while experimental evidence indicates that μ_t takes different values for different $\overline{u_i u_j}$ terms in certain cases such as strongly swirling flows. Moreover, the effects of curvature, rotation and buoyancy forces have to be modelled separately. In order to eliminate these limitations the so called stress equation models have been developed.

3.3.4 Stress Equation Models

In the stress equation models, the turbulent viscosity hypothesis is not employed and a partial differential transport equation is developed for each component of the Reynolds stresses. In addition, the transport equation for turbulent kinetic energy dissiaption rate ϵ is also needed. The stress equation models include Reynolds stress models which solve the transport equations for the Reynolds stresses directly through modelling assumptions, and algebraic stress models in which an algebraic relation is derived from the Reynolds stress transport equations through some modelling assumptions. The stress equation models are also

referred to as second order closure models in some literature.

Reynolds Stress Models

The Reynolds stress transport equations can be derived from the Navier-Stokes equations by multiplying the momentum equations using the fluctuating components and then time averaging them. For incompressible flows, the Reynolds stress transport equations may be written in the following form:

$$\frac{D\overline{u_i u_j}}{Dt} = -\left[\overline{u_j u_k}\frac{\partial U_i}{\partial x_k} + \overline{u_i u_k}\frac{\partial U_j}{\partial x_k}\right] - 2\nu\overline{\frac{\partial u_i \partial u_j}{\partial x_k \partial x_k}} + \overline{\frac{p}{\rho}\left(\frac{\partial u_i}{\partial x_j} + \frac{\partial u_j}{\partial x_i}\right)} - \frac{\partial}{\partial x_k}\left[\overline{u_i u_j u_k} - \nu\frac{\partial \overline{u_i u_j}}{\partial x_k} + \overline{\frac{p}{\rho}(\delta_{jk}u_i + \delta_{ik}u_j)}\right] \quad (3.48)$$

the first term on the right hand side serves to exchange kinetic energy between the mean flow and the turbulence. Normally, the energy exchange involves a loss to the mean flow and profit to the turbulence. Therefore, this term represents the generation of turbulent kinetic energy. The second term represents the rate at which viscous stresses perform deformation work against the fluctuating strain rate. This is always a drain of turbulent kinetic energy, hence it is called the viscous dissipation rate or turbulent kinetic energy dissipation rate. The third and fourth terms are called pressure strain and diffusion terms respectively according to Launder et al (87).

The transport equations for the six independent Reynolds stresses have been derived. However, a number of unknowns have also been created in the process. In principle, transport equations could be derived for each of the new terms introduced in Eq.(3.48) but the number of new unknowns would increase much

faster than the number of new transport equations. Therefore, this is not a practical way to derive more transport equations. Reynolds stress models stop at the Reynolds stress transport equations and model the unknowns as empirical functions of the mean velocities, Reynolds stresses and their derivaties. They are also called second order (momentum) closure or Reynolds stress closure such as those developed by Hanjalic and Launder (88), Daly and Harlow (85) and Launder et al (87).

The unknowns which need to be modelled in Eq.(3.48) are as follows:

1). The triple correlations among various components of velocity fluctuations.

2). The dissipation rate term.

3). The correlation of velocity fluctuations with the pressure field.

The triple correlation term in Eq.(3.48) represents the rate at which the Reynolds stress is carried by the turbulence fluctuations. This term may be called the turbulent diffusional flux of the Reynolds stresses which can be a large or even a dominant term in many situations. Daly and Harlow (85) modelled this term employing the simple gradient-diffusion hypothesis by analogy with the approximation for the flux of a scalar. Launder et al (87) modelled this term through severe simplications of the exact transport equation for $\overline{u_i u_j u_k}$ as:

$$-\overline{u_i u_j u_k} = C_s \frac{k}{\epsilon}\left[\overline{u_i u_l}\frac{\partial \overline{u_j u_k}}{\partial x_l} + \overline{u_j u_l}\frac{\partial \overline{u_k u_i}}{\partial x_l} + \overline{u_k u_l}\frac{\partial \overline{u_i u_j}}{\partial x_l}\right] \qquad (3.49)$$

where C_s is a constant assigned the value 0.11 on the basis of computer optimization.

The dissipation rate term is modelled by almost all research workers assuming

that the dissipation motions are isotropic

$$2\nu\overline{\left(\frac{\partial u_i}{\partial x_k}\right)\left(\frac{\partial u_j}{\partial x_k}\right)} = \frac{2}{3}\delta_{ij}\epsilon \tag{3.50}$$

Although experimental evidence has shown that turbulence does not remain locally isotropic in the presence of strong strain fields Eq.(3.50) seemed to be the best of the simple hypotheses.

The pressure-induced diffusion in the diffusion term in Eq.(3.48) was represented as a simple diffusion term by Daly and Harlow (85). However, Launder et al (87) stated that it was usually neglected following the practice of most other workers although there seemed to be no direct evidence to sustain or demolish the assumption.

The only remaining term to be modelled is the pressure-strain correlation which is of particualr importance for anistropic turbulence and seems to be the most difficult to model. The appropriate starting point is to derive a Poisson equation for mean and fluctuating pressure from the momentum equations, which represents pressure as a function of the velocity field. This transforms the problem to one in which only multiple velocity correlations are involved. For isothermal incompressible flow, the Poisson equation for pressure is

$$-\frac{\nabla^2(P+p)}{\rho} = 2\frac{\partial U_i}{\partial x_j}\frac{\partial u_j}{\partial x_i} + \frac{\partial^2 u_i u_j}{\partial x_j \partial x_i} + \frac{\partial U_i}{\partial x_j}\frac{\partial U_j}{\partial x_i} \tag{3.51}$$

integrating the above equation by Green's formula yields the following expression for pressure:

$$P(x_0,y_0,z_0) + p(x_0,y_0,z_0) = -\frac{1}{4\pi}\int\int\int_v \nabla^2(P+p)\frac{dVol}{r} + S \tag{3.52}$$

where S is a surface integral which is negligible away from the solid boundary and hence is neglected hereafter. Multiplying both sides of Eq.(3.52) by $\left(\frac{\partial u_i}{\partial x_j} + \frac{\partial u_j}{\partial x_i}\right)$ and taking the time average, the pressure-strain correlation may be re-expressed in the following form:

$$\frac{p}{\rho}\left(\frac{\partial u_i}{\partial x_j} + \frac{\partial u_j}{\partial x_i}\right) = \Phi_{ij,1} + \Phi_{ij,2} \tag{3.53}$$

$$\Phi_{ij,1} = \frac{1}{4\pi}\int\left\{\left(\frac{\partial^2 u_l u_m}{\partial x_l \partial x_m}\right)'\left(\frac{\partial u_i}{\partial x_j} + \frac{\partial u_j}{\partial x_i}\right)\right\}\frac{dVol}{r} \tag{3.54}$$

$$\Phi_{ij,2} = \frac{2}{4\pi}\int\left\{\left(\frac{\partial U_l}{\partial x_m}\right)'\overline{\left(\frac{\partial u_m}{\partial x_l}\right)'\left(\frac{\partial u_i}{\partial x_j} + \frac{\partial u_j}{\partial x_i}\right)}\right\}\frac{dVol}{r} \tag{3.55}$$

where the prime superscript indicates that the quantity involved is evaluated at a distance r from the one in question. $\Phi_{ij,1}$ involves only fluctuating quantities and $\Phi_{ij,2}$ involves products of turbulence quantities and the mean rates of strain. These two parts are modelled separately by almost all the research workers. $\Phi_{ij,1}$ is referred to as the "return-to-isotropy" term as it serves to interchange turbulence energy among the various components, i.e., equaling the normal Reynolds stresses and diminishing shear stresses. This term has significant influence for problems involving anisotropic homogeneous flow where the mean velocity is small or zero. A closure approximation for $\Phi_{ij,1}$ as first proposed by Rotta (89) and adopted by most workers may take the following form:

$$\Phi_{ij,1} = -C_1\frac{\epsilon}{k}(\overline{u_i u_j} - \frac{2}{3}\delta_{ij}k) \tag{3.56}$$

This form is consistent with the assumption that the rate of return to isotropy is directly proportional to the anisotropy (the term in brackets in the above equation). Details about modelling the second part, $\Phi_{ij,2}$, can be found in (78, 87,

88). Most workers adopt Rotta's proposals for this term and the final expression takes the form (87):

$$\Phi_{ij,2} = -\frac{(C_2+8)}{11}[P_{ij} - \frac{2}{3}P\delta_{ij}] - \frac{(30C_2-2)}{55}k\left[\frac{\partial u_i}{\partial x_j} + \frac{\partial u_j}{\partial x_i}\right] - \frac{(8C_2-2)}{11}[G_{ij} - \frac{2}{3}P\delta_{ij}] \qquad (3.57)$$

where $P_{ij} = -\left[\overline{u_i u_k}\frac{\partial U_j}{\partial x_k} + \overline{u_j u_k}\frac{\partial U_i}{\partial x_k}\right]$, $G_{ij} = -\left[\overline{u_i u_k}\frac{\partial U_k}{\partial x_j} + \overline{u_j u_k}\frac{\partial U_k}{\partial x_i}\right]$. P represents the rate of turbulent kinetic energy production. Launder et al argued that the first group on the right hand side in Eq.(3.57) was the dominant one, and as a result the equation was expressed in a simplified form as:

$$\Phi_{ij,2} = -\gamma(P_{ij} - \frac{2}{3}P\delta_{ij}) \qquad (3.58)$$

where γ is a constant whose value is around 0.6, P_{ij} and P are the same production terms given before. The above equation is employed in the present study.

Near wall effects have not been taken into account in the modelling process so far. A wall reduces the fluctuating velocity components normal to the wall and enhances those parallel to it. The pressure-strain term, as stated before, serves to redistribute turbulence energy among the Reynolds stresses. Thus, it would not be appropriate to neglect the surface integral in Eq.(3.52) in the region near a wall. It has been suggested by various workers that near wall corrections should be incorporated into the expression for $\Phi_{ij,1}$ and $\Phi_{ij,2}$. The final form of near wall correction to the pressure-strain given by Launder et al (87) is as follows:

$$\Phi_{ij,w} = \left[0.125\frac{\epsilon}{k}(\overline{u_i u_j} - \frac{2}{3}\delta_{ij}k) + 0.015(P_{ij} - G_{ij})\right]\frac{k^{3/2}}{\epsilon x_1} \qquad (3.59)$$

where x_1 is the normal distance to the surface of a wall. Upon rearranging all the modelled terms the final expression for the modelled Reynolds stress transport

equations may be written in Cartesian tensor form as:

$$\frac{D\overline{u_iu_j}}{Dt} = -\left[\overline{u_ju_k}\frac{\partial U_i}{\partial x_k} + \overline{u_iu_k}\frac{\partial U_j}{\partial x_k}\right] - \frac{2}{3}\delta_{ij}\epsilon - C_1\frac{\epsilon}{k}(\overline{u_iu_j} - \frac{2}{3}\delta_{ij}k)$$
$$+\Phi_{ij,2} + \Phi_{ij,w} + C_s\frac{\partial}{\partial x_k}\frac{k}{\epsilon}\left[\overline{u_iu_l}\frac{\partial\overline{u_ju_k}}{\partial x_l} + \overline{u_ju_l}\frac{\partial\overline{u_ku_i}}{\partial x_l} + \overline{u_ku_l}\frac{\partial\overline{u_iu_j}}{\partial x_l}\right] \quad (3.60)$$

where $\Phi_{ij,2}$is given by Eq.(3.57) or Eq.(3.58), $\Phi_{ij,w}$ is the near wall correction given by Eq.(3.59). The above equation can be also written in a compact form as:

$$\frac{D\overline{u_iu_j}}{Dt} = P_{ij} - \frac{2}{3}\delta_{ij}\epsilon + \Phi_{ij} + D_{ij} \quad (3.61)$$

where

$$P_{ij} \equiv Production\ \ tensor \quad (3.62)$$

$$\Phi_{ij} \equiv Pressure - strain\ \ tensor \quad (3.63)$$

$$D_{ij} \equiv Diffusion\ \ tensor \quad (3.64)$$

In order to solve the above equation one needs to know the turbulent kinetic energy dissipation rate. The exact transport equation for ϵ at high Reynolds number is (84, 87)

$$\frac{D\epsilon}{Dt} = -\frac{\partial}{\partial x_k}\left[\overline{\nu u_k\left(\frac{\partial u_i}{\partial x_l}\right)^2} + \frac{\nu}{\rho}\overline{\frac{\partial p}{\partial x_i}\frac{\partial u_k}{\partial x_i}}\right] - 2\nu\overline{\frac{\partial u_i}{\partial x_k}\frac{\partial u_i}{\partial x_l}\frac{\partial u_k}{\partial x_l}} - 2\left[\overline{\nu\frac{\partial^2 u_i}{\partial x_k\partial x_l}}\right]^2 \quad (3.65)$$

This transport equation contains several unknowns which need to be modelled to make the equation solvable. The modelled equation given by Hanjalic and Launder (88) takes the following form:

$$\frac{D\epsilon}{Dt} = C_\epsilon\frac{\partial}{\partial x_k}\left(\frac{k}{\epsilon}\overline{u_ku_l}\frac{\partial\epsilon}{\partial x_l}\right) - C_{\epsilon 1}\frac{\epsilon\overline{u_iu_k}}{k}\frac{\partial U_i}{\partial x_k} - C_{\epsilon 2}\frac{\epsilon^2}{k} \quad (3.66)$$

the first term on the right hand side approximates the corresponding term in Eq.(3.64) responsible for the diffusion of ϵ. The second and third terms represent the generation of ϵ and its destruction by viscous action.

The values of constants given by Launder et al (87) are as follows:

$C_1 = 1.5 \quad C_2 = 0.4 \quad C_s = 0.11 \quad \gamma = 0.6 \quad C_\epsilon = 0.15 \quad C_{\epsilon 1} = 1.44 \quad C_{\epsilon 2} = 1.90$

Algebraic Stress Models

In Reynolds stress models there are six Reynolds stress transport equations in addition to the transport equation for ϵ. Solving such a set of equations needs enormous computer time. Rodi (90, 91) proposed an algebraic relation from Eq.(3.60) for calculating the Reynolds stresses in order to reduce computational effort. It can be seen from Eq.(3.60) that there are only two terms involving the gradient of the Reynolds stresses, i.e., the term on the left hand side and the diffiusion term D_{ij} on the right. The Reynolds stress transport equations would become algebraic equations if these two terms could be approximated involving only algebraic relations for the Reynolds stresses by modelling assumptions. Rodi (90, 91) assumed that convective and diffusive transport of $\overline{u_i u_j}$ are proportional to those of k and the proportionality factor is $\overline{u_i u_j}/k$. Mathematically, these assumptions may take the following forms:

$$\frac{D\overline{u_i u_j}}{Dt} = \frac{\overline{u_i u_j}}{k}\frac{Dk}{Dt} \tag{3.67}$$

$$D_{ij} = \frac{\overline{u_i u_j}}{k} D(k) \tag{3.68}$$

where D(k) represents the diffusion of k. It is argued by Rodi that the above assumptions are appropriate if the rate of variation of $\overline{u_i u_j}/k$ along a streamline

is much less than that of $\overline{u_i u_j}$, and if the spatial gradient of $\overline{u_i u_j}$ is large compared with that of $\overline{u_i u_j}/k$. Also, the transport equation for k can be written as:

$$\frac{Dk}{Dt} = P - \epsilon + D(k) \tag{3.69}$$

substituting Eq.(3.69) into Eq.(3.67), one has:

$$\frac{D\overline{u_i u_j}}{Dt} = \frac{\overline{u_i u_j}}{k}[P - \epsilon + D(k)] \tag{3.70}$$

combining Eq.(3.68) and Eq.(3.70) with Eq.(3.61) yields an algebraic equation for $\overline{u_i u_j}$ in tensor form as:

$$\frac{\overline{u_i u_j}}{k}(P - \epsilon) = P_{ij} - \frac{2}{3}\delta_{ij}\epsilon + \Phi_{ij} \tag{3.71}$$

as k and ϵ appear in the above equation so k and ϵ equations need to be solved as well.

Invariance and Realizability

The ideal turbulence models should have general applicability and be flow independent. The development of Reynolds stress models is a step towards this ideal as more physical processes such as those due to curvature, rotation, buoyancy, and so on, can be accounted for automatically. For general applicability it has been shown (78, 79, 92, 93) that these models have to satisfy many constraints. Tensor invariance requires the replaced terms to have the same tensor form as the original terms so that they can be transformed properly in different coordinate systems. This type of modelling is called invariant modelling (92). The concept of realizability was first introduced by Schumann (93). He stated that no matter

what equation is used to predict $\overline{u_i u_j}$ it must have the property which does not allow negative component energies and requires all off-diagonal components of the Reynolds stress to satisfy Schwartz's inequality. These and the additional conditions put forth by Schumann can be written in a numerically most convenient form as (93):

$$R_{11} \geq 0 \tag{3.72}$$

$$R_{11}R_{22} - R_{12}^2 \geq 0 \tag{3.73}$$

$$R_{11}(R_{22}R_{33} - R_{23}^2) - R_{12}(R_{12}R_{33} - R_{23}R_{13}) + R_{13}(R_{12}R_{23} - R_{22}R_{13}) \geq 0 \tag{3.74}$$

Similar conditions apply for scalar fluxes. Schumann shows that the exact Reynolds stress transport equations satisfy the realizability condition. However, it is also indicated by him that some of the existing models do not satisfy such a condition. Nevertheless, attempts to satisfy the realizability condition lead invariably to complicated model expressions. Therefore, at present no special efforts are taken to ensure that models satisfy the realizability condition.

There is no doubt that stress equation models are relatively more general than other models discussed previously. They are not restricted by the Boussinesq assumption relating turbulent stresses to the rate of mean strain. However, approximations and assumptions are still used in modelling various terms which presently cannot be measured. Moreover, Reynolds stress models have not been well tested for many types of complex flows and it may take some time before they have been fully tested and refined to the point that they become commonplace in engineering calculations.

3.3.5 Multiple-Scale Models

It is recongized that fully developed turbulence (when Reynolds number is well above the critical value) consists of fluctuating motion with a wide spectrum of eddy size and time scales. For instance, in turbulent pipe flow the largest turbulence eddies are of a size comparable with the diameter of the pipe while the smaller eddies are so small that viscous action becomes dominant. The large-scale eddies contain much of the kinetic energy of turbulence and dissipate little energy by viscous effects. These large-scale eddies interact with each other, generating smaller eddies in which viscous dissipation becomes important. Since different turbulent interactions are associated with different parts of the spectrum it would be desirable to have turbulence models accounting for this detailed structure of turbulence. Unfortunately, all the turbulence models discussed above are based on a single-scale scheme. Hanjalic et al (94) proposed a multiple-scale model based on a rational extension of widely used single-scale equations and ideas. An outline of their model is briefly described below.

A typical energy spectrum of turbulence is known to consist of, generally speaking, three regions. These are the production region (low wave number region); the dissipation region (high wave number region) and between these two regions, with an intermediate range of wave number, is the so called transfer region (also called the inertial region). Since there is negligible kinetic energy of turbulence in the dissipation region the total turbulent kinetic energy k is assumed to comprise k_p in the production region and k_t in the transfer region. Turbulent kinetic energy leaves the first region (the production region) at a rate

ϵ_p, enters the dissipation region at a rate ϵ and across the transfer region at an assumed representive spectral energy transfer rate ϵ_t. This simplified energy spectrum is the basis of the model of Hanjalic et al. They argue that the spectral division appears to be too coarse but the single-scale models take no cognizance of changes in the shape of the energy spectrum, and there is implicit the assumption that $\epsilon_p = \epsilon_t = \epsilon$. The transport equations for k_p, k_t, ϵ_p, ϵ_t are formulated. In a homogeneous flow the transport equations for k_p and k_t are (94):

$$\frac{Dk_p}{Dt} = -\overline{u_i u_j}\frac{\partial U_i}{\partial x_j} - \epsilon_p \tag{3.75}$$

$$\frac{Dk_t}{Dt} = \epsilon_p - \epsilon \tag{3.76}$$

and the transport equations for ϵ_p, ϵ_t given by Hanjalic et al (94) take the following forms:

$$\frac{D\epsilon_p}{Dt} = -\overline{u_i u_j}C_{p1}\frac{\epsilon_p}{k_p}\frac{\partial U_i}{\partial x_j} - C_{p2}\frac{\epsilon_p^2}{k_p} + D_{\epsilon p} \tag{3.77}$$

$$\frac{D\epsilon_t}{Dt} = C_{t1}\frac{\epsilon_p \epsilon_t}{k_t} - C_{t2}\frac{\epsilon_t^2}{k_p} + D_{\epsilon t} \tag{3.78}$$

where D_ϕ (ϕ stands for k_p, k_t, ϵ_p, ϵ_t) is the diffusion term and can be uniformly represented as:

$$D_\phi = 0.22\frac{\partial}{\partial x_k}\left(\overline{u_k u_l}\frac{k_p}{\epsilon_p}\frac{\partial \phi}{\partial x_l}\right) \tag{3.79}$$

This model was used to predict axisymmetrical jets and boundary layers (94). Good agreement was obtained between the prediction of the jet spread rate and experimental data. For the boundary layers the prediction with this model is in closer agreement with experimental data than the single-scale model of Launder et al (87). This shows the potential advantages of including some account of the

spectral character of turbulence in traditional second-moment closures. However, this model has not been tested further.

3.3.6 Other Approachs to Turbulence Modelling

Apart from the models discussed above there are some other approachs to turbulence modelling such as two-point closure and large-eddy-simulation. The stress equation models (second-order modelling), including multi-scale models, are only one-point closure. This involves merely averaging the Navier-Stokes equations and approximating the unknowns introduced in the averaging procedure through modelling auusmptions. Usually, the approaches to solve turbulent flows can be classified into three categories, i.e., one-point closure (which is the most widely used technique so far), two-point closure and large-eddy-simulation.

Two-point closure considers differential equations for two point correlations or the spectrum tensor. This technique is intermediate in complexity between large-eddy-simulation (with sub-grid-scale modelling) and one-point closure (second-order modelling). The potential advantage of the two-point closure lies in its relative simplicity when compared with large-eddy-simulation and its flexibility and universality when compared with the common one-point closure. In particular, it can be used to identify proper coefficients to be used in the one-point closure.

Large-eddy-simulation has been developed recently. Deardorff (83) first suggested this approach and used it to predict channel flows and atmospheric boundary layers. This approach consists of averaging the Navier-Stokes equations over

a time T shorter than the time scale of the large turbulent structures of the motion. Only the time-dependent fluctuations with a time scale smaller than T are smoothed out which are then approximated by the so called sub-grid-scale modelling. Such calculations have shown much promise. However, this technique is too costly at present to be considered as a practical way for engineering calculations.

Chapter 4

SOLUTION PROCEDURE

The governing equations presented in the previous chapter are non-linear, coupled, and second-order partial differential equations. The analytical solution is formidable due to not only non-linearity but also the complex flow structure of turbulence. Hence, a method of numerical solution has to be employed to solve the governing nonlinear partial differential equations.

As numerical schemes and the methods to discretize the governing partial differential equations are fairly standard and well documented (2, 6, 7, 16, 25, 64), only a brief introduction will be given in this chapter. However, the proper differencing of the pressure gradient and the evaluation of density at the control volume boundaries are of great importance in supersonic flow. In addition, the treatment of velocity-pressure coupling becomes very crucial to the whole solution procedure when pressure is chosen as a main dependent variable. Therefore, the discussion will be focussed on these two important issues.

4.1 The Finite Difference Equations

The method employed to derive the finite difference equations is the control volume approach due to its clear physical meaning. It entails dividing the computational domain into a great number of finite volumes (control volumes) called 'cells'. The finite difference counterparts of the governing partial differential equations are derived for each cell by a combination of formal integration and some approximations so as to preserve physical realism and computational stability.

A staggered grid system is employed here to avoid an unrealistic solution. All the variables except the axial and radial velocity components are stored at the nodes. The U and V velocity components are stored mid-way between the grid nodes. This arrangement has the following advantages:

1). The velocities are between the pressures which drive them. This may avoid an unrealistic pressure field.

2). The velocities are directly available for the evaluation of the convective fluxes across the control volume boundaries of the nodes. This is also convenient for the solution procedure adopted for the continuity equation.

The numerical scheme employed to approximate the convective terms is the so called 'hybrid scheme' which is a combination of the central- and upwind-differencing schemes. Whether the central- or upwind- differencing scheme is used or not depends on the local convection/diffusion ratio as measured by the local Peclet number, defined as follows:

$$Pe = \frac{U_P \delta x}{\nu} \tag{4.1}$$

where ν is the kinematic viscosity and δx is the mesh increment. When the local Pe is equal to 2 or less the central differencing scheme is used. When the local Pe is over 2 the upwind differencing scheme is used instead of the central differencing scheme in order to avoid numerical instability. The hybrid scheme has been proved to be stable and superior to both the central- and upwind-differencing schemes. Moreover, the QUICK (Quadratic Upstream Interpolation for Convective Kinematics) differencing scheme, which is more accurate, has also been incorporated into the computer code.

4.2 Solution of the Difference Equations

The algebraic finite difference equations obtained from the governing partial differential equations are also non-linear and coupled and cannot be solved directly. Hence, an iterative solution method has to be used to solve these equations. The non-linearities are usually handled by expressing the quantities at the current iteration level in terms of the values available at the previous iteration level. In the present work, the non-linear algebraic finite difference equations are linearized through the calculation of coefficients based on the currently available flow field values. This practise results in the coefficients lagging behind by one iteration. However, when the solution converges all the equations are satisfied and this effect is eliminated automatically.

A form of the Gauss-Seidel line by line iteration method is then employed to solve the linearized algebraic finite difference equations in such a way that each

variable is solved separately instead of a simultaneous solution of all the variables. The variables along each grid line are calculated by the use of the Tri-Diagonal Matrix Algorithm (TDMA) which is given in more detail in (7).

4.3 Boundary Conditions

It is believed that most of the flow patterns of common gases and liquids can be described by the same governing partial differential equations, the Navier-Stokes equations. The flows (solutions) are distingushed only by boundary and initial conditions, and by the flow parameters such as Re, Pr etc. It is therefore understandable that the specification of the computational boundary conditions plays a very crucial role in the solution procedure. The proper specification of the boundary conditions, apart from affecting numerical stability, greatly affects the accuracy of the solution of the finite difference equations. This is of great importance to compressible flow as the mathematical theory for the computational boundary conditions is not so well established for the compressible Navier-Stokes equations as it is for the incompressible form of the governing equations.

For confined flow, the boundaries can be classified, generally speaking, into four categories:

1). Inlet (Inflow) boundary,

2). Wall boundary,

3). Symmetry boundary,

4). Outlet (outflow) boundary.

Wall and symmetry boundaries can be also grouped as no-flow boundaries, i.e., the fluid cannot cross this kind of boundary.

The slip and no-slip wall boundary conditions are usually used for inviscid and viscous flows resprectively. More detailes can be found in (2).

Across a symmetry surface the reflection method is usually adopted, e.g., if a line of node points j=s are on the line of symmetry, one has

$$V_{s-1} = -V_{s+1} \tag{4.2}$$

$$V_s = 0 \tag{4.3}$$

$$F_{s-1} = F_{s+1} \tag{4.4}$$

where F=ρ, U, W or T etc.

The treatment of the inlet and outlet boundary conditions, especially for compressible flow, is very important but the established treatment of outlet boundary conditions for supersonic flow is misleading. This will be discussed in more detail in chapter six.

4.4 Treatment of Velocity-Pressure Coupling

It was pointed out previously that when pressure is chosen as a main dependent variable the difficulty is how to evalute pressure as there is not a governing equation for pressure in the original set of equations. However, there are several ways of calculating pressure indirectly, such as the Poisson equation method, which have been discussed in chapter two. Among these methods, pressure correction

methods have gained more favor than the others and found wide application. In this section, the pressure correction method for incompressible flow used in the present study will be briefly outlined and its extension to compressible flow presented.

4.4.1 The SIMPLE Algorithm

The obstacle arising from the choice of pressure as a main dependent variable can be removed by devising a mechanism by which the continuity and momentum equations are linked together to evaluate pressure. The basic idea of pressure correction methods is to first guess a pressure field, then get an approximate solution to the velocity field. The velocity field obtained using the guessed pressure field does generally not satisfy the continuity equation, and corrections to the pressure field are made in such a way so as to bring the velocity field into conformity with the continuity equation. The key point of this is approach to derive a so called pressure-correction equation from the finite difference form of the continuity and momentum equations. In the present study, the pressure correction method employed is the SIMPLE (Semi-Implicit Method for Pressure-Linked Equations) algorithm proposed by Pantakar and Spalding (6, 7) which is outlined for the two dimensional case as follows:

1). Guess the initial values of the flow field variables, which are usually specified as zero.

2). The following momentum equations are solved using the guessed pressure

field P^* to get the intermediate velocity field U^*, V^*:

$$a_P U_P^* = \Sigma a_{nb} U_{nb}^* - A_P^U (P_P^* - P_W^*) + S^U \tag{4.5}$$

$$a_P V_P^* = \Sigma a_{nb} V_{nb}^* - A_P^V (P_P^* - P_S^*) + S^V \tag{4.6}$$

where 'nb' denotes the neighboring points, S is the source term, A is the area of cell boundary normal to the velocity in question.

3). The velocity field obtained will not satisfy the continuity equation unless the pressure field has been guessed correctly. Suppose the correct pressure field is the present pressure field plus a correction pressure field expressed in the following form:

$$P_P = P_P^* + P_P' \tag{4.7}$$

correspondingly, the velocity field will also change due to the pressure field change, which may be expressed in the following form:

$$U_P = U_P^* + U_P' \tag{4.8}$$

$$V_P = V_P^* + V_P' \tag{4.9}$$

substituting the above relations into equations (4.5) and (4.6), one has:

$$a_P U_P = \Sigma a_{nb} U_{nb} - A_P^U (P_P - P_W) + S^U \tag{4.10}$$

$$a_P V_P = \Sigma a_{nb} V_{nb} - A_P^V (P_P - P_S) + S^V \tag{4.11}$$

from equations (4.5), (4.6) and (4.10), (4.11) the following relations can be obtained:

$$a_P U_P' = \Sigma a_{nb} U_{nb}' - A_P^U (P_P' - P_W') \tag{4.12}$$

$$a_P V'_P = \Sigma a_{nb} V'_{nb} - A^V_P (P'_P - P'_S) \tag{4.13}$$

neglecting $\Sigma a_{nb} U'_{nb}$ and $\Sigma a_{nb} V'_{nb}$, the relationship between the pressure change and the corresponding velocity change can be expressed as follows:

$$U'_P = D^U_P (P'_W - P'_P) \tag{4.14}$$

$$V'_P = D^V_P (P'_S - P'_P) \tag{4.15}$$

D^U_P, D^V_P can be evaluated from the relevant momentum equations:

$$D^U_P = A^U_P / a^U_P \tag{4.16}$$

$$D^V_P = A^V_P / a^V_P \tag{4.17}$$

4). P' is calculated from the pressure-correction equation which is derived as follows:

subsituting the following relations

$$U_P = U^*_P + D^U_P (P'_W - P'_P) \tag{4.18}$$

$$V_P = V^*_P + D^V_P (P'_S - P'_P) \tag{4.19}$$

into the finite difference form of the continuity equation and after some manipulation, the resultant pressure-correction equation is:

$$a_P P'_P = a_W P'_W + a_E P'_E + a_N P'_N + a_S P'_S + S_o \tag{4.20}$$

$$a_W = \rho_w A^U_W D^U_W \tag{4.21}$$

$$a_E = \rho_e A^U_E D^U_E \tag{4.22}$$

$$a_S = \rho_s A^V_S D^V_S \tag{4.23}$$

$$a_N = \rho_n A_N^V D_N^V \tag{4.24}$$

$$a_P = a_W + a_E + a_S + a_N \tag{4.25}$$

where S_o is the residue (source term) in mass flow rate due to the imbalance in mass-continuity at each node in the flow field and is equal to:

$$S_o = A_W^U(\rho U^*)_w - A_E^U(\rho U^*)_e + A_S^V(\rho V^*)_s - A_N^V(\rho V^*)_n \tag{4.26}$$

The pressure and velocity fields are then updated using P' obtained from the above pressure-correction equation. However, in the calculation the relaxation method has to be used to ensure convergence.

5). Some other transport equations are solved if necessary.

6). A new iteration is started until a fully convergent solution is reached (momentum and continuity are both satisfied).

4.4.2 Modifications for Subsonic Flow

The only difference between the incompressible and compressible subsonic flows is that density changes which creates the effect of 'compressibility'. When Mach number is low (less than 0.3) density varies little and compressibility is negligible, and hence low Mach number subsonic flow can be treated in the same way as incompressible flow. However, if the Mach number is higher, density variation has to be accounted for. Nevertheless, it is understandable that minor modifications to the original SIMPLE algorithm will be enough for subsonic flow.

Intuitively, density has to be calculated for compressible flow instead of keeping it constant as in the case of incompressible flow. However, the pressure field

obtained using the SIMPLE algorithm is based on an arbitrary pressure at the specified reference point, and usually it is set equal to zero. Therefore, the pressure field cannot be used to calculate density directly unless the correct pressure is given at the specified reference point. As a result, one important step is to specify a correct pressure for compressible subsonic (the same for supersonic) flow. This pressure is given either experimentally or analytically. Moreover, if temperature needs to be calculated then the transport equation of stagnation enthalpy should be solved. The calculation of density is switched on using the gas state law after a reasonable pressure field is established, i.e., after a certain number of iterations so as to avoid an unrealistic pressure field since negative pressure may be present at the very begining of calculation. The modified solution procedure is then as follows:

1).—— 4). The same as before,

5). The transport equation of stagnation enthalpy is solved to get the temperature field.

6). The calculation of density is switched on after a certain number of iterations.

7). Some other transport equations are solved if necessary.

8). A new iteration is started until a fully convergent solution is reached.

It has been found that the modified solution procedure performs quite well for subsonic flow in several cases. It can be claimed with confidence that the modified solution procedure can handle subsonic flow in general if the computational boundary conditions are specified properly. This aspect will be discussed

in more detail in chapter six.

4.4.3 Modifications for Supersonic Flow

For supersonic flow, it was suggested (62) that more modifications should be introduced to account for the hyperbolic nature which applies only to supersonic flow, i.e., when Mach number is over one. The original solution procedure cannot handle the hyperbolic nature of such flow as it treats the whole computational domain elliptically. Although numerous unsteady numerical methods have been developed for calculating supersonic flow they are only applicable to high Mach number flow and may not be efficient when only the steady solution is of concern. To the best of the author's knowledge, the iterative numerical solution procedures available for all Mach number flows and solving the steady compressible Navier-Stokes equations are the extension of the SIMPLE algorithm by Issa and Lockwood (62) and SIMPLER by Karki (64).

According to Issa and Lockwood (62), the SIMPLE algorithm has three sources of 'ellipticity' which are as follows:

1). The variables at each node are linked to the variables at neighboring nodes. This means that downstream influences could have effects upstream.

2). The 'staggered grid' arrangement ensures that each velocity is driven by the pressure difference across the two grid nodes lying on both sides of the velocity cell. This implies that downstream pressure influences upstream velocity.

3). The calculation of the mass fluxes at control volume boundaries is based on the linearly interpolated values of densities between nodes, which also means

that the downstream pertubations can be transmitted upstream.

Issa and Lockwood argued that modifications should be introduced to eliminate these downstream influences so as to make the solution procedure able to handle the hyperbolic nature of supersonic flow.

The first elliptical numerical influence is automatically eliminated due to the use of a hybrid differencing scheme which employs an upwind differencing scheme for the convective terms and ingores diffusional effects when the convection/diffusion ratio is large. This is definitely satisfied for supersonic flow. Therefore there is no need to introduce any modification for the first elliptical source.

With respect to the second elliptical influence, this was done (62) in such a simple way that the pressure difference across the adjacent two upstream nodes was taken instead of the two nodes lying on both sides of the velocity. For example, the unmodified pressure gradient $(P(I,J) - P(I-1,J))/\delta x$ for the velocity U(I,J) will be $(P(I-1,J) - P(I-2,J))/\delta x$ after modification. This treatment of the pressure gradient is doubtful and will be discussed later.

The third elliptical effect was removed by using only upstream densities when the supersonic fluxes were calculated, i.e., density was upwinded when supersonic mass fluxes were calculated.

Karki (64) also argued that the evaluation of density at the control volume boundaries and the differencing of the pressure gradient were two very critical issues, which determined the validity of a solution procedure in the transonic and supersonic flow regions. These two very important issues are actually the

second and third elliptical sources as defined by Issa and Lockwood (64). Their argurements, not surprisingly, are exactly the same bearing in mind that the first elliptical source can be eliminated automatically by the use of the hybrid differencing scheme. The difference is how they modified the solution procedure to account for these effects.

For the third elliptical source, i.e., how to evaluate density at the control volume boundaries, upstream densities were used for the supersonic mass flux calculations in Issa and Lockwood's modified solution procedure as mentioned above. It was shown by Karki (64) that using an upwind biased density was equivalent to the effect of adding the artificial viscosity. Bearing this in mind, it is understandable why upstream densities are used for the supersonic mass flux calculations. However, Karki (64) also argued that the use of two different methods to evaluate density for subsonic and supersonic flow respectively might cause some numerical problems near the switch-over point, and the switch-over point itself might be problem dependent. Therefore, density was always upwinded no matter what the Mach number was in Karki's modified solution procedure. This treatment seems to provide enough numerical diffusion but also adds damping even in subsonic flow regions where it is not required. In the present study, density is therefore upwinded only when local Mach number is over one, and it has been found that this treatment does not cause any problem near the switch-over point.

The second elliptical source, i.e., the treatment of the pressure gradient, seems to be quite confusing. The hyperbolic nature of supersonic flow tells us that small

disturbanes at a point downstream cannot be felt upstream, and transmit to only a certain zone downstream bounded by the characteristics passing through that point. Issa and Lockwood (62), therefore, argued that the downstream pressure influence should be eliminated so as to simulate this hyperbolic nature of supersonic flow. Karki (64) also argued that the treatment of the pressure gradient should exhibit an elliptical behavior in the subsonic flow region and hyperbolic behavior in the supersonic flow region. However, it should be noticed that the 'disturbances' must be 'small' whereas pressure changes, in most cases, are always relatively large, and hence it may be physically unrealistic to follow the above arguements that the downstream pressure influences or changes should be eliminated. In fact, take the quasi-one dimensional convergent-divergent nozzle flow as an example, if the downstream pressure changes could never be felt upstream, and hence a shock could not propagate upstream, it would be, therefore, not possible to turn off an induced indraft wind tunnel!. In addition, Issa and Lockwood's treatment of the pressure gradient, i.e., take the pressure difference across the adjacent two upstream nodes, may violate the conservation of momentum and mass due to the abrupt switch to a different scheme as experienced by the present author. Karki (64) finally decided to use central differencing for the pressure gradient by considering the methods developed for potential flows for discretizing the pressure gradient despite his arguement that it should exhibit the hyperbolic behavior.

Kurzrock (110) experimented with forward, backward, and central differencing schemes for the pressure gradient. His experiments and his stability calcula-

tions show that the central differencing scheme is perferable. Moreover, almost all the unsteady methods developed for compressible flow (26, 27, 33, 37, 53) employ the same differencing scheme for the pressure gradient no matter whether supersonic or subsonic flow is calculated.

Due to all the reasons and facts presented above the present modified solution procedure uses the central differencing scheme for the pressure gradient in both supersonic and subsonic flow regions. It has been found that this practise has given good performance for several supersonic flow cases. It is worth pointing out that the specification of the computational boundary conditions is more crucial in compressible flow calculations, especially in supersonic flow calculations as the established principle is misleading as pointed out above, this will be discussed in more detail in chapter six.

4.4.4 The Pressure-Correction Equation

The pressure-correction equation is derived from the momentum and continuity equations by assuming that the current velocities calculated using the guessed pressure field will not satisfy the continuity equation, and hence there must be an adjustment or a change to the pressure field. As a result of this, velocities will change correspondingly as expressed in Eq.(4.8) and Eq.(4.9). However, when compressible flow is under consideration density will also change due to the pressure change which can be expressed as follows:

$$\rho = \rho^* + \rho' \tag{4.27}$$

the density change ρ' is related to the pressure change through the equation of state, and can be expressed in the following form:

$$\rho' = KP' \tag{4.28}$$

where K can be evaluated from the equation of state as follows:

$$\rho = \frac{P}{RT} \tag{4.29}$$

$$K = \frac{\partial \rho}{\partial P} = \frac{1}{RT} \tag{4.30}$$

where R is the gas constant and T is temperature.

The finite difference form of the continuity equation in the two dimensional case is:

$$(\rho U)_e - (\rho U)_w + (\rho V)_n - (\rho V)_s = 0 \tag{4.31}$$

When the pressure field changes the velocity and density fields will also change. The mass flux, e.g., $(\rho U)_e$ can be evaluated as follows:

$$(\rho U)_e = (\rho^* + \rho')_e (U^* + U')_e \tag{4.32}$$

expanding the above equation, one has:

$$(\rho U)_e = (\rho^* U^*)_e + (\rho^* U')_e + (\rho' U^*)_e + (\rho' U')_e \tag{4.33}$$

The fourth term on the right hand side of the above equation is one order smaller and hence can be neglected. The above equation then reduces to the following form:

$$(\rho U)_e = (\rho^* U^*)_e + (\rho^* U')_e + (\rho' U^*)_e \tag{4.34}$$

As the central differencing scheme is still used for the pressure gradient, Eq.(4.14) and Eq.(4.28) are then substituted into the above equation to yield the following equation:

$$(\rho U)_e = (\rho^* U^*)_e + (\rho^* D^U)_e (P'_P - P'_E) + (U^* K P')_e \tag{4.35}$$

$(\rho U)_w$, $(\rho V)_n$, $(\rho V)_s$ can be also obtained in the same way and expressed as follows:

$$(\rho U)_w = (\rho^* U^*)_w + (\rho^* D^U)_w (P'_W - P'_P) + (U^* K P')_w \tag{4.36}$$

$$(\rho V)_n = (\rho^* V^*)_n + (\rho^* D^V)_n (P'_P - P'_N) + (V^* K P')_n \tag{4.37}$$

$$(\rho V)_s = (\rho^* V^*)_s + (\rho^* D^V)_s (P'_S - P'_P) + (V^* K P')_s \tag{4.38}$$

When the upwind differencing scheme is used the values of density correction at the control volume boundaries, taking e as an example, can be evaluated as follows:

$$(\rho' U^*)_e = \rho'_P max[U^*_e, 0.0] + \rho'_E max[-U^*_e, 0.0] \tag{4.39}$$

substituting these relations into Eq.(4.32) and after some manipulation, the modified pressure-correction equation is:

$$a_P P'_P = a_W P'_W + a_E P'_E + a_N P'_N + a_S P'_S + S_o \tag{4.40}$$

$$a_W = A^U_W (\rho^*_w D^U_W + K_W max[U^*_w, 0.0]) \tag{4.41}$$

$$a_E = A^U_E (\rho^*_e D^U_E + K_E max[-U^*_e, 0.0]) \tag{4.42}$$

$$a_N = A^V_N (\rho^*_n D^V_N + K_N max[-U^*_n, 0.0]) \tag{4.43}$$

$$a_S = A^V_S (\rho^*_s D^V_S + K_S max[U^*_s, 0.0]) \tag{4.44}$$

$$a_P = A_W^U(\rho_w^* D_W^U + K_P max[-U_w^*, 0.0]) + A_E^U(\rho_e^* D_E^U + K_P max[U_e^*, 0.0])$$

$$+A_N^V(\rho_n^* D_N^V + K_P max[U_n^*, 0.0]) + A_S^V(\rho_s^* D_S^V + K_P max[-U_s^*, 0.0]) \quad (4.45)$$

$$S_o = A_W^U(\rho^* U^*)_w - A_E^U(\rho^* U^*)_e + A_S^V(\rho^* V^*)_s - A_N^V(\rho^* V^*)_n \quad (4.46)$$

Karki (64), however, employed the above modified pressure-correction equation to update only the velocity field whereas the pressure field was corrected by another pressure-correction equation which he termed the 'first' pressure-correction equation. This so called 'first' was also derived from the momentum and continuity equations in more or less the same way as the derivation in SIMPLER (7, 19). It differs from the above pressure-correction equation in that the full momentum equations were used, i.e., the two terms $\Sigma a_{nb} U'_{nb}$, $\Sigma a_{nb} V'_{nb}$ in Eq(4.12) and Eq.(4.13) were not neglected in the derivation. Details can be found in (64).

However, it has been experienced by the present author that the above modified pressure-correction equation (4.42) does not show any superiority to the unmodified one. In principle, density changes should be accounted for in deriving the pressure-correction equation in the case of compressible flow. Nevertheless, the density field is renewed once a new pressure field is obtained, which means that density changes will be accounted for after one iteration. In other words, density changes lag behind one iteration in the case of compressible flow when the unmodified pressure-correction equation is used. It is worth pointing out that this treatment of density is exactly the same way in which the non-linearities of the momentum equations are treated. Therefore, the original pressure-correction equation is employed in the present study, and the results obtained confirm that

it did lead to a convergent solution for compressible flow provided the calculation of density was switched on after a reasonable pressure field had been established and the computational boundary conditions were specified properly.

4.4.5 Summary of the Solution Procedure

In this chapter, a brief introduction was given to the derivation of the finite difference equations from the corresponding governing partial differential equations, the solution of these equations and so on. Detailed discussion was presented about the evaluation of density at the control volume boundaries and the differencing scheme for the pressure gradient in the case of supersonic flow. It was clearly stated that the idea to completely eliminate downstream pressure influence to simulate the hyperbolic nature of supersonic flow sounded correct superficially but actually was misleading. The pressure-correction equation was also discussed in more detail with the conclusion that the pressure-correction equation did not need to be modified necessarily for compressible flow. The overall solution procedure is as follows:

1). The initial values of the flow field variables are specified or simply set equal to zero.

2). The momentum equations are solved using the currently available pressure field.

3). The pressure-correction equation is solved and the pressure and velocity fields are updated.

4). The transport equation of the stagnation enthalpy is solved to get tem-

perature.

5). The calculation of density is switched on after a reasonable pressure field is established, that is after a certain number of iterations if compressible flow is under study.

6). Other transport equations are solved if necessary.

7). A new iteration is then started until a fully convergent solution is reached.

Chapter 5

APPLICATIONS TO STRONGLY SWIRLING FLOWS

In this chapter, the prediction procedure is applied to strongly swirling confined incompressible turbulent flows in vortex throttles. As stated in previous chapters there is usually no difficulty in obtaining a good numerical solution for incompressible flows, and the SIMPLE algorithm incorporated in the prediction procedure has been well tested for incompressible flows (13, 14, 15, 16, 17, 18). However, turbulence modelling is still a challenge in the case of strongly swirling turbulent flows. It is expected that for strongly swirling flows, the anistropy becomes more and more important, resulting in the components of turbulent viscosity, μ_{rx}, $\mu_{r\theta}$ etc. adopting different values (95, 96). The conventional two equation k-ϵ model uses the same value for all the components of turbulent vis-

cosity according to the Boussinesq assumption, which is appropriate for isotropic turbulent flows. It is generally accepted that Reynolds stress models, predicting each component of the Reynolds stresses separately, offer more universality but they have not been thoroughly tested for recirculating, swirling flows etc. An attempt is made in the present study to employ a Reynolds stress model and compare the performance of such a Reynolds stress model with that of the two equation k-ϵ model in the case of strongly swirling confined turbulent flows. In addition, a conventional wall treatment (97) and a modified wall treatment, based on Chieng-Launder (98) and Johnson-Launder wall treatment (97), are employed in order to model the near wall region more carefully, and their relative performance compared. In all cases the results are compared with experimental data.

5.1 Introduction

Swirling flows are very important phenomena found in nature and they have become of interest in association with a wide range of applications. In nonreactive cases applications include, for example: vortex amplifiers, cyclone separators, agricultural spraying machines, heat exchangers etc. In combustion systems, such as in gasoline engines, gas turbines, industrial furnaces, the dramatic effects of swirl to stabilize flames and to improve combustion efficiency have been known and appreciated for many years. Better understanding of swirling flows will undoubtedly help the improved design of the various devices and bring about more

new applications. However, the strongly coupled, nonlinear governing partial differential equations and the complex nature of turbulence impose formidable difficulty to solution by analytical methods. An alternative approach is the numerical solution procedure.

For the strongly swirling incompressible turbulent flow computations, the most difficult problem to deal with is the turbulence modelling. The conventional two equation k-ϵ model has been well tested and successfully applied to numerous engineering calculations but its performance becomes poor for certain situations such as recirculating and swirling flows, especially for strongly swirling flows (4, 17, 96, 99, 100). This may be attributed to the assumption of isotropic turbulence which is not appropriate for swirling flows as anisotropy becomes more and more important. Experimental study of swirling flow (101), free swirling jets (102) and the flow field near the recirculation zone at the exit of a swirl generator (103) have shown that the axial and radial components of turbulent viscosity change significantly, yielding a considerable degree of anisotropy. Modifications could be made to account for the anisotropy by specifying the rθ-viscosity number etc., $\sigma_{r\theta} = \frac{\mu_{rx}}{\mu_{r\theta}} \neq 1$, which is in general larger than 1 (96). However, since this is too empirical and flow dependent it can be hardly accepted in terms of universality. Boysan and Swithenbank (17) applied an algebraic stress model to the prediction of strongly swirling confined turbulent flow in a cyclone chamber and showed that some important flow features could be captured using the algebraic stress model whereas the two equation k-ϵ model failed to reproduce them. An evaluation of the performance of the two equation k-ϵ model and algebraic stress models was

presented by Nallasamy (4), concluding that the performance of the conventional two equation k-ϵ model becomes poor for attached flow, recirculating flow, swirl flow etc. and algebraic stress models perform better. It is also pointed out by him that Reynolds stress models have not been thoroughly tested for recirculating and swirling flows.

In this chapter, calculations have been performed for strongly swirling confined turbulent incompressible flows in 76mm and 102mm chamber diameter vortex throttles. Both the widely tested conventional k-ϵ model and a Reynolds stress model are employed in the study for the sake of comparison. Wall functions are used to simplify the calculations in the near wall region, and both a conventional wall treatment (97) and a modified wall treatment, based on Ching-Launder (98) and Johnson-Launder wall treatment (97), are adopted. The predicted pressure drops through the vortex throttles over a certain range of flow rate are compared with experimental data. The predicted streamlines, velocity profiles etc. are presented and the flow field structure is analyzed. Moreover, numerical experiments have been made to assess the effect of inlet swirl intensity (the ratio of inlet tangential velocity to inlet radial velocity), the inlet Reynolds number, and inlet turbulent intensity on the flow fields. Finally, further exploration of pressure drop in such vortex throttles is given and some other possible applications are discussed.

5.2 Governing Equations

It is assumed that flows in the vortex throttles are axisymmetrical, hence, the governing transport equations in a cylindrical coordinate system are as follows:

5.2.1 The Reynolds stress model

The continuity and momentum equations are time-averaged as described in chapter three to yield the following averaged equations:

$$\frac{\partial U}{\partial x} + \frac{1}{r}\frac{\partial rV}{\partial r} = 0 \tag{5.1}$$

$$\frac{\partial}{\partial x}(\rho U^2) + \frac{1}{r}\frac{\partial}{\partial r}(r\rho UV) = -\frac{\partial P}{\partial x} + \frac{\partial}{\partial x}\left(\mu\frac{\partial U}{\partial x}\right) + \frac{1}{r}\frac{\partial}{\partial r}\left(r\mu\frac{\partial U}{\partial r}\right) - \frac{\partial}{\partial x}(\rho\overline{u^2}) - \frac{1}{r}\frac{\partial}{\partial r}(r\rho\overline{uv}) \tag{5.2}$$

$$\frac{\partial}{\partial x}(\rho UV) + \frac{1}{r}\frac{\partial}{\partial r}(r\rho V^2) - \frac{\rho W^2}{r} = -\frac{\partial P}{\partial r} + \frac{\partial}{\partial x}\left(\mu\frac{\partial V}{\partial x}\right) + \frac{1}{r}\frac{\partial}{\partial r}\left(r\mu\frac{\partial V}{\partial r}\right) - \frac{\mu V}{r^2} - \frac{\partial}{\partial x}(\rho\overline{uv}) - \frac{1}{r}\frac{\partial}{\partial r}(r\rho\overline{v^2}) + \frac{\rho\overline{w^2}}{r} \tag{5.3}$$

$$\frac{\partial}{\partial x}(\rho UW) + \frac{1}{r}\frac{\partial}{\partial r}(r\rho VW) + \frac{\rho VW}{r} = \frac{\partial}{\partial x}\left(\mu\frac{\partial W}{\partial x}\right) + \frac{1}{r}\frac{\partial}{\partial r}\left(r\mu\frac{\partial W}{\partial r}\right) - \frac{\mu W}{r^2} - \frac{\partial}{\partial x}(\rho\overline{uw}) - \frac{1}{r}\frac{\partial}{\partial r}(r\rho\overline{vw}) - \frac{\rho\overline{vw}}{r} \tag{5.4}$$

where U, V, W represent the mean velocity components, and u, v, w represent the corresponding fluctuating parts in axial, radial and tangential directions respectively. However, the above equations cannot be solved as more unknowns, called the Reynolds stresses, appear in the equations due to the averaging procedure. Therefore, a turbulence model has to be employed to predict the six

Reynolds stresses directly or indirectly. In the Reynolds stress model employed in this study, the modelled transport equations for k, $\overline{v^2}-\overline{u^2}$, $\overline{v^2}-\overline{w^2}$, $\overline{uv}$, $\overline{uw}$, $\overline{vw}$ and ϵ are as follows:

$$\frac{\partial}{\partial x}(Uk)+\frac{1}{r}\frac{\partial}{\partial r}(rVk)=\frac{\partial}{\partial x}\left[(\nu+\Gamma)\frac{\partial k}{\partial x}\right]+\frac{1}{r}\frac{\partial}{\partial r}\left[r(\nu+\Gamma)\frac{\partial k}{\partial r}\right]-\epsilon$$
$$-\overline{uv}\left(\frac{\partial U}{\partial r}+\frac{\partial V}{\partial x}\right)-\overline{u^2}\frac{\partial U}{\partial x}-\overline{v^2}\frac{\partial V}{\partial r}-\overline{w^2}\frac{V}{r}-\overline{vw}\frac{\partial W}{\partial r}-\overline{uw}\frac{\partial W}{\partial x}+\overline{vw}\frac{W}{r} \quad (5.5)$$

$$\frac{\partial}{\partial x}[U(\overline{v^2}-\overline{u^2})]+\frac{1}{r}\frac{\partial}{\partial r}[rV(\overline{v^2}-\overline{u^2})]-2\overline{vw}\frac{W}{r}=\frac{\partial}{\partial x}\left[(\nu+\Gamma)\frac{\partial(\overline{v^2}-\overline{u^2})}{\partial x}\right]$$
$$+\frac{1}{r}\frac{\partial}{\partial r}\left[r(\nu+\Gamma)\frac{\partial(\overline{v^2}-\overline{u^2})}{\partial r}\right]-\frac{2\Gamma}{r^2}(\overline{v^2}-\overline{u^2})-C_1\frac{\epsilon}{k}(\overline{v^2}-\overline{u^2})$$
$$-2(1-\alpha)\left[\overline{uv}\left(\frac{\partial V}{\partial x}-\frac{\partial U}{\partial r}\right)+\overline{v^2}\frac{\partial V}{\partial r}-\overline{u^2}\frac{\partial U}{\partial x}-\overline{vw}\frac{W}{r}\right] \quad (5.6)$$

$$\frac{\partial}{\partial x}[U(\overline{v^2}-\overline{w^2})]+\frac{1}{r}\frac{\partial}{\partial r}[rV(\overline{v^2}-\overline{w^2})]-4\overline{vw}\frac{W}{r}=\frac{\partial}{\partial x}\left[(\nu+\Gamma)\frac{\partial(\overline{v^2}-\overline{w^2})}{\partial x}\right]$$
$$+\frac{1}{r}\frac{\partial}{\partial r}\left[r(\nu+\Gamma)\frac{\partial(\overline{v^2}-\overline{w^2})}{\partial r}\right]-\frac{4\Gamma}{r^2}(\overline{v^2}-\overline{w^2})-C_1\frac{\epsilon}{k}(\overline{v^2}-\overline{w^2})$$
$$-2(1-\alpha)\left[\overline{uv}\frac{\partial V}{\partial x}+\overline{v^2}\frac{\partial V}{\partial r}-\overline{w^2}\frac{V}{r}-\overline{vw}\left(\frac{\partial W}{\partial r}+\frac{W}{r}\right)-\overline{uw}\frac{\partial W}{\partial x}\right] \quad (5.7)$$

$$\frac{\partial}{\partial x}(U\overline{uv})+\frac{1}{r}\frac{\partial}{\partial r}(rV\overline{uv})-\overline{uw}\frac{W}{r}=\frac{\partial}{\partial x}\left[(\nu+\Gamma)\frac{\partial\overline{uv}}{\partial x}\right]+$$
$$\frac{1}{r}\frac{\partial}{\partial r}\left[r(\nu+\Gamma)\frac{\partial\overline{uv}}{\partial r}\right]-\frac{\Gamma}{r^2}\overline{uv}-C_1\frac{\epsilon}{k}\overline{uv}-$$
$$(1-\alpha)\left[\overline{v^2}\frac{\partial U}{\partial r}+\overline{u^2}\frac{\partial V}{\partial x}+\overline{uv}\left(\frac{\partial U}{\partial x}+\frac{\partial V}{\partial r}\right)-\overline{uw}\frac{W}{r}\right] \quad (5.8)$$

$$\frac{\partial}{\partial x}(U\overline{uw})+\frac{1}{r}\frac{\partial}{\partial r}(rV\overline{uw})+\overline{uv}\frac{W}{r}=\frac{\partial}{\partial x}\left[(\nu+\Gamma)\frac{\partial\overline{uw}}{\partial x}\right]+$$
$$\frac{1}{r}\frac{\partial}{\partial r}\left[r(\nu+\Gamma)\frac{\partial\overline{uw}}{\partial r}\right]-\frac{\Gamma}{r^2}\overline{uw}-C_1\frac{\epsilon}{k}\overline{uw}-$$
$$(1-\alpha)\left[\overline{vw}\frac{\partial U}{\partial r}+\overline{uw}\left(\frac{\partial U}{\partial x}+\frac{V}{r}\right)+\overline{uv}\frac{\partial W}{\partial r}+\overline{u^2}\frac{\partial W}{\partial x}\right] \quad (5.9)$$

$$\frac{\partial}{\partial x}(U\overline{vw}) + \frac{1}{r}\frac{\partial}{\partial r}(rV\overline{vw}) + (\overline{v^2} - \overline{w^2})\frac{W}{r} = \frac{\partial}{\partial x}\left[(\nu + \Gamma)\frac{\partial \overline{vw}}{\partial x}\right] +$$
$$\frac{1}{r}\frac{\partial}{\partial r}\left[r(\nu + \Gamma)\frac{\partial \overline{vw}}{\partial r}\right] - \frac{4\Gamma}{r^2}\overline{vw} - C_1\frac{\epsilon}{k}\overline{vw} -$$
$$(1-\alpha)\left[\overline{uw}\frac{\partial V}{\partial x} + \overline{v^2}\frac{\partial W}{\partial r} + \overline{vw}\left(\frac{\partial V}{\partial r} + \frac{V}{r}\right) + \overline{uv}\frac{\partial W}{\partial x} - \overline{w^2}\frac{W}{r}\right] \qquad (5.10)$$

$$\frac{\partial}{\partial x}(U\epsilon) + \frac{1}{r}\frac{\partial}{\partial r}(rV\epsilon) = \frac{\partial}{\partial x}\left[(\nu + \Gamma_\epsilon)\frac{\partial \epsilon}{\partial x}\right] +$$
$$\frac{1}{r}\frac{\partial}{\partial r}\left[r(\nu + \Gamma_\epsilon)\frac{\partial \epsilon}{\partial r}\right] + \frac{\epsilon}{k}\left[C_{\epsilon 1}G - C_{\epsilon 2}\epsilon\right] \qquad (5.11)$$

$$G = -\overline{uv}\left(\frac{\partial U}{\partial r} + \frac{\partial V}{\partial x}\right) - \overline{u^2}\frac{\partial U}{\partial x} - \overline{v^2}\frac{\partial V}{\partial r} - \overline{w^2}\frac{V}{r} - \overline{vw}\frac{\partial W}{\partial r} -$$
$$\overline{uw}\frac{\partial W}{\partial x} + \overline{vw}\frac{W}{r} \qquad (5.12)$$

where the scalar turbulent diffusivity, $\Gamma = C_T\frac{k^2}{\epsilon}$, $\Gamma_\epsilon = C_\epsilon\frac{k^2}{\epsilon}$.

5.2.2 The k-ϵ Model

The continuity equation is the same as above,

$$\frac{\partial U}{\partial x} + \frac{1}{r}\frac{\partial rV}{\partial r} = 0 \qquad (5.13)$$

In the k-ϵ model, the six Reynolds stresses are not solved directly but indirectly using the following equations according to the Boussinesq assumption:

$$-\rho\overline{u^2} = 2\mu_{tur}\frac{\partial U}{\partial x} - \frac{2}{3}\rho k \qquad (5.14)$$

$$-\rho\overline{v^2} = 2\mu_{tur}\frac{\partial V}{\partial r} - \frac{2}{3}\rho k \qquad (5.15)$$

$$-\rho\overline{w^2} = 2\mu_{tur}\frac{V}{r} - \frac{2}{3}\rho k \qquad (5.16)$$

$$-\rho\overline{uv} = \mu_{tur}\left(\frac{\partial V}{\partial x} + \frac{\partial U}{\partial r}\right) \qquad (5.17)$$

$$-\rho\overline{uw} = \mu_{tur}\frac{\partial W}{\partial x} \tag{5.18}$$

$$-\rho\overline{vw} = \mu_{tur}\left(\frac{\partial W}{\partial r} - \frac{W}{r}\right) \tag{5.19}$$

Substituting the above relations into the averaged momentum equations and after some manipulations the momentum equations have the following forms:

$$\frac{\partial}{\partial x}(\rho U^2) + \frac{1}{r}\frac{\partial}{\partial r}(r\rho UV) = -\frac{\partial P}{\partial x} + \frac{\partial}{\partial x}\left(\mu_{eff}\frac{\partial U}{\partial x}\right) + \frac{1}{r}\frac{\partial}{\partial r}\left(r\mu_{eff}\frac{\partial U}{\partial r}\right) \tag{5.20}$$

$$\frac{\partial}{\partial x}(\rho UV) + \frac{1}{r}\frac{\partial}{\partial r}(r\rho V^2) - \frac{\rho W^2}{r} = -\frac{\partial P}{\partial r} + \frac{\partial}{\partial x}\left(\mu_{eff}\frac{\partial V}{\partial x}\right) + \frac{1}{r}\frac{\partial}{\partial r}\left(r\mu_{eff}\frac{\partial V}{\partial r}\right) - \frac{\mu_{eff}V}{r^2} \tag{5.21}$$

$$\frac{\partial}{\partial x}(\rho UW) + \frac{1}{r}\frac{\partial}{\partial r}(r\rho VW) + \frac{\rho VW}{r} = \frac{\partial}{\partial x}\left(\mu_{eff}\frac{\partial W}{\partial x}\right) + \frac{1}{r}\frac{\partial}{\partial r}\left(r\mu_{eff}\frac{\partial W}{\partial r}\right) - \frac{\mu_{eff}W}{r^2} \tag{5.22}$$

where U, V, W represent the mean velocity components in axial, radial and tangential directions respectively. μ_{eff} is the effective viscosity expressed as follows:

$$\mu_{eff} = \mu + \mu_{tur} \tag{5.23}$$

where μ_{tur} is the turbulent viscosity which is obtained from the following equation

$$\mu_{tur} = C_\mu\rho\frac{k^2}{\epsilon} \tag{5.24}$$

and the transport equations for k and ϵ are as follows:

$$\frac{\partial}{\partial x}(\rho Uk) + \frac{1}{r}\frac{\partial}{\partial r}(r\rho Vk) = \frac{\partial}{\partial x}\left[\left(\mu + \frac{\mu_{tur}}{Pr_k}\right)\frac{\partial k}{\partial x}\right] + \frac{1}{r}\frac{\partial}{\partial r}\left[r\left(\mu + \frac{\mu_{tur}}{Pr_k}\right)\frac{\partial k}{\partial r}\right] + G_k - \rho\epsilon \tag{5.25}$$

$$\frac{\partial}{\partial x}(\rho U\epsilon)+\frac{1}{r}\frac{\partial}{\partial r}(r\rho V\epsilon)=\frac{\partial}{\partial x}\left[\left(\mu+\frac{\mu_{tur}}{Pr_\epsilon}\right)\frac{\partial \epsilon}{\partial x}\right]+$$
$$\frac{1}{r}\frac{\partial}{\partial r}\left[r\left(\mu+\frac{\mu_{tur}}{Pr_\epsilon}\right)\frac{\partial \epsilon}{\partial r}\right]+\frac{\epsilon}{k}(C_{\epsilon 1}G_k-C_{\epsilon 2}\rho\epsilon) \tag{5.26}$$

$$G_k=2\mu_{tur}\left[\left(\frac{\partial U}{\partial x}\right)^2+\left(\frac{\partial V}{\partial r}\right)^2+\left(\frac{V}{r}\right)^2\right]+$$
$$\mu_{tur}\left\{\left(\frac{\partial U}{\partial r}+\frac{\partial V}{\partial x}\right)^2+\left(\frac{\partial W}{\partial x}\right)^2+\left[r\frac{\partial}{\partial r}\left(\frac{W}{r}\right)\right]^2\right\} \tag{5.27}$$

The numerical constants used in the above equations take the following values in both models:

C_μ	C_1	C_T	α	Pr_k	Pr_ϵ	C_ϵ	$C_{\epsilon 1}$	$C_{\epsilon 2}$
0.09	1.5	0.1	0.4	1.0	1.3	0.07	1.44	1.92

5.3 Wall Treatment

For wall-bounded flows, a special treatment should be employed to handle a region near the wall where viscous effects become important and the turbulence levels decrease. There are usually two ways by which one can achieve this, i.e., either using low Reynolds number turbulence models or using wall functions. The latter approach is adopted in this study and more details about the wall treatment is given elsewhere (97). Here an outline is presented.

5.3.1 The Conventional Wall Treatment

The expression for the wall shear stress given in (97) is as follows:

$$\tau_w=\frac{\rho\kappa U_P C_\mu^{1/4}k_P^{1/2}}{\ln Ey^+} \tag{5.28}$$

where subscript P refers to values at a point P in the inertial sub-layer and E is a constant, κ is the von Karman constant. The values of these two constants are determined from the experimental logarithmic law as, $\kappa = 0.4187$, E=9.793. $y^+ = \frac{yk_P^{1/2}C_\mu^{1/4}}{\nu}$, y is the distance from the wall and ν is the kinematic viscosity. C_μ is a constant whose value is 0.09. It is assumed that the shear stress in the viscous sub-layer is constant and equal to that of the inertial sub-layer. Therefore, the shear stress in both the viscous and inertial sub-layer is the same as that of the wall shear stress which is then used in the momentum equations in the wall-adjacent grid cells.

The same needs to be done in the wall-adjacent grid cells for k and ϵ. For k, the generation and dissipation rates must be specified. The generation rate is assumed to be

$$\tau_w \left(\frac{dU}{dy} + \frac{dW}{dy} \right) = \tau_w \left(\frac{U_P - 0}{y_P - 0} + \frac{W_p - 0}{y_P - 0} \right) = \frac{\tau_w (U_P + W_P)}{y_P} \tag{5.29}$$

The dissipation rate for both k and ϵ is assumed to be

$$\epsilon = \frac{k^{3/2}}{C_l y_P} \tag{5.30}$$

where C_l is a constant defined as

$$C_l = \frac{\kappa}{C_\mu^{3/4}} \tag{5.31}$$

This conventional wall treatment has been used traditionally by the Imperial college group and hence is denoted as the IC wall treatment in (97).

5.3.2 The Modified Wall Treatment

The assumption that shear stress is constant in the near wall region could lead to the result that the turbulent kinetic energy k is also constant in the same region. This is not physically realistic. Therefore, it is assumed that τ is a linear function of distance from the wall and k is also a linear function in the inertial sub-layer. They are expressed mathematically as follows:

$$\tau = sy + \tau_w \qquad 0 \leq y \leq y_e \tag{5.32}$$

$$k = my + b \qquad y_v \leq y \leq y_e \tag{5.33}$$

$$k = k_v \left(\frac{y}{y_v}\right)^2 \qquad 0 \leq y \leq y_v \tag{5.34}$$

where τ_w is the wall shear stress, s and m are the slopes of τ and k, b is a constant, the subscripts v and e denote the edge of viscous and inertial sub-layer respectively, k_v is the turbulent kinetic energy at the edge of viscous sub-layer. Upon integrating the following equation,

$$sy + \tau_w = \mu \frac{dU}{dy} \tag{5.35}$$

using laminar viscosity for the viscous sub-layer and the expression, $\mu_t = C_l C_\mu k^{1/2} y$, for the inertial sub-layer, and after considerable manipulations the following expression for τ_w can be obtained (97)

$$\tau_w = \frac{\rho \kappa^* U_P b^{1/2} - s b^{1/2} \left[\frac{y_v^2 \kappa^*}{2\nu} + \frac{2(y_P - y_v)}{k_P^{1/2} + k_v^{1/2}}\right]}{\ln E^{**} y_P \frac{k_v^{1/2}}{\nu}} \tag{5.36}$$

where

$$\kappa^* = \kappa C_\mu^{1/4} \tag{5.37}$$

$$Re_v = \frac{y_v k_v^{1/2}}{\nu} = 20 \tag{5.38}$$

$$E^{**} = \frac{(k_v^{1/2} + b^{1/2})^2}{(k_P^{1/2} + b^{1/2})^2} \frac{e^{\frac{b^{1/2}\kappa^* Re_v}{k_v^{1/2}}}}{Re_v} \tag{5.39}$$

For k, the mean generation rate is obtained by

$$Mean - Generation - Rate(MGR) = \frac{1}{y_e} \int_{y_v}^{y_e} (sy + \tau_w) \frac{dU}{dy} dy \tag{5.40}$$

upon integrating and simplifying, the final expression (97) is

$$MGR = \frac{\tau_w}{y_e}(U_e - U_v) + \frac{2s\tau_w(y_e - y_v)}{\rho\kappa^* y_e(k_e^{1/2} + k_v^{1/2})} \tag{5.41}$$

and the mean dissiaption rate is given (97) as follows:

$$MDP = \frac{2\nu k_v}{y_e y_v} + \frac{1}{y_e C_l}\left[\frac{2}{3}(k_e^{3/2} - k_v^{3/2}) + 2b(k_e^{1/2} - k_v^{1/2})\right] + \frac{b^{3/2}}{y_e C_l} \ln\left[\frac{y_e}{y_v}\frac{(k_v^{1/2} + b^{1/2})^2}{(k_e^{1/2} + b^{1/2})^2}\right] \tag{5.42}$$

For ϵ, the same expression as before is employed

$$\epsilon_P = \frac{k^{3/2}}{C_l y_P} \tag{5.43}$$

There are several unknowns which need to be evaluated in the above equations. It is important that some measures be taken to make sure that they adopt appropriate values. It is assumed that turbulent kinetic energy, k = my+b, and the shear stress, $\tau = sy + \tau_w$, increase away from the wall in both the viscous and inertial sub-layers so that the slopes m and s should be positive. Moreover, at the edge of the viscous sub-layer one has, $k_v = my_v + b \longrightarrow b = k_v - my_v$, so that b should be smaller than k_v which should be smaller than k_P.

5.4 Boundary Conditions

The treatment of the boundary conditions for incompressible flows is well documented in (2). The boundary conditions used in this study are given briefly as follows:

5.4.1 Inlet Boundary

The values of the variables are usually known or can be calculated from the given conditions at the inlet boundary. The values are used in the boundary control volumes in the discretization equations and nothing special requires to be done. One point which should be noted is that a boundary condition for pressure is not required due to the use of staggered grids. Therefore, in the present work only the velocities were specified at the inlet boundary.

5.4.2 Outlet Boundary

The fluid leaves the computational domain at the outlet boundary and usually there is no information about the variables. This boundary is often an artificial boundary used to limit the computational domain to a finite region. Hence, the outlet boundary should placed and treated such that it minimizes the influences on the results in the region of interest. In this study, the tangential and radial velocity component gradients were assumed to be zero and the axial velocity component was adjusted to satisfy overall mass conservation.

5.4.3 Wall Boundary and Symmetry Line

At the solid wall, the no-slip condition is usually applied for viscous flows. According to this condition the velocity of the fluid at the wall should be the same as that of the wall. In the study, all the walls are fixed and hence the velocities at the wall were zero. At a symmetry line, the normal component of velocity and the normal gradient of the parallel component of velocity are zero. In this case at the axis of the symmetry, the tangential and radial velocities, W and V, vanish under the assumption of axi-symmetric flow.

5.5 Geometry of Vortex Throttles

Figure 5.1 shows the geometry of vortex throttles used in this study. They are of the square-edged type with symmetrical structure. Flow enters at the tangential port, forms a vortex in the chamber and leaves through the axial port. The following table gives details of the value of the various dimensions in millimeters, as defined in Figure 5.1.

D	h	w	d_a	l	s	D_p	D_i
102	13.12	10.05	12.75	12.95	14	38	19
76	13.12	10.20	12.85	13.05	13	38	19

The inlet tangential and radial velocities are calculated from the given flow rate and Reynolds number.

5.6 Results and Comparisons

Fig. 5.2 and Fig. 5.3 compare measured and predicted pressure drops with the two equation k-ϵ model for various water flowrates through both the 76mm and 102mm chamber diameter vortex throttles respectively. It can be seen that better agreement has been achieved between the experimental data and the results predicted using the modified wall treatment, compared with the relatively poor predictions obtained using the conventional wall treatment. This confirms that it is important to handle the near wall region carefully since the conventional two equation k-ϵ model and some of the other turbulence models are appropriate to high Reynolds number flows only. This also indicates that the wall shear stresses play a important role in determining the pressure drop in the vortex throttles as will be discussed below. All predictions presented hereafter are obtained with the modified wall treatment.

Fig. 5.4 shows experimental data and the two equation predictions of pressure drop versus the flowrates through both the 76mm and 102mm chamber diameter vortex throttles. It can be seen that measured pressure drops across the 76mm diameter vortex throttle are slightly larger than those of the 102mm diameter one. This again indicates the importance of internal wall friction (wall shear stresses) in determining the pressure drop as mentioned before. In the absence of internal wall friction, the strength of the potential vortex in the vortex chamber would increase with increasing chamber diameter. In practice, however, internal wall friction forces limit this effect. It can also be seen from this figure that the

two equation k-ϵ model fails to predict the higher pressure drop as measured in the 76mm chamber diameter vortex throttle.

Fig. 5.5 compares the Reynolds stress model predictions of pressure drops with experimental data in both the 76mm and 102mm chamber diameter vortex throttles. It can be seen that the Reynolds stress model predictions give not only closer agreement with the experimental data but also slightly higher pressure drops in the 76mm chamber diameter vortex throttle. This verifies that the Reynolds stress model offers more universality and gives better predictions than the two equation k-ϵ model in the case of highly swirling flows despite its complication and requiring more CPU time.

Fig. 5.6 shows the ideal free vortex tangential velocity profile and the predicted profiles for Re=11078 in the 102mm chamber diameter vortex throttle at x/R=0.065. For a free vortex the tangential velocity can be expressed as Wr=C, where C is a constant and r is the distance from the axis. Hence the tangential velocity goes to infinity at the axis in the case of a free vortex. In reality, however, the tangential velocity is zero at the axis of symmetry and has the Rankine free-forced vortex form in the vortex chamber as shown. It can also be seen that the peak value of the tangential velocity predicted by the Reynolds stress model is larger than that predicted by the k-ϵ model, which agrees with the higher pressure drop predicted by the Reynolds stress model as will be discussed later.

Fig. 5.7 shows the experimental and predicted data plotted as Euler number versus Reynolds number for the 102mm throttle, based on the the flow condition at the inlet tangential port. The Reynolds stress model predictions are again

closer to the experimental data than the k-ϵ model predictions. It can be also seen that the performance of the throttle is a strong function of Reynolds number below about Re=10,000, with Euler number rising from a minimum value of about 10 to a maximun value of about 60. However, when Reynolds number is over 10,000 Euler number is seen to be fairly constant at the maximum value.

Fig. 5.9 and Fig. 5.10 compare the Reynolds stress model and k-ϵ model predictions of tangential and axial velocity profiles for the 102mm throttle at Re=11078. Fig. 5.9 shows that the Reynolds stress model predicts a sharper tangential velocity profile in the vortex chamber, as can also be seen from Fig. 5.6. By comparison, the two equation k-ϵ model predicts a flatter and smoother tangential velocity profile. This may be attributed to the overprediction of the turbulent kinetic energy by the k-ϵ model, as can be seen in Fig. 5.8 which shows turbulent kinetic energy predicted by the Reynolds stress model and the k-ϵ model respectively for Re=11078 in the 102mm diameter vortex chamber at x/R=0.065. Near the axis the Reynolds stress model predicts a lower tangential velocity compared with the k-ϵ model. This may be because the Reynolds stress model predicts a stronger recirculation region along the axis, bringing more fluid with very low tangential velocity back, which can be seen from the axial profiles as shown.

Fig. 5.11 shows streamlines in the 102mm chamber diameter vortex throttle obtained by the Reynolds stress model and the k-ϵ model at Re=11078. Some differences can be observed between the Reynolds stress model predictions and the k-ϵ model predictions, especially in the vortex chamber where slightly differ-

ent flow patterns have been predictied. This is probably due to the difference of tangential velocity predicted by the two models. Higher tangential velocity is predicted by the Reynolds stress model in the chamber near the axial port, resulting in higher centrifugal force which causes more outward radial flows, hence a strong recirculation zone is predicted in the vortex chamber. The recirculation zone is also predicted, though to a lesser extent, by the two equation k-ϵ model. At the axial port exit the flow patterns predicted by both the Reynolds stress model and the k-ϵ model are very similar and a recirculation zone which is usually referred to as CTRZ (Central Toroidal Recirculation Zone) is predicted by both models. Details of the flow structure will be discussed in the next section.

The results for the 76mm diameter vortex throttle are almost the same as those for the 102mm diameter one so that it is not necessary to present them again. They are not presented in the following discussion for the same reason.

5.7 Discussions of the Results

It has been well established that swirl flows can be classified into two groups according to the degree of swirl strength. They are the low swirl and high swirl flows respectively, and the flow characteristics are quite different in the two cases. The degree of swirl is usually characterized by the so called swirl number S, which stands for the ratio of axial flux of swirl momentum to axial flux of axial momentum (96). At higher degrees of swirl (S is larger than 0.6), strong radial and axial pressure gradients are set up, resulting in axial recirculation in the

form of a CTRZ (Central Toroidal Recirculation Zone) as metioned above. The study undertaken belongs to the high swirl flows, and one point which needs to be noted is that the inlet swirl intensity (the ratio of inlet tangential velocity to inlet radial velocity) is used to characterize the flow field for convenience instead of swirl number S in the present study.

5.7.1 Pressure Field

Fig. 5.12 shows the pressure profiles and the pressure contours predicted by the Reynolds stress model in the 102mm diameter throttle at Re=11078. The radial pressure gradient in the vortex chamber near the axis is apparent (as can be seen from both the profile and contours) and the axial pressure gradient can be seen clearly along the axis. From the pressure profile in the vortex chamber one can see that a low pressure zone occurs around the axis in the vortex chamber as a result of the centrifugal force. This is the cause of the axial pressure gradient which results in the axial recirculation. Out of the axial port, pressure is almost constant due to the decay of tangential velocity. In the vortex chamber the total pressure, $P_{total} = P + \frac{W^2}{2}$(radial and axial velocities are negligible), is almost constant. However, out of the axial port both tangential velocity and pressure are very low, as shown in Fig. 5.9 and Fig. 5.12, which means that a large amount of total pressure (energy) is lost through the axial port due to wall friction and the sudden expansion at the exit of the axial port. This indicates the importance of the design of the axial port and the expansion part in determining throttle performance.

5.7.2 Flow Field

Fig. 5.13 shows the k-ϵ prediction of streamlines and velocity vectors in the 102mm diameter throttle at Re=5565. The salient features of the flow field predicted are the two recirculation zones, one is in the vortex chamber and another is along the axis and is referred to as the CTRZ mentioned above, which occurs in swirl flows when the swirl number is over 0.6. In the particular case under study it is due to the inlet high swirl intensity (the ratio of inlet tangential velocity to radial velocity), which creates a large centrifugal force in the vortex chamber, causing a low pressure zone around the axis as explained above. With respect to the recirculation zone in the vortex chamber it may be explained as follows:

Because of the viscous action, there is a tangential boundary layer on the walls in the vortex chamber. In the boundary layer the reduced tangential velocity leads to a reduced centrifugal force and thus the fluid tends to move inwards as shown in Fig. 5.13 due to the radial pressure gradient force and the inertial force. Outside the boundary layer, however, the centrifugal force on a particle of fluid tends to be balanced by the radial pressure gradient force and the inertial force. When the inlet swirl intensity increases the tangential velocity rises as well, and so does the centrifugal force. Eventually a point is reached where the tangential velocity in the main body of the vortex chamber produces a centrifugal force which just balances the radial pressure gradient force plus the radial inertial force, this can be defined as a critical point beyond which the larger centrifugal force will cause outward radial flow and hence the recirculation zone occurs in the vortex chamber. However, the chamber recirculation zone is not only dependent on the inlet swirl

intensity but also on the inlet Reynold number as well, which will be discussed later. Moreover, one may notice at the corner region in the vortex chamber near the axial port where the boundary layer ends, a flow separation can be observed which is similar to the usual separation in boundary layers. In this particular case it is because the radial pressure gradient force and the inertial force are not large enough to maintain inward flow due to an increase of the centrifugal force just outside the boundary layer. These phenomena are not predicted when the inlet swirl intensity is small enough as will be discussed later. In addition, when Reynolds number is changed the flow field also changes which will be discussed next.

5.7.3 The Effects of Reynolds Number

Fig. 5.14 shows the k-ϵ model predictions of streamlines in the 102mm diameter throttle at different Reynolds numbers. For all the cases the Central Toroidal Recirculation Zone can be clearly seen, and so can the separation zone at the corner near the axial port in the vortex chamber. In Fig 5.14(a) at Re=3385 and Fig. 5.14(b) at Re=5565 a strong recirculation zone is observed in the vortex chamber. This is also apparent, though to a lesser extent, in Fig. 5.14(c) at Re=11078. However, when the inlet Reynolds number is raised to 14600 the reverse flow in the vortex chamber disappears as shown in Fig. 5.14(d). According to what is stated above, this means the centrifugal force is no longer larger than the pressure gradient force plus the radial inertial force. This is probably because the inertial radial force increases proportionally with the increase of inlet Reynolds number.

The centrifugal force rises as well but not so rapidly as the radial inertial force. In conclusion, the inlet Reynolds number has great effects on the flow pattern in the vortex chamber but out of the chamber the flow field does not change too much.

5.7.4 Effect of Inlet Swirl Intensity

It is well known that one of the most important factors influencing a swirling flow field is the swirl number. In this study, however, the inlet swirl intensity (denoted hereafter as SI) is adopted for convenience as mentioned before. One would imagine that the inlet SI will also have great effect on the flow field. All the results presented above have been obtained when the inlet SI is about 32, which is the value for the vortex throttles used. For a certain vortex throttle design the inlet SI is determined solely by the inlet geometry of the throttle. The results shown below do not refer to any practical vortex throttle and they are just numerical experiments to assess the effects of the inlet SI on the flow field.

Fig. 5.15 gives the k-ϵ predictions of streamlines in the 102mm throttle at the same inlet Reynolds number but when the inlet SI is changed. When the inlet SI is reduced to 15 the flow field does not change too much as can be seen in Fig. 5.15 (b). By comparison, in the case of low inlet SI, as shown in Fig. 5.15 (c) and Fig. 5.15 (d), dramatic changes occur. The recirculation zone in the vortex chamber disappears completely and the size of the CTRZ reduces as well. When the inlet SI is reduced to 1 both the CTRZ and the separation region at the corner disappear entirely. This shows that the inlet SI has a great effect on

the flow field as does the swirl number, confirming that it is equivalent to use the inlet SI instead of swirl number to characterize the flow field.

5.7.5 Effect of Inlet Turbulent Intensity

Solving the transport equation for turbulent kinetic energy needs the specification of the inlet condition, but unfortunately no experimental data is available. In most cases the inlet turbulent intensity is assumed around 10 to 20 percent. For the case undertaken 10 percent has been assumed. However, in order to assess the effect of inlet turbulent intensity several values from 1 percent to 30 percent have been adopted. It has been found that the change of inlet turbulent intensity has hardly any influence on pressure drop and mean velocities nor even on the turbulent kinetic energy and its dissipation rate. This indicates that turbulent kinetic energy is mainly produced inside the flow field in this case.

5.7.6 Pressure Drop

It would be too broad to discuss pressure drop in general flow fields and it is also beyond the scope of this thesis. In the following part of the discussion the pressure drop in the vortex throttles will be discussed, in particular, the important factors influencing the pressure drop in such a device will be given. Moreover, some difference between the mechanism causing pressure drop in the swirling flows in vortex throttles and in pipe flows will be presented.

Pressure drop or pressure loss is actually an energy loss from the point of view of energy conservation. In the case of swirling flows in vortex throttles, pressure

drop (energy loss) occurs mainly through the axial port by dissipating the high tangential velocity and depends on several factors. This will be discussed as follows:

In the vortex chamber there is a small amount energy loss due to wall friction and viscous dissipation although a large pressure gradient exists because of centrifugal force. The total pressure, $P_{total} = P + \frac{W^2}{2}$(radial and axial velocities are negligible), is almost constant. However, outside of the axial port both tangential velocity and pressure are very low, as shown in Fig. 5.9 and Fig. 5.12, which means that a large amount of total pressure (energy) is lost through the axial port and at the exit of the axial port due to the sudden expansion. This indicates that higher tangential velocity near the axial port would lead to higher energy loss as tangential velocity decays very quickly. Therefore, any means to create a stronger vortex, resulting in higher tangential velocity, would increase the pressure drop. The ideal case is the free vortex as shown in Fig. 5.6, but this is impossible in reality due to the viscosity of fluids and wall friction. In normal pipe flows, increasing wall friction results in higher pressure drop but in the case under study increasing wall friction in the vortex chamber would reduce the vortex strength, resulting in lower tangential velocity and hence lower pressure drop.

Energy is mainly lost through the axial port due to wall friction of the port and due to the viscous interaction in the fluid because of the sudden expansion at the outlet of the axial port as well as interaction with the recirculation flow along the axis. This may be verified by Fig. 5.16 which shows contours of turbulent

kinetic energy disspation rate. It can be seen from the contours that turbulent kinetic energy is mainly dissipated through the axial port. One may infer that the mean kinetic energy is also largely dissipated through the axial port due to wall friction of the port and the sudden expansion. This means that pressure drop across vortex throttles mainly occurs through the axial port. Therefore the design of the axial port is very crucial, and the wall of the axial port should be made as rough as possible so as to get higher wall friction. However, the wall of the vortex chamber should be made as smooth as possible in order to reduce energy loss in the vortex chamber and hence increase the vortex strength.

The mechanism of turbulence tells us that turbulence extracts energy from the mean motion by various means such as shear stress, buoyancy and other ways. Larger eddies formed initially decay into smaller ones until the viscous action becomes very important and turbulent kinetic energy is then dissipated. This is essentially irreversible process. Applying this mechanism to the swirling flows in vortex throttles, it can be concluded that turbulence influences pressure drop by way of extracting energy from mean motion in the vortex chamber, which reduces the vortex strength and hence lowers the tangential velocity near the axis. This is illustrated further by Fig. 5.9 which shows turbulent kinetic energy predicted by the Reynolds stress model and the k-ϵ model respectively. It can be seen that much higher turbulent kinetic energy in the chamber has been predicted by the k-ϵ model, which agrees with a slightly lower pressure drop predicted by the k-ϵ model as compared with the Reynolds stress model.

In conclusion, increasing any energy loss in the vortex chamber would lead to

the reduction of the vortex strength and hence lower tangential velocity, consequently, lower pressure drop. Whereas increasing energy loss through the axial port and out of it would result in higher pressure drop.

In some applications it would be useful to exploit the high centrifugal force and tangential velocity created within a vortex, without the penalty of the high overall pressure loss. This would require recovery of the vortex energy, as opposed its dissipation in the throttle. Turbulence usually extracts energy from the mean flow and dissipates it by viscous action, which is against this objective. However, turbulent kinetic energy is, in most situations, very small compared with the total kinetic energy and in our case, the Reynolds stress model predictd the turbulent kinetic energy in the chamber to be only about 3.5%. of the total kinetic energy. Therefore, Significant energy recovery would be possible if viscous losses due to the axial recirculation, the sudden expansion of the axial port, and friction losses within the port, could be minimised.

5.8 Conclusions

Both the widely used two equation k-ϵ model and a more complicated Reynolds stress model have been employed to simulate numerically the strongly swirling confined turbulent flows in vortex throttles. The influence of the inlet swirl intensity, inlet Reynolds number, and inlet turbulence intensity on the flow field have been analyzed. Several conclusions may be reached.

The wall shear stresses greatly influence the performence of vortex throttles,

and careful modelling in the near wall region leads to better results.

The conventional k-ϵ model gives relatively poor predictions compared with measured pressure drop and fails to predict higher measured pressure drops in a 76mm diameter vortex throttle as compared with a 102mm one.

The Reynolds stress model gives better predictions than the conventional two equation k-ϵ model for the highly swirling flows, producing good agreement with measured pressure drop data and successfully predicting the better performance of the 76mm throttle.

The turbulent kinetic energy predicted by the conventional k-ϵ model in the vortex chamber is much higher than that predicted by the Reynolds stress model. This explains why the Reynolds stress model predicts higher pressure drops since the vortex is stronger if turbulent kinetic energy is lower as discussed before.

The swirl intensity can be equally used as the swirl number to characterize the flow field in vortex throttles. Numerical experiments showed that the flow field changed enormously when the inlet swirl intensity reduced, and all the re-circulating flow in the high inlet swirl intensity disappeared when the inlet swirl intensity reduced to one.

The inlet Reynolds number influences mainly the flow field in the vortex chamber. The recirculation zone reduces when the inlet Reynolds number increases and it disappears completely when the inlet Reynolds number is above approximately 14600 according to the predictions.

The inlet turbulence intensity has little influence on the overall predictions. This was shown when the inlet turbulence intensity was changed from 1% to 30%

since the mean variables hardly changed.

The pressure drop through vortex throttles differs from that in pipe flows due to the mechanism of swirl conservation. It depends on mainly dissipating the high tangential velocity created in the vortex chamber through the axial port. Therefore, any means to produce higher tangential velocity can result in higher possible pressure drop.

Design of the axial port of throttles is very important as energy is mainly dissipated through the axial port. In addition, the walls of the vortex chamber should be made as smooth as possible so as to get higher tangential velocity, and the walls of the axial port should be made as rough as possible in order to dissipate energy as much as possible.

Two mesh sizes were used for one imcompressible flow case (30*30, 45*45), and it was found that the difference between the results was negligible (discrepancy within 3%). This means that the predicted results are grid independent and therefore, all the predicted results were obtained using a 30*30 grid.

In all the predictions, step grids were used to simulate different geometries.

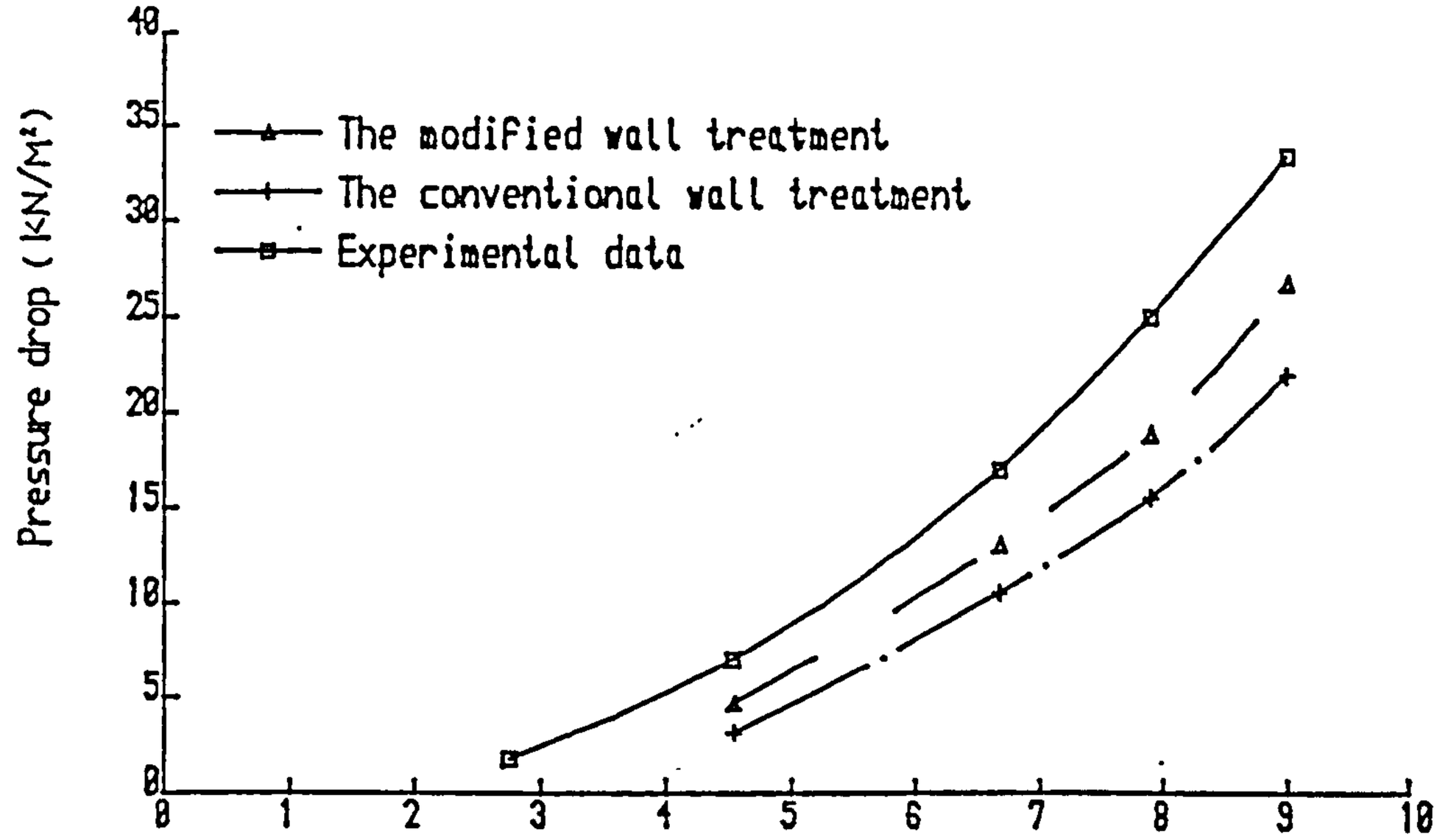

Fig. 5.2 Comparison between measured and predicted pressure drop by the K-E model using both the conventional wall and the modified wall treatment fot the 76mm throttles.

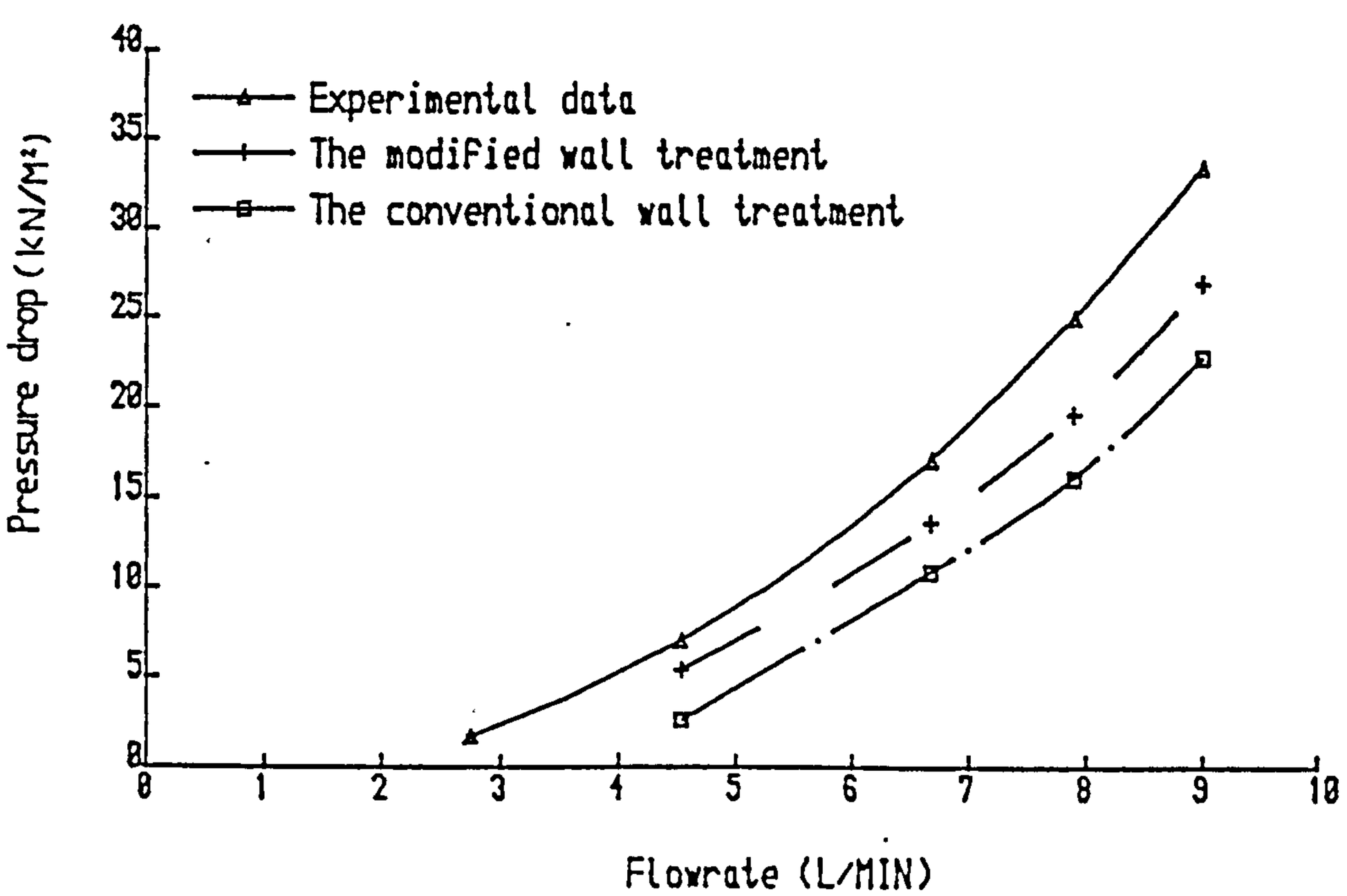

Fig. 5.3 Comparison between measured and predicted pressure drop by the K-E model using both the conventional wall and the modified wall treatment for the 102mm throttle.

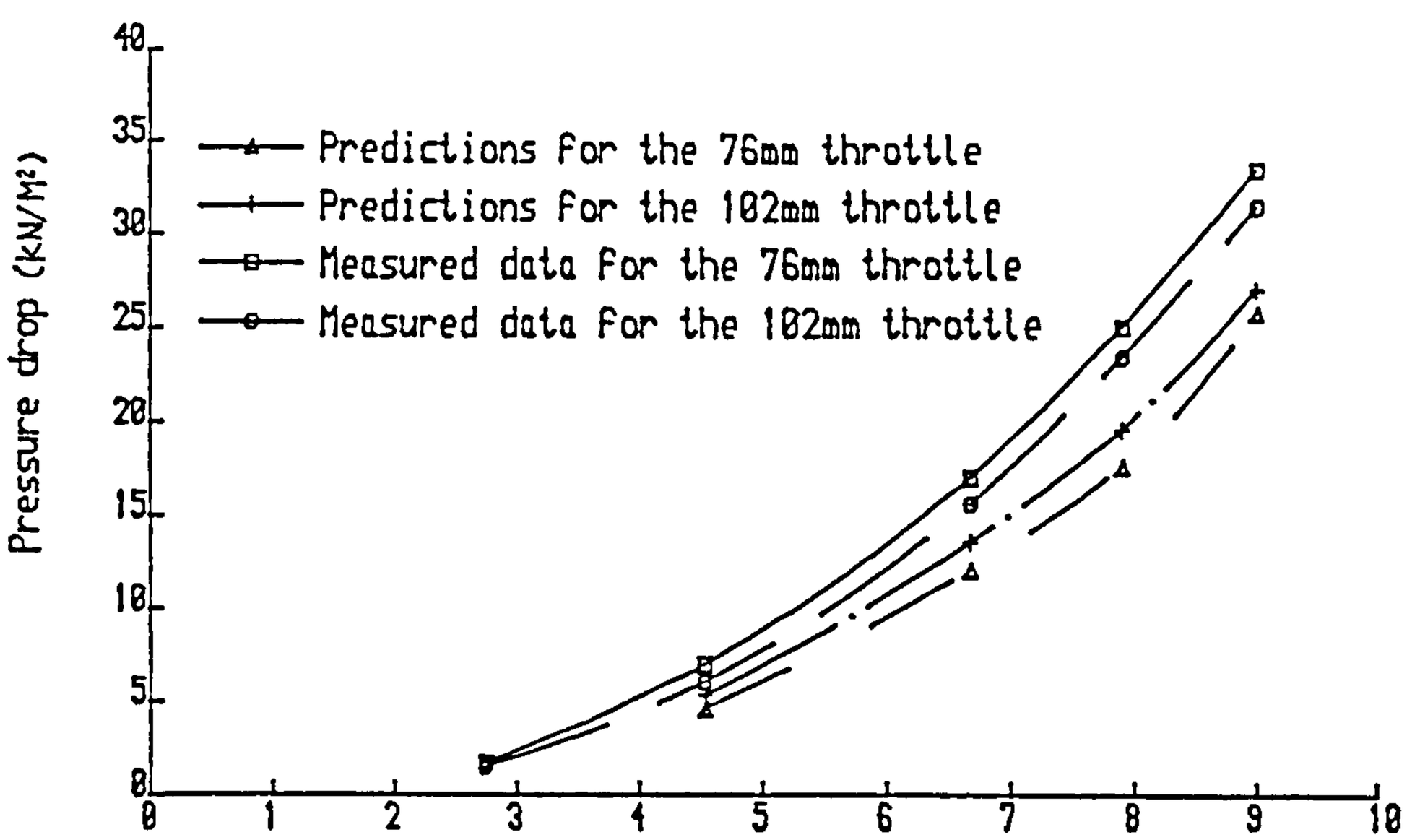

Fig. 5.4 Comparison between measured and predicted pressure drop by K-E model for both the 76mm and 102mm diameter vortex throttles

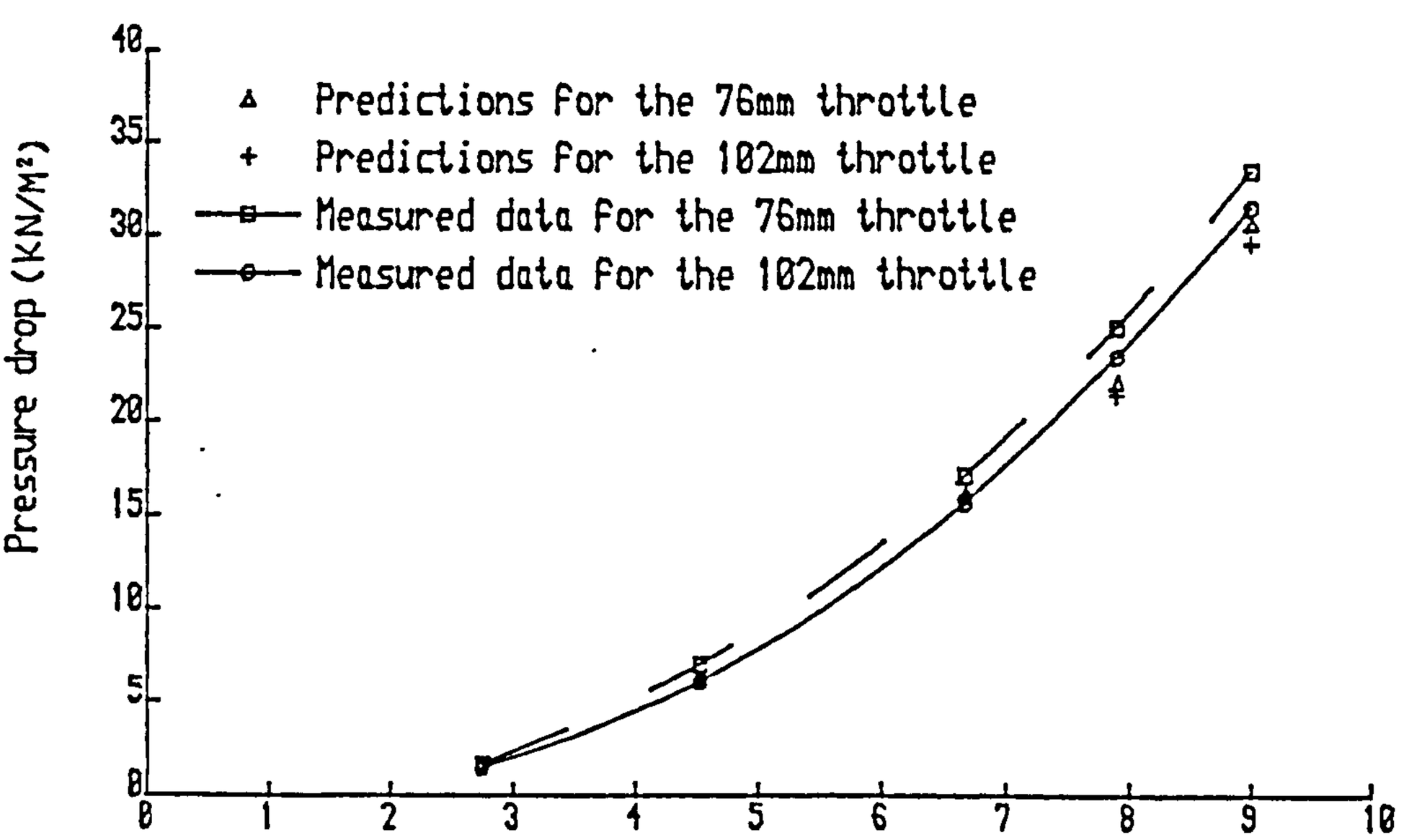

Fig. 5.5 Comparison between measured and predicted pressure drop by the Reynolds stress model for both the 76mm and 102mm diamete vortex throttles.

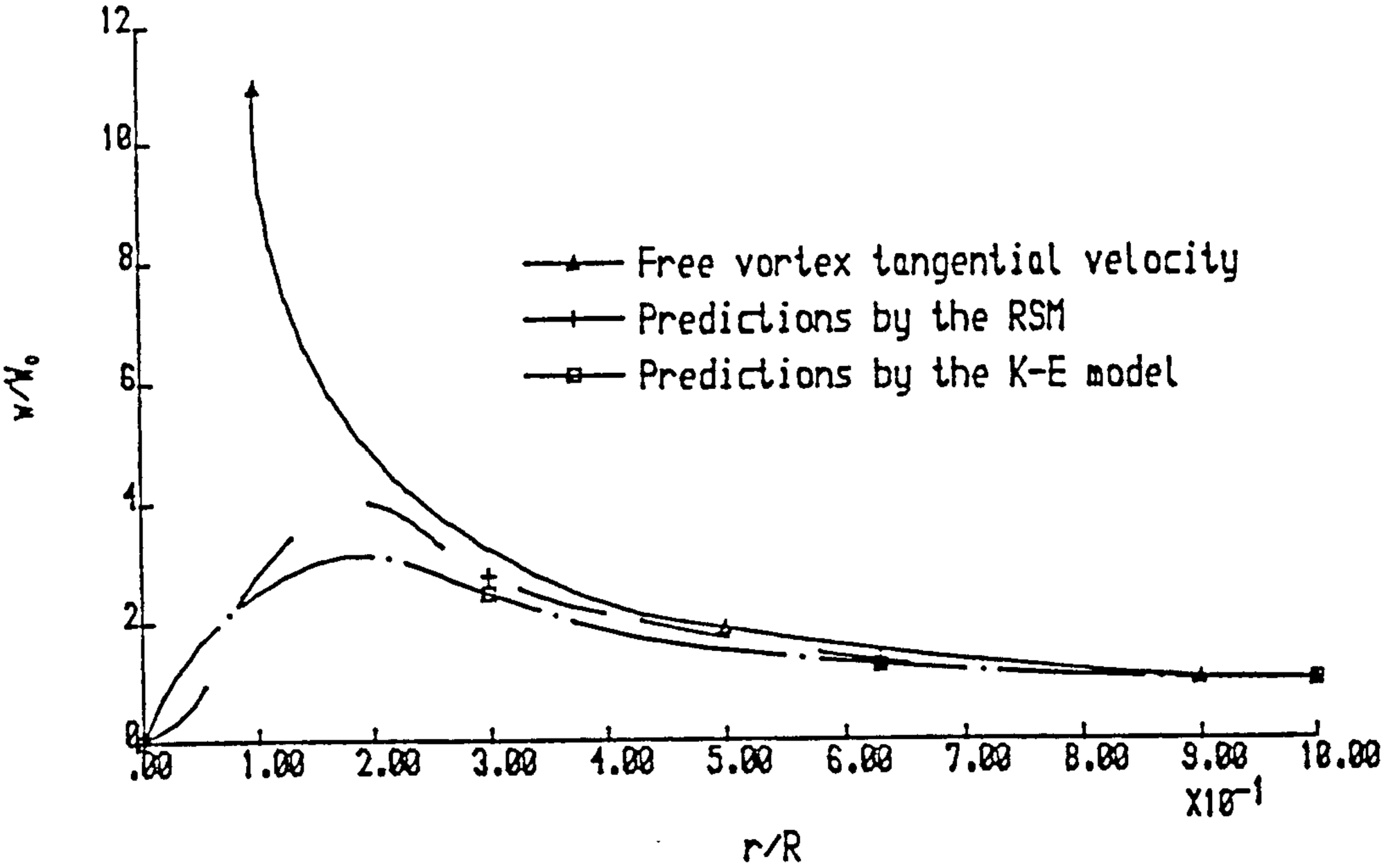

Fig. 5.6 Comparison between the ideal free vortex tangential velocity profile and the predictied profiles in the 102mm vortex chamber at x/R=0.065.

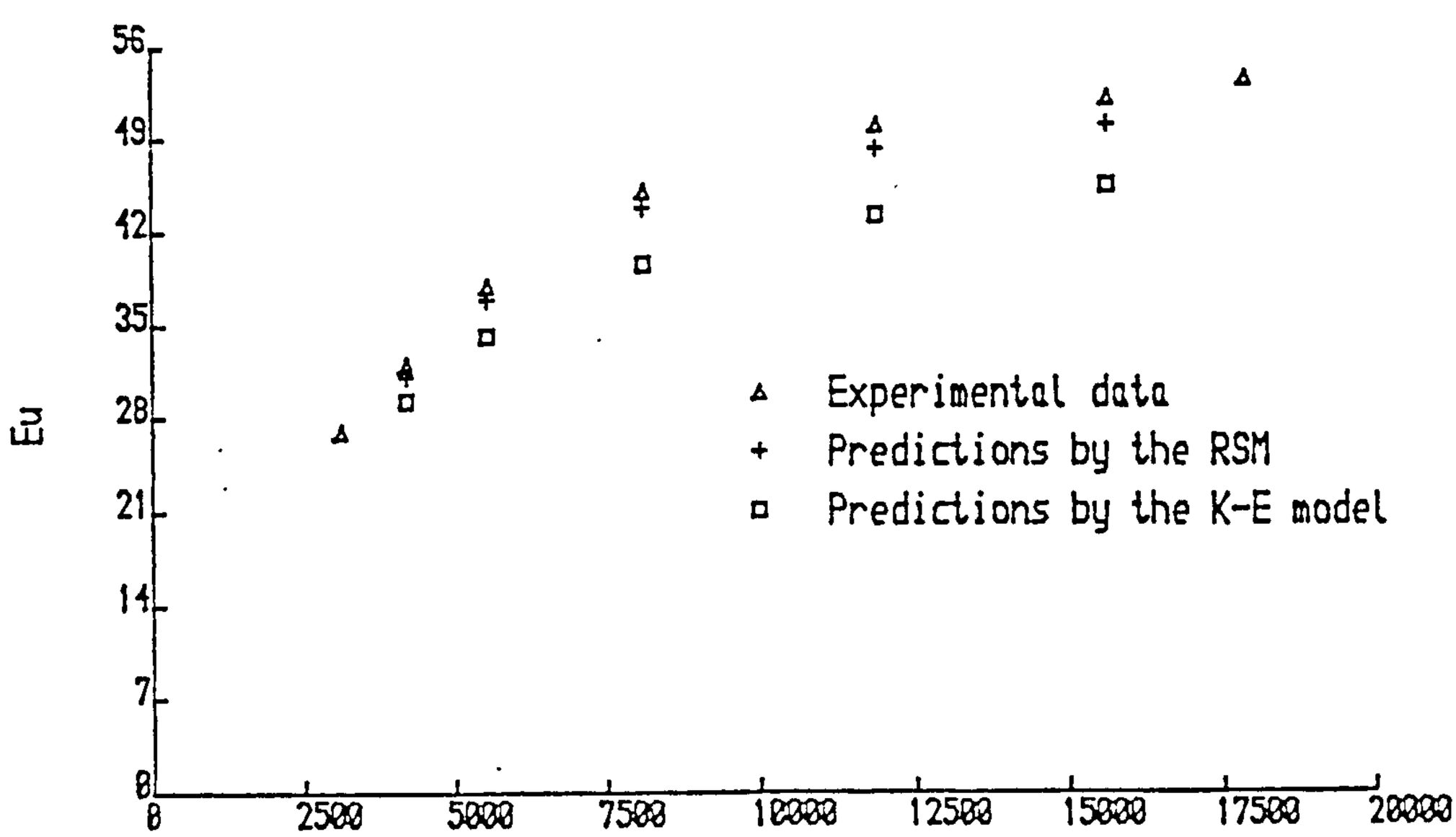

Fig. 5.7 Comparison between experimental and the predicted Euler number against Reynolds number for the 102mm throttle by both the Reynolds stress and the K-E models.

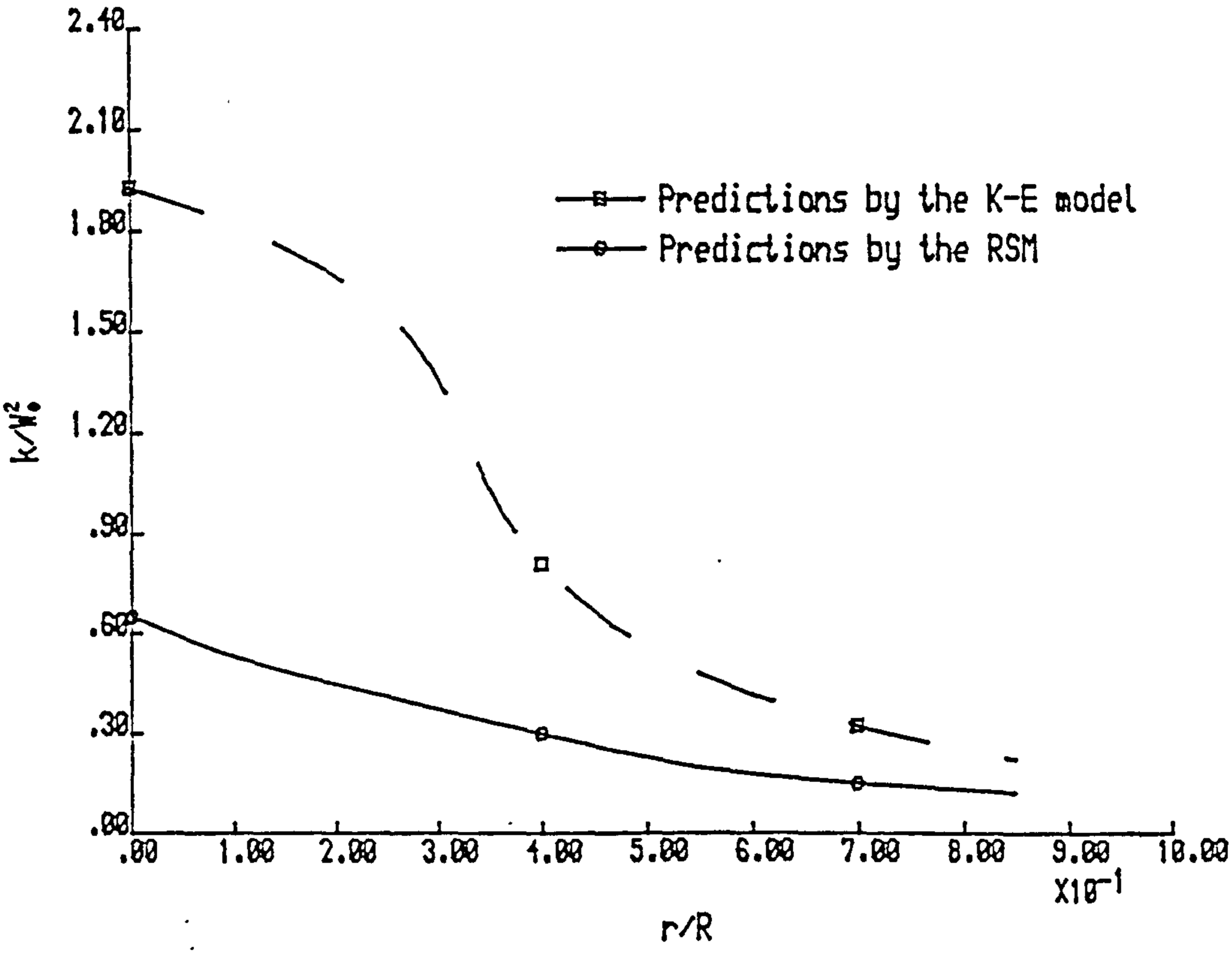

Fig. 5.8 Turbulent kinetic energy profiles in the 102mm vortex chamber predicted by the RSM and the K-E model respectively at x/R=0.065.

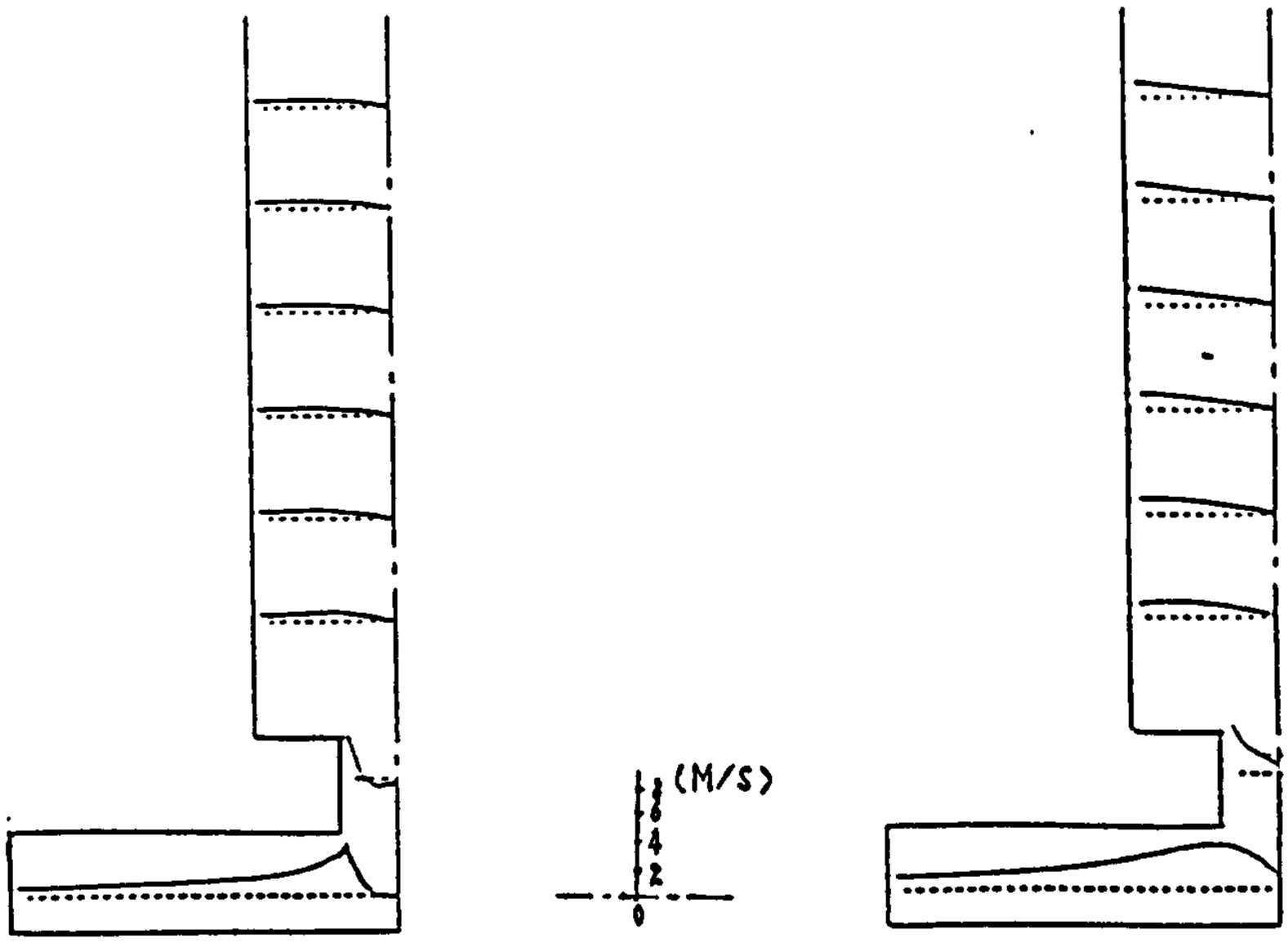

The RSM predictions The K-E predictions

Fig. 5.9 The tangential velocity profiles predicted by both models in the 102mm throttle at Re=11078.

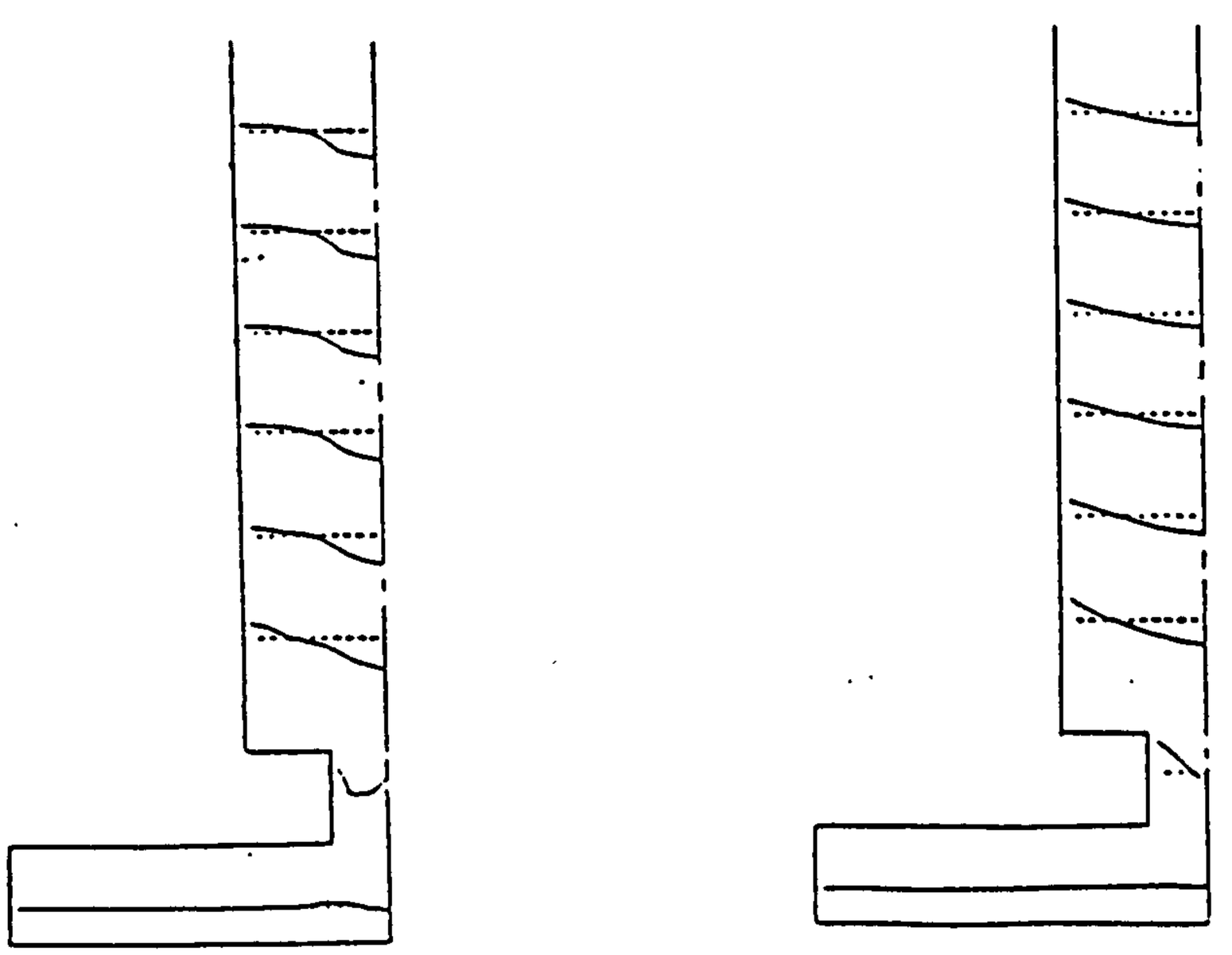

The RSM predictions The K-E predictions

Fig. 5.10 The axial velocity profiles predicted by both models in the 102mm throttle at Re=11078.

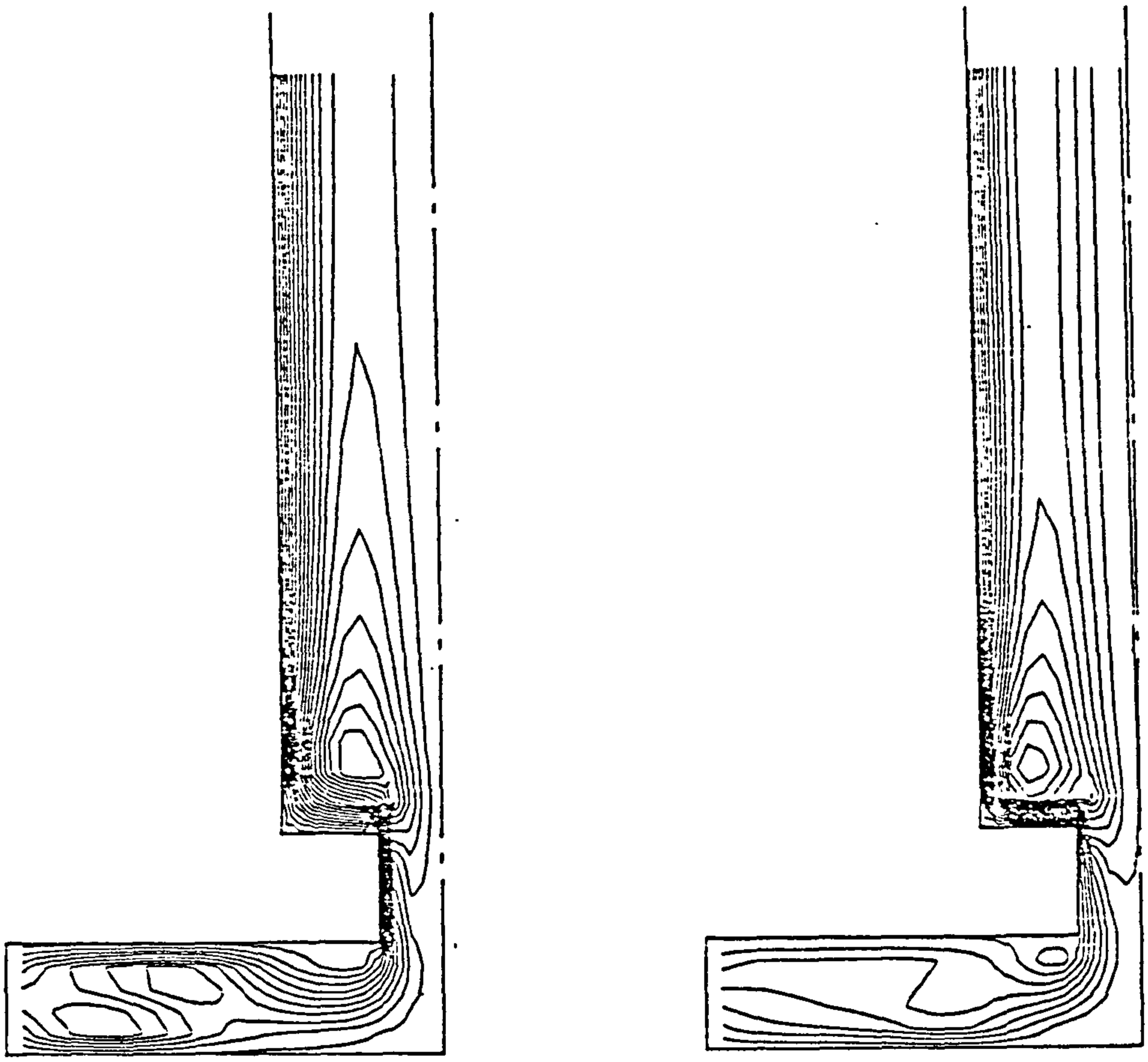

The RSM predictions

The K-E predictions

Fig. 5.11 The streamlines predicted by both models
in the 102mm throttle at Re=11078

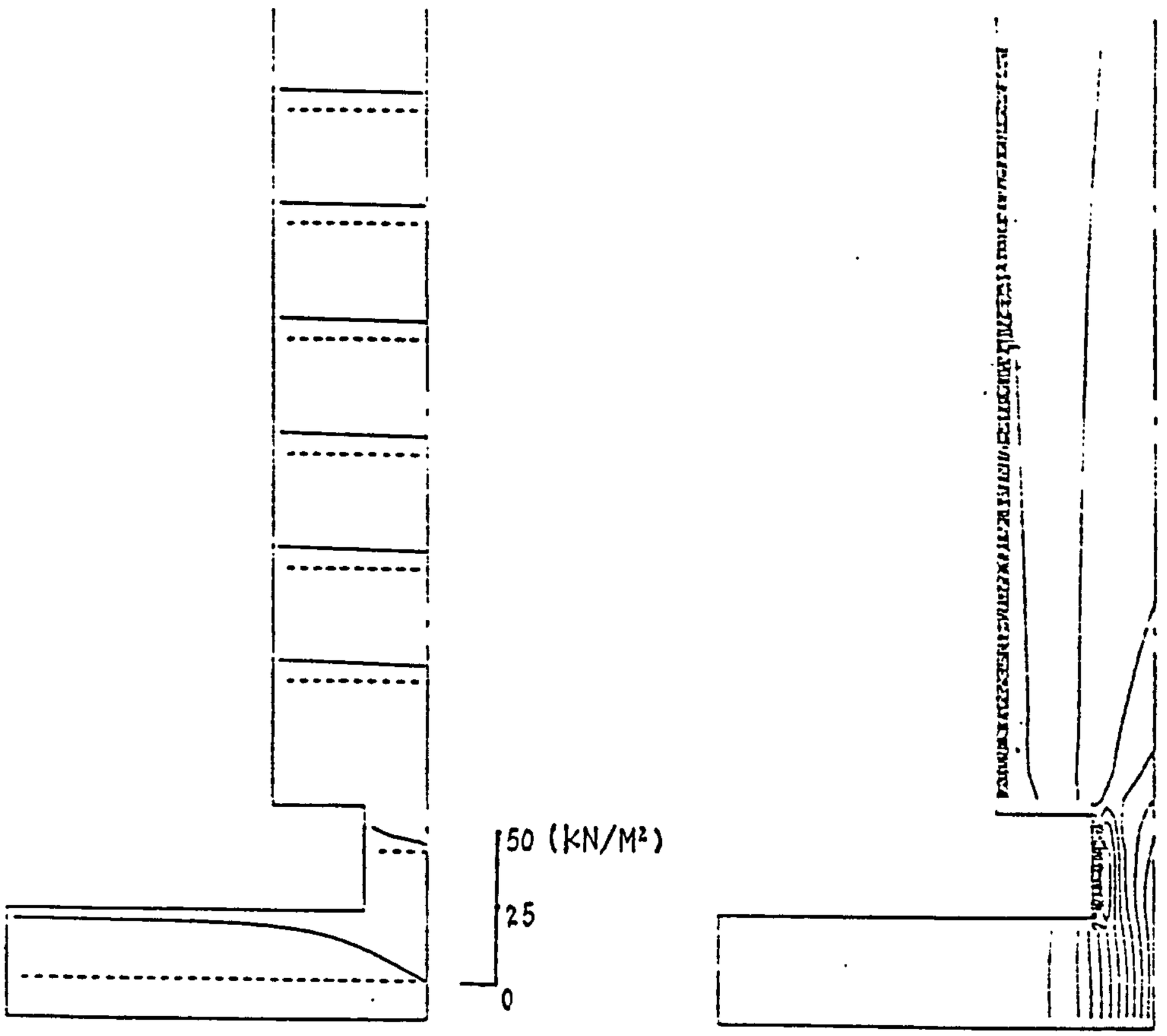

Profiles

Contours

Fig. 5.12 The pressure profiles and contours predicted by the Reynolds stress model in the 102mm throttle at Re=11078

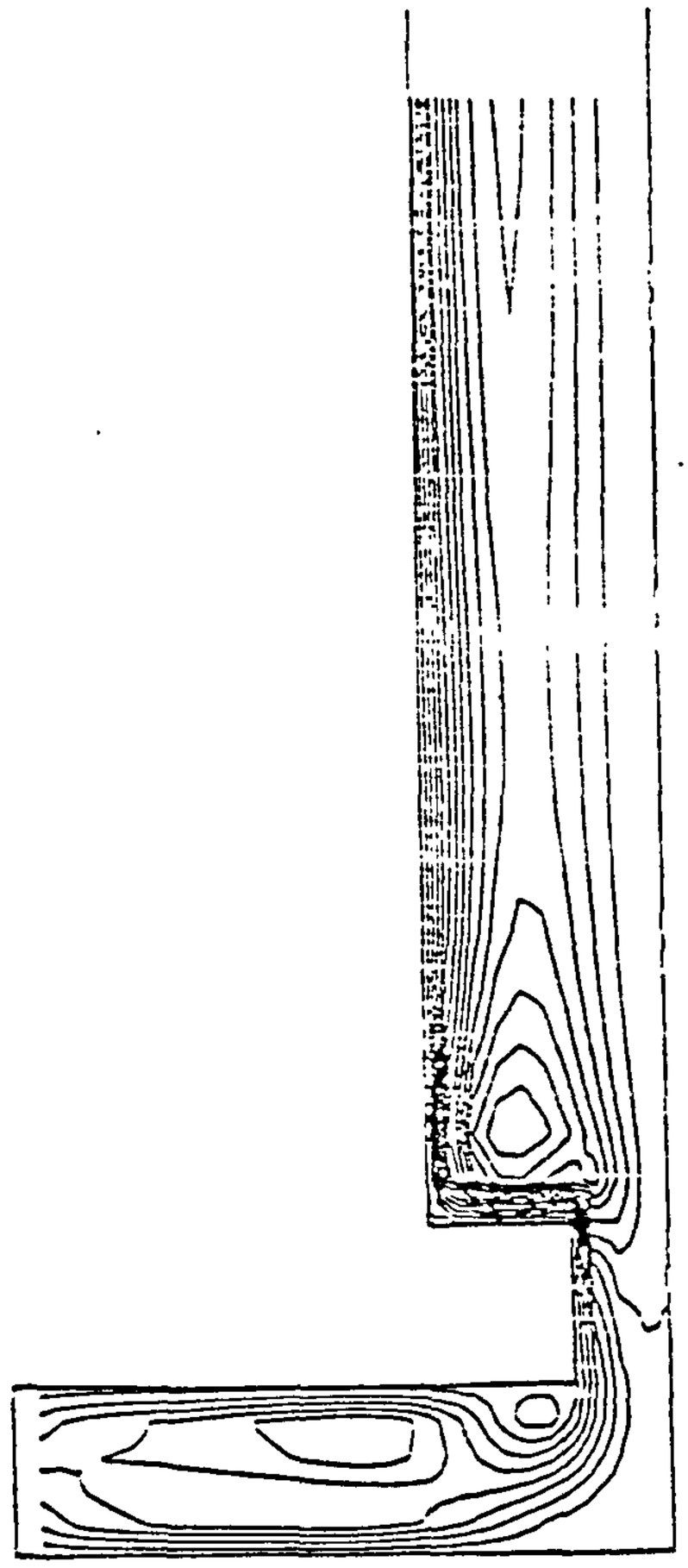

The streamlines

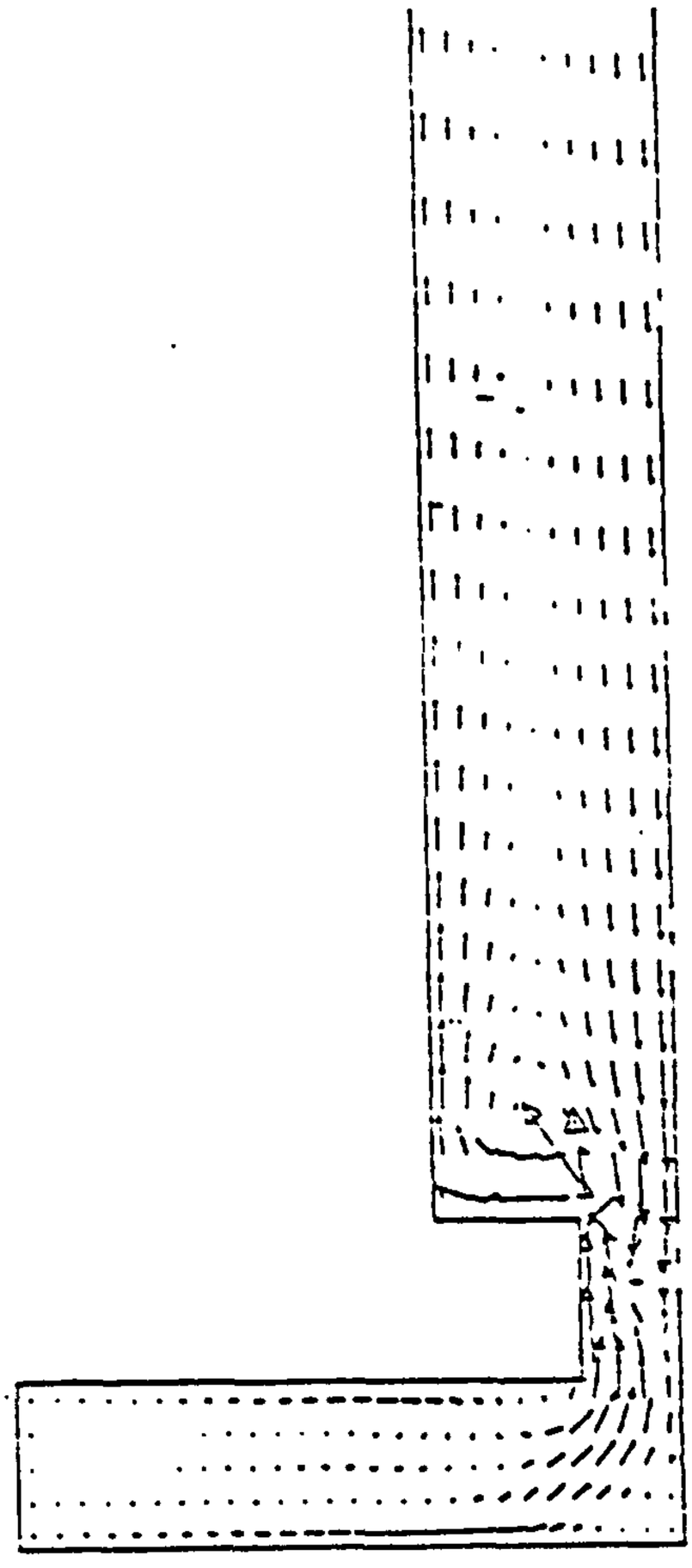

The velocity vectors

Fig. 5.13 The streamlines and velocity vectors predicted by the K-E model in the 102mm throttle at Re=5565.

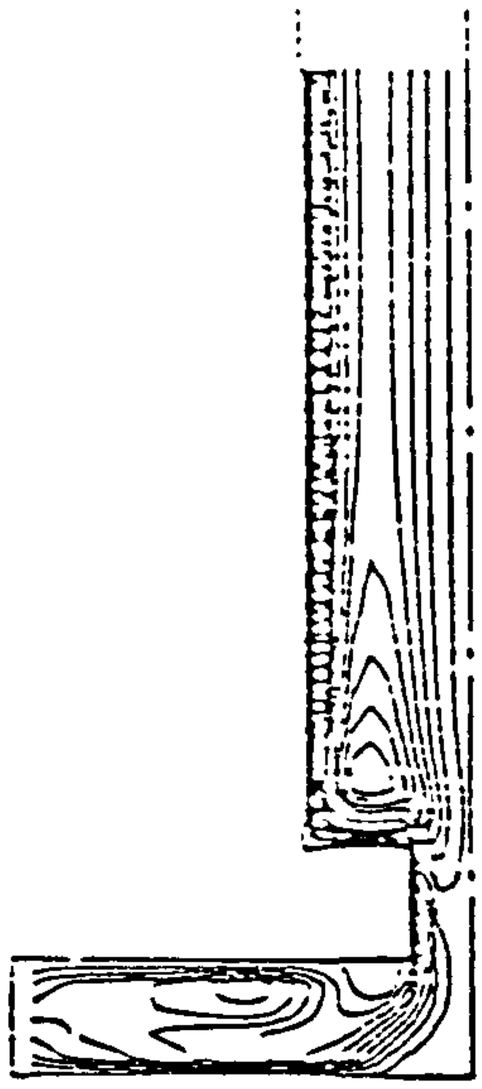

Re=3385

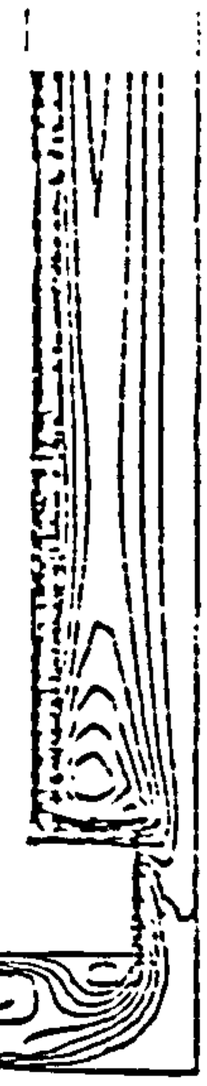

Re=5565

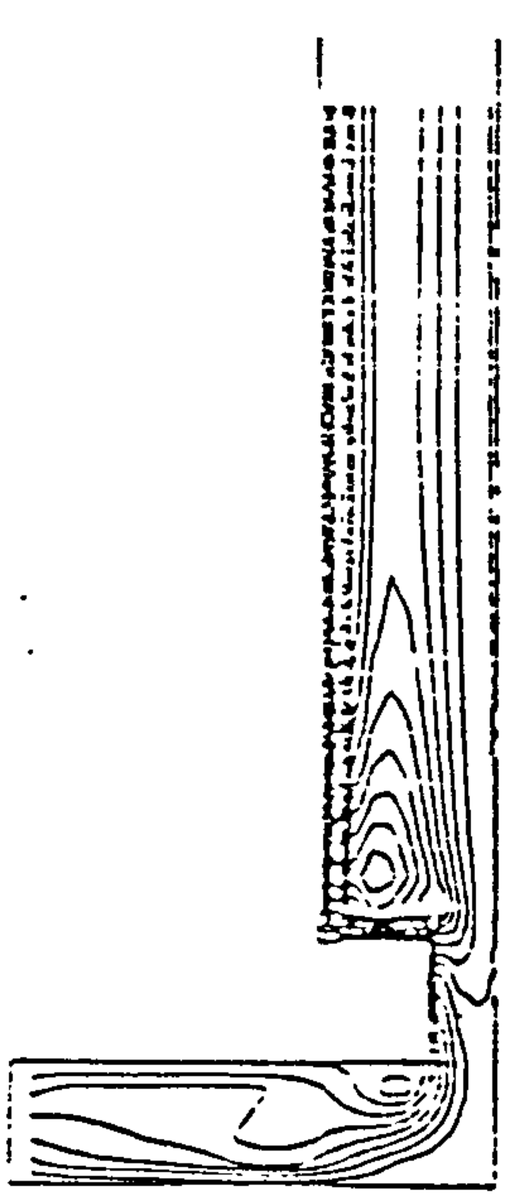

Re=11078

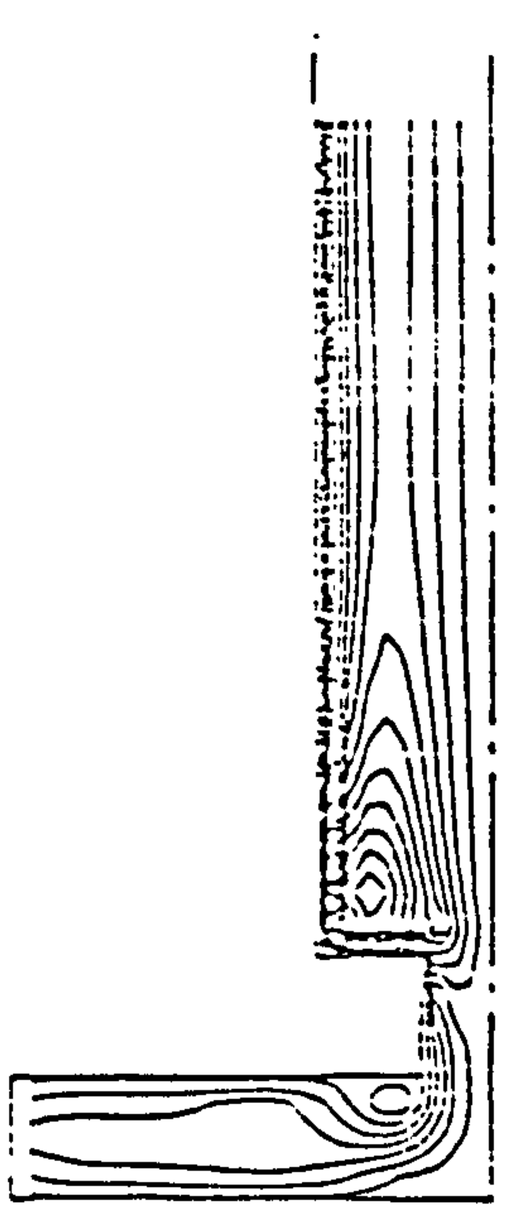

Re=14600

Fig. 5.14 The streamlines predicted by the K-Ξ model in the 102mm throttle at different Reynolds numbers.

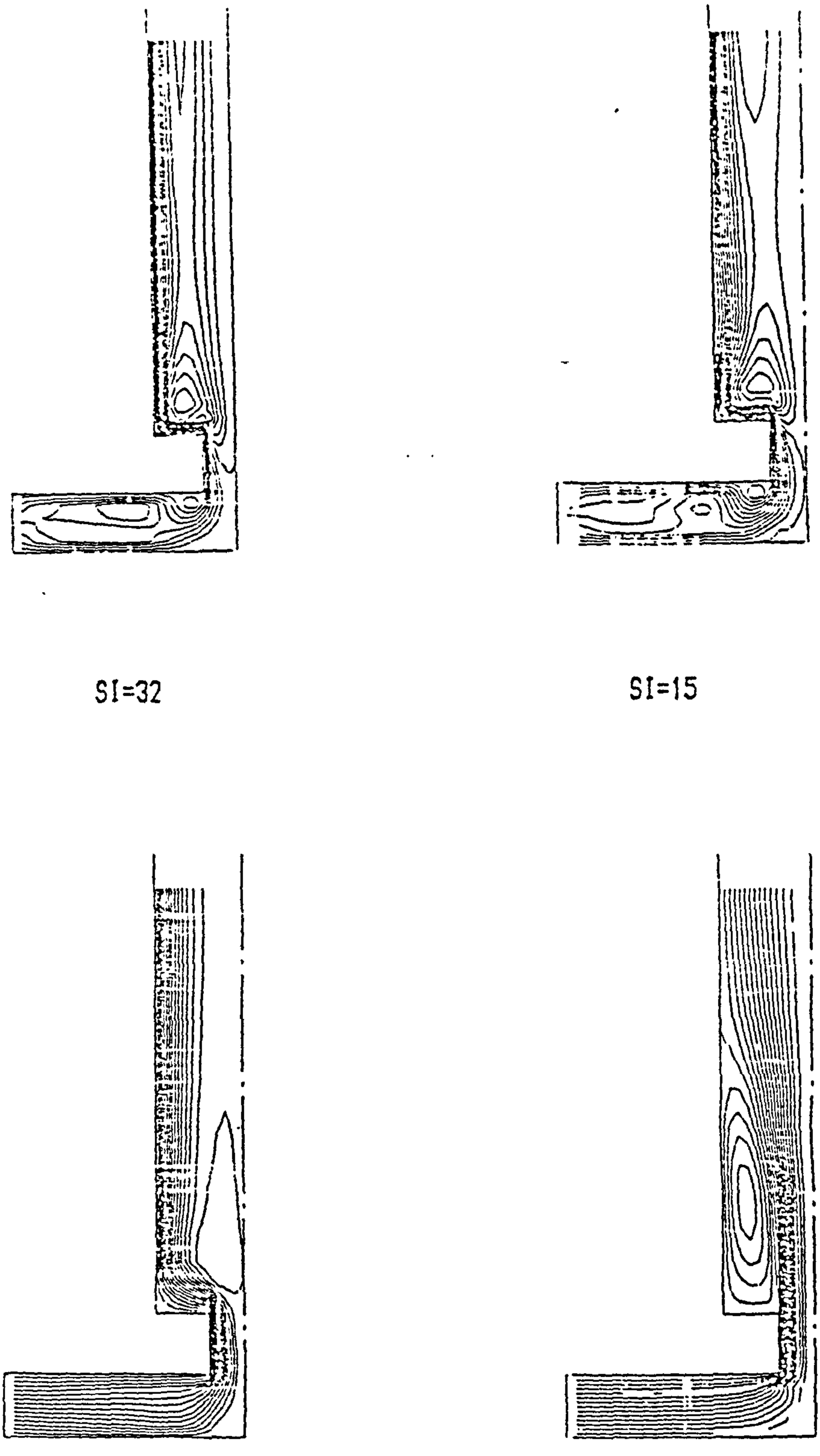

SI=32 SI=15

SI=5 SI=1

Fig. 5.15 The streamlines predicted by the K-E model in the 102mm throttle at different inlet Swirl Intensity (SI)

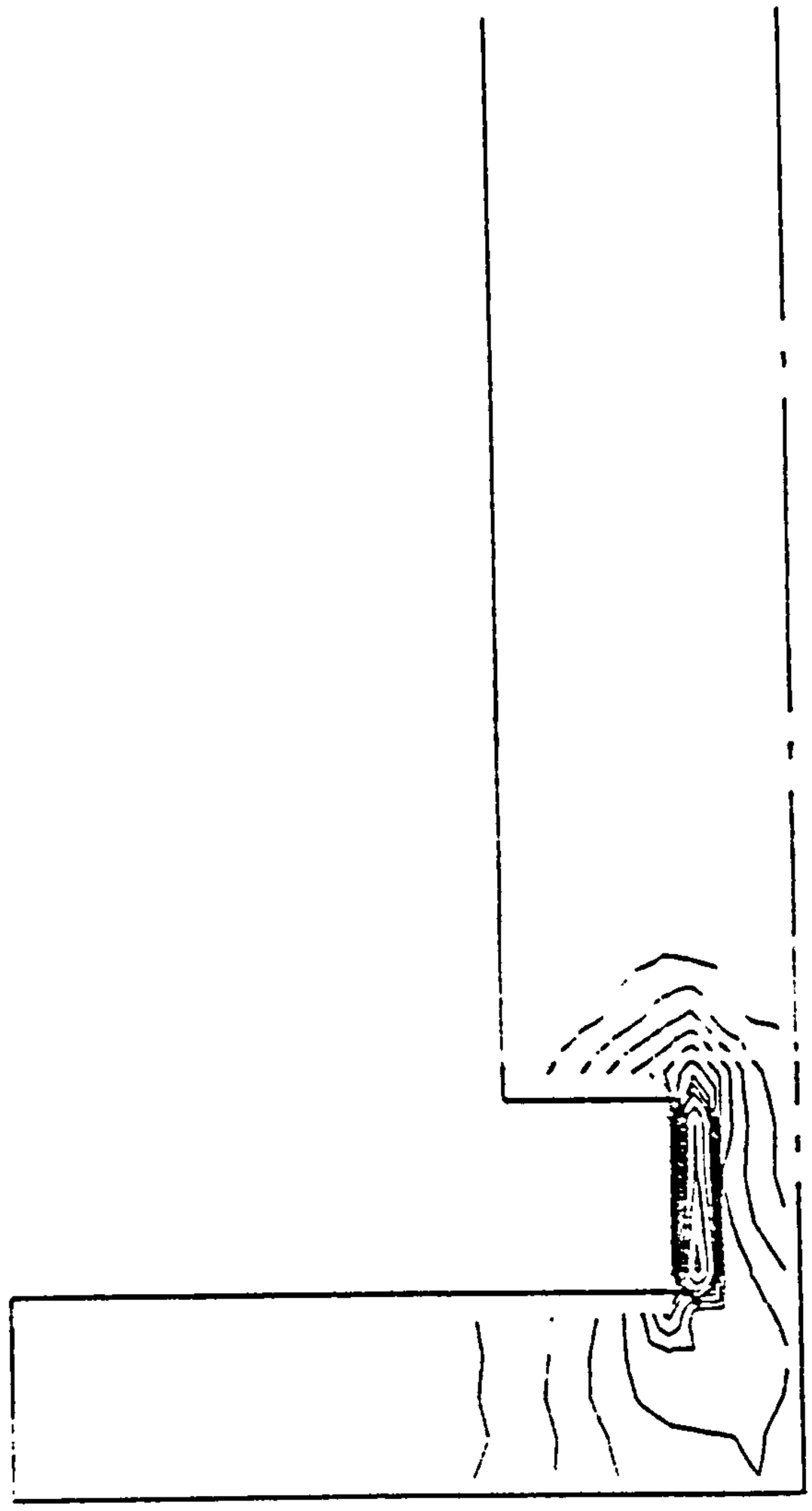

Fig. 5.16 The contours of turbulent kinetic energy dissipation rate predicted by the RSM in the 102mm throttle at Re=11078.

Chapter 6

APPLICATIONS TO COMPRESSIBLE FLOWS

In this chapter, the prediction procedure is applied to steady compressible subsonic, transonic and supersonic flows. The prediction procedure is tested for accuracy against known analytical solutions for inviscid subsonic, transonic and supersonic flows in convergent and divergent nozzles. The accuracy of this numerical scheme is further assessed by comparing the results with those obtained using Godunov first and second-order methods (104) for two dimensional subsonic, transonic and supersonic flows in a channel with a circular arc bump. This problem was selected as a test case for a workshop (105) and since then has become a standard test problem. The prediction procedure has also been applied to a more severe case, i.e., supersonic flow behind a rearward-facing step where a recirculating subsonic flow region is embedded.

The results obtained clearly indicate that the prediction procedure is able to

handle laminar subsonic, transonic and supersonic flows. However, when compressible turbulent flows are considered additional problems related to the modelling of turbulence may arise so that turbulent flows are not considered as test problems in the present study.

6.1 Governing Equations

The governing equations employed are the two dimensional Navier-Stokes equations which, in the case of inviscid flows, are actually the Euler equations. In addition, the energy equation and the state equation are also needed. The governing equations have already been presented in chapter three, and they can be found in many textbooks and articles (2, 25, 58, 59, 60, 106).

6.2 Convergent and Divergent Nozzle Flows

The convergent and divergent nozzle flows were selected as the first test problem mainly because the analytical results are available for comparison with the numerical solutions. Moreover, the flow fields are relatively simple so that the accuracy of the numerical scheme can be assessed more correctly from the comparison between the analytical results and the numerical solutions, and confidence can be gained from this about the capability of the prediction procedure to handle subsonic, transonic and supersonic flows.

6.2.1 Analytical Solution

It is assumed that the flow in nozzles is one dimensional, steady and isentropic when the analytical method is used. Therefore, the following relations can be obtained (106)

$$\frac{T^*}{T} = 1 + \frac{(\gamma - 1)}{2} M^2 \tag{6.1}$$

$$\frac{P^*}{P} = \left[1 + \frac{(\gamma - 1)}{2} M^2\right]^{\frac{\gamma}{\gamma - 1}} \tag{6.2}$$

$$\frac{\rho^*}{\rho} = \left[1 + \frac{(\gamma - 1)}{2} M^2\right]^{\frac{1}{\gamma - 1}} \tag{6.3}$$

where M is the Mach number, γ is the specific heat ratio which is usually taken to be 1.4, T^*, P^*, ρ^* are the local reservoir values or stagnation values. Mach number is defined as follows:

$$M = \frac{U}{a} \tag{6.4}$$

where U is the velocity, and a is the local sound velocity which can be obtained by the following relation

$$a = \sqrt{\gamma RT} \tag{6.5}$$

where R is the gas constant which is 287 $\frac{m^2}{s^2 K}$ for air. Moreover, if the throat of a nozzle becomes sonic then the area-Mach number relation is found to be (106)

$$\left(\frac{A}{A^*}\right)^2 = \frac{1}{M^2}\left[\frac{2}{\gamma + 1}\left(1 + \frac{\gamma - 1}{2} M^2\right)\right]^{\frac{\gamma + 1}{\gamma - 1}} \tag{6.6}$$

where A^* is the throat area. Therefore, once a nozzle geometry is specified, all the variables along the nozzle can be obtained from the above relations.

6.2.2 Numerical Solution

Calculations of the inviscid subsonic, transonic and supersonic nozzle flows were performed assuming two dimensional axisymmetrical flows with the tangential velocity equal to zero. In addition, the stagnation enthalpy was constant as inviscid and adiabatic flows were assumed so that there was no need to solve the energy equation.

The stagnation values were taken to be

$$T^* = 303 \qquad K \tag{6.7}$$

$$P^* = 100000 \qquad N/m^2 \tag{6.8}$$

The inlet conditions could be worked out by the relations presented in the section on the analytical solution. They are given as follows:

For the subsonic and transonic flows

$$M_{in} = 0.24 \tag{6.9}$$

$$P_{in} = 96070 \qquad N/m^2 \tag{6.10}$$

$$T_{in} = 300 \qquad K \tag{6.11}$$

$$U_{in} = 83.3 \qquad m/s \tag{6.12}$$

For the supersonic flow

$$M_{in} = 1.17 \tag{6.13}$$

$$P_{in} = 42870 \qquad N/m^2 \tag{6.14}$$

$$T_{in} = 238 \qquad K \tag{6.15}$$

$$U_{in} = 361.8 \qquad m/s \tag{6.16}$$

Geometry of Nozzles

Fig. 6.1 shows the geometry of the nozzles used in this study. The subsonic flow is obtained in the convergent nozzle, the supersonic flow is produced in the divergent nozzle and the transonic flow is created in the convergent and divergent nozzle by specifying appropriate inlet and outlet boundary conditions. The details of dimensions are given in millmeters as follows:

The convergent nozzle

$D_1 = 31.6$ $D_2 = 20$ $L = 35$

The convergent-divergent nozzle

$D_1 = 31.6$ $D_2 = 20$ $L = 70$

The divergent nozzle

$D_1 = 20.22$ $D_2 = 31.6$ $L = 35$

Boundary Conditions

Proper specification of the boundary conditions is a crucial aspect in computing compressible flows. There are, unfortunately, only a few cases where mathematical theory can tell us what boundary conditions should be imposed so as to ensure the uniqueness of the solution. Hence, boundary conditions for compressible flows are usually treated in a heuristic way. Nevertheless, an FDE solution with mathematically inconsistent boundary conditions may still give an approximation to the PDE.

The wall and symmetry boundary conditions for compressible and incompressible flows are more or less the same, and they are fully discussed in reference

(2). Therefore, the discussion here will focus on the inlet and outlet boundary conditions for not only the nozzle flows but also for compressible flows in general.

Inlet Boundary

It is generally accepted that if the inflow is supersonic, all the variables must be specified at the inlet boundary. However, when the inflow is subsonic, there are different choices as to which variables are specifi ed. For a two dimensional subsonic flow, the system of partial differential equations requires three boundary conditions (107). In addition, the numerical methods need a fourth boundary condition. There are, therefore, basically two ways of specifying the inlet boundary conditions. One is to specify three boundary conditions which are usually the velocity components along with either density or temperature, and the fourth boundary condition is extrapolated (107). Another is to specify the inlet boundary conditions completely (2, 107). This is a stable boundary condition and stated as overspecification of the inlet boundary in (107). Nevertheless, most of the published two dimensional compressible flow computations have adopted this method. More detailed discussion is given in (107).

In the present study of subsonic nozzle flow, the stagnation pressure, the stagnation temperature, the inlet Mach number and the inlet flow angle were given so that the inlet velocity components, inlet density and inlet temperature could be worked out using the relations presented in the section on the analytical solution. The inlet boundary conditions were specified completely in the present calculations.

Outlet Boundary

For a two dimensional subsonic outflow boundary, the partial differential equations require one boundary condition and the numerical solution requires three additional boundary conditions. Usually, the static pressure is specified and other variables are extrapolated. However, in some cases, when nothing is available at the outlet boundary, all variables have to be extrapolated. This is not correct mathematically and it was pointed out in (107) that the steady-state solution depended strongly on the initial flow field. Detailed discussion about the subsonic outflow boundary conditions is given in (107).

In the present study of the subsonic nozzle flow, density was specified at the outlet boundary. The axial velocity was adjusted until the overall mass flowrate was satisfied. Other variables were extrapolated.

For supersonic flow, there is a general point that outlet boundary conditions are not important if the outflow is supersonic since supersonic flow limits the upstream effect. However, this is incorrect as argued by Roache (2), and the present author, having some experience in supersonic computations, agrees with Roache's arguments. As stated by Roache (2); if the boundaries had no effect at all, it would be impossible to "turn off "an indraft supersonic wind tunnel. It is also stated in (2) that the downstream outflow problem is more important in supersonic flow than in subsonic flow. The above statements are not difficult to understand when one considers quasi-one-dimensional inviscid flow in the convergent-divergent nozzle as shown in Fig. 6.1, where the inlet boundary conditions are fixed. The back pressure can have great influence on the flow pattern in the nozzle. When the outflow is already supersonic, a reduction in the back

pressure will not be felt upstream. However, if the back pressure is raised, a shock wave will move into the nozzle, its final position depending on the back pressure. If the back psressure is further raised above a critical value, the flow will become subsonic through the whole nozzle. Therefore, in Crocco's (108) calculation of quasi-one-dimensional flow in a duct, two downstream variables, pressure and temperature, had to be specified to approach a steady solution. Benison and Rubin (109) also had to fix density at the outflow boundary in their quasi-one-dimensional calculations. More detailed discussion is given in (2).

In the present study, it has been found that at least one variable, either static pressure or density, has to be specified at the outlet boundary, and in the calculation, density was fixed at the supersonic outflow boundary. Other variables were extrapolated and the axial velocity was adjusted to satisfy overall mass conservation.

6.2.3 Results and Comparison

When the numerical solutions are compared with the one dimensional analytical results, the average value of the numerical solutions at each x location is taken. This is because the numerical solutions are two dimensional.

Subsonic Flow

Fig. 6.2 shows the predicted Mach number profile and the analytical result for the subsonic flow in the convergent nozzle. Two grid sizes were used to make sure that the solution is grid independent. It can be seen that very good agreement

between the predictions and the analytical solutions has been achieved, and the results obtained by different grids are almost the same. This means that the numerical solutions are independent of the grid size and the results are reliable in this respect.

Fig. 6.3 compares the predicted pressure profile with the pressure profile obtained by the analytical method for subsonic flow in the convergent nozzle. It can be seen from the figure that the agreement between the predictions and the analytical solutions is again very good. This indicates that the prediction procedure performs quite well for subsonic steady inviscid nozzle flow.

Transonic Flow

For the transonic and supersonic flows, only one grid size was used since the numerical solutions for the subsonic flow, as shown above, changed very little when different grid sizes were used.

Fig. 6.4 compares the predicted Mach number profile with the Mach number profile obtained by the analytical method for transonic flow in the convergent-divergent nozzle. Good agreement can be seen from this figure, however, near the throat where a transonic flow region exists, the predicted Mach number is a little bit lower than the analytical result. This may be partly due to the fact that the geometry is not simulated exactly since step grids were used instead of using body fitted coordinates, and partly due to the switch of the different numerical schemes for density evaluation.

Fig. 6.5 shows the predicted pressure profile and the pressure profile obtained

by the analytical method along the convergent-divergent nozzle. The agreement is, as can be seen from the figure, quite good overall apart from the near throat region where the predicted pressure is higher than that obtained by the analytical method. This corresponds to the prediction of the Mach number in this region discussed above.

Supersonic Flow

Fig. 6.6 compares the predicted Mach number profile with the analytical Mach number profile for supersonic flow in the divergent nozzle. As can be seen from the figure, generally good agreement has been reached but not as good as that for the subsonic flow. This may be attributed partly to the use of the step grids and partly to the reason that the prediction procedure cannot fully simulate the nature of supersonic flow as stated before.

Fig. 6.7 shows the predicted pressure profile together with the pressure profile obtained using the analytical method. Once again only a general good agreement has been achieved, which corresponds to the prediction of the Mach number as shown in Fig. 6.6.

Fig. 6.8 and Fig. 6.9 show the predicted velocity vectors in the convergent and the divergent nozzles respectively. It can be seen from the figures that the flows are almost one dimensional in both cases since the radial velocity is quite small compared with the axial velocity. This indicates that the assumption of one dimensional flow in the nozzles is very close to reality.

From the above results it can be said that the prediction procedure performs

quite well for the subsonic, transonic and supersonic steady inviscid nozzle flows. However, further tests in different flow situations should be made to assess the general validity of the prediction procedure.

6.3 Channel Flow

The second test problem chosen in this study is the two dimensional subsonic, transonic and supersonic flow in a channel with a circular arc bump on the lower wall. This problem was selected to assess the accuracy of the prediction procedure since it is a standard test problem as stated before, and it is well suited for computer code development and testing. In addition, there are results obtained by Godunov first- and second-order methods available for comparison with the present numerical solution.

6.3.1 Geometry of the Channel

Fig. 6.10 shows the channel used in the present study. It has a circular arc bump on the lower wall. The distance between the upper and the lower walls is equal to the chord length. The total length of the channel is three times the chord length. Two circular arc bump thickness-to-chord ratios were used in the study: 10% for the subsonic and transonic flow modelling, 4% for the supersonic flow modelling. Step grids were used to simulate the geometry of the circular arc bump.

6.3.2 Boundary Conditions

A detailed discussion on the boundary conditions for compressible flow has been presented in the previous section. It is argued that one variable should be specified at the outlet boundary for not only subsonic flow but also for supersonic flow if possible. For the flow considered here in the channel, at the inlet, the total temperature, the total pressure and the Mach number were specified. Density was specified at the outlet boundary. The axial velocity was adjusted until the overall mass flowrate was satisfied.

6.3.3 Results and Comparison

Fig. 6.11 compares the predicted Mach number profile with the results obtained by the first- and second-order Godunov methods (104) at the lower wall of the channel for subsonic flow. It can be seen from the figure that good overall agreement has been achieved. However, at around the mid-chord the prediction procedure overpredicted the Mach number by about 3%. This may be attributed to the use of the step grid to simulate the circular arc bump. Near the outlet, the present prediction is much closer to the results obtained by the second-order Godunov method compared with the first-order Godunov method.

The comparison between the present prediction and the results given by the first- and second-order Godunov methods at the upper wall of the channel is shown in Fig. 6.12. Very good agreement has been achieved as can be seen from the figure.

From Fig. 6.11, it could be said that the prediction procedure performed

better than the first-order Godunov method as the overall prediction is closer to the results by the second-order Godunov method. Nevertheless, at around the mid-chord the result given by the first-order Godunov method is closer to the result obtained from the second-order Godunov method. In addition, one can hardly distinguish the difference between the present prediction and the result of the first-order Godunov method from Fig. 6.12. Therefore, it is fair to say that the prediction procedure is only of first-order accuracy in the case of subsonic flow.

For transonic flow, the comparison between the present prediction and the results obtained by the first- and second-order Godunov methods at the lower wall and the upper wall of the channel are presented respectively in Fig. 6.13 and Fig. 6.14.

Fig. 6.13 shows the results at the lower wall of the channel. In this case, a supersonic flow region appears around mid-chord and is terminated by a shock at about two-thirds length of the chord. It is seen that the prediction procedure underpredicted the shock strength by about 8% compared with the second-order Godunov method. However, the results obtained by the first-order method agree very well with the present prediction. This indicates that in the case of transonic flow the prediction procedure is also of first-order accuracy.

Fig. 6.14 compares the present prediction with the results by the Godunov methods at the upper wall. As can be seen from the figure, the overall agreement between the prediction and the results obtained by the first-order Godunov method is better which confirms that the prediction procedure is of first-order accuracy.

Fig. 6.15 compares the prediction of Mach number with the results by the first- and second-order Godunov methods at the lower wall for the case of supersonic flow. In this case, there is an oblique shock wave at the leading edge of the circular arc bump. It can be seen from Fig. 6.15 that Mach number dropped suddenly at the leading edge which indicates that the oblique shock wave is predicted. However, the present prediction is rather poor compared with the results obtained by the second-order Godunov method but comparable with the results by the first-order Godunov method. At the end of the circular arc bump, i.e., at the trailing edge, a shock wave also exists. This can be also seen from the figure since there is another sudden drop of Mach number. The present prediction is again rather poor compared with the results by the second-order Godunov method and can only be comparable with those by the first-order Godunov method.

Fig. 6.16 presents the comparison at the upper wall of the channel for the same case. The results by the second-order Godunov method show a very sharp drop of Mach number at about two-thirds of the channel length where the oblique shock wave formed at the leading edge intersects the top wall. However, the present prediction is rather poor even compared with the results by the first-order Godunov method. The shock wave is too oversmeared by the present prediction procedure as can be seen from Fig. 6.16. This indicates that in order to get good resolution of shock waves alternative numerical techniques have to be employed.

It can be seen from the above comparative study that the present prediction procedure is only comparable with the first-order method. The overall predictions

are, generally speaking, quite good but some other special numerical technique has to be employed in order to get a better prediction of supersonic flow with strong shock waves.

6.4 Flow Behind a Rearward-Facing Step

The previous test cases have clearly demonstrated that the prediction procedure can handle the quasi-one dimensional subsonic, transonic and supersonic nozzle flows. For two dimensional subsonic, transonic and supersonic flows in the channel with a circular arc bump, overall good agreement has been achieved between the present predictions and the results obtained by the Godunov methods. In this section, in order to check the general validity of the prediction procedure a more complicated flow case is chosen as a more severe test for the prediction procedure. This is supersonic laminar flow behind a rearward-facing step with a subsonic recirculating flow region. This kind of flow can be found in important engineering applications such as the flow in a supersonic combustor.

6.4.1 Flow Geometry

Fig. 6.17 shows the flow geometry under investigation. The Reynolds number of the laminar approach flow at the step is 1.2×10^6 which corresponds to a static pressure of 2900 Pa and a static temperature of 80 K (32). The air inflow Mach number is 3.5 which corresponds to a inlet velocity of 627.5 m/s at the step.

6.4.2 Boundary Conditions

The specification of computational boundary conditions for compressible flow has been fully discussed above. For this particular case, the velocity, static pressure and temperature were specified at the inlet boundary and density was specified at the outlet boundary. The no-slip boundary condition was applied at the wall and reflection boundary conditions as presented before were employed for the upper boundary.

6.4.3 Results and Comparison

Fig. 6.18 presents the comparison between the predicted wall pressure distribution and the experimental data (32) behind the step. The pressure was normalized by the inflow static pressure. It can be seen from the figure that quite good agreement has been achieved.

Fig. 6.19 compares the predicted static pressure profile with the experimental data at a location downstream of a step at x/h = 0.0537. The pressure was normalized by the inflow static pressure. An overall good agreement has been obtained as shown in the figure.

Fig. 6.20 and Fig. 6.21 presents the comparisons between the predicted normalized static pressure profiles and the experimental data at locations downstream of steps at x/h = 2.137, 4.279. It can be seen again that general overall good agreement has been achieved. However, there are some discrepances between the predictions and the experimental data near the wall. This may be attributed to the fact that the flow attaches to the lower wall between two locations

and hence more complicated phenomena such as a shock wave, flow separation and transition may occur which the prediction procedure cannot simulate exactly.

Fig. 6.22 presents the predicted velocity vectors. It can be seen that the flow field near the upper boundary does not change much. This verifies that it is appropriate to employ the reflection boundary conditions for the upper boundary.

6.5 Closure

The prediction procedure has been applied to several compressible flow cases which include subsonic, transonic and supersonic flows. The one crucial issue in computing compressible flow is the specification of the computational boundary conditions. These are, in particular, of great importance for supersonic flow as the established principle is misleading. The results shown above confirm that the prediction procedure can not only handle simple quasi-one dimensional subsonic, transonic and supersonic flows but also can predict quite well two-dimensional subsonic, transonic and supersonic channel flows and the even more complicated supersonic flow behind a rearward-facing step with a subsonic recirculating flow region. However, the present prediction procedure cannot give good resolution of shock waves. This indicates that other numerical techniques have to be employed in order to get a better prediction of supersonic flow with shock waves.

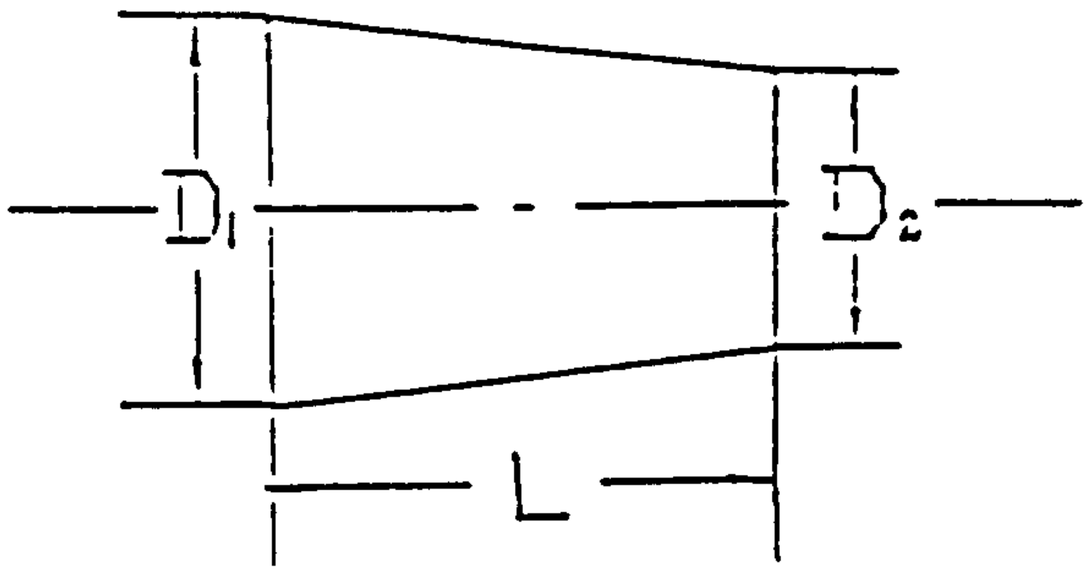

The convergent nozzle

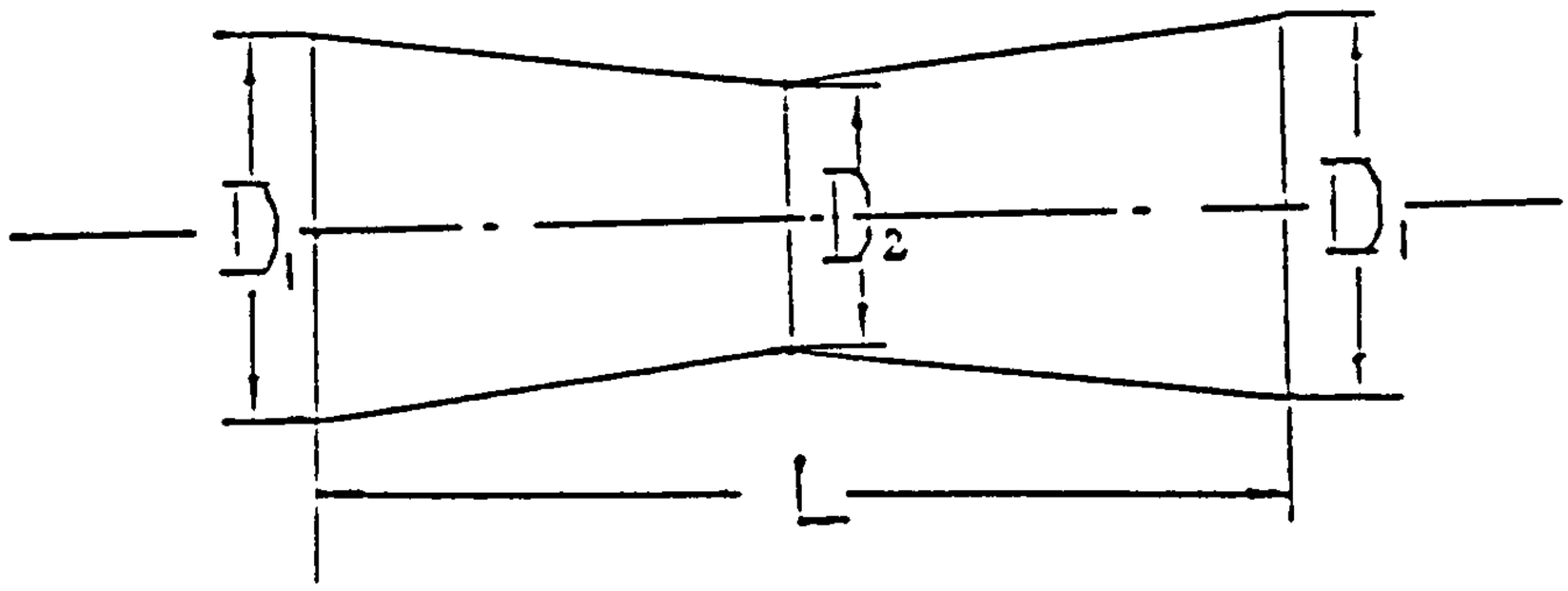

The convergent–divergent nozzle

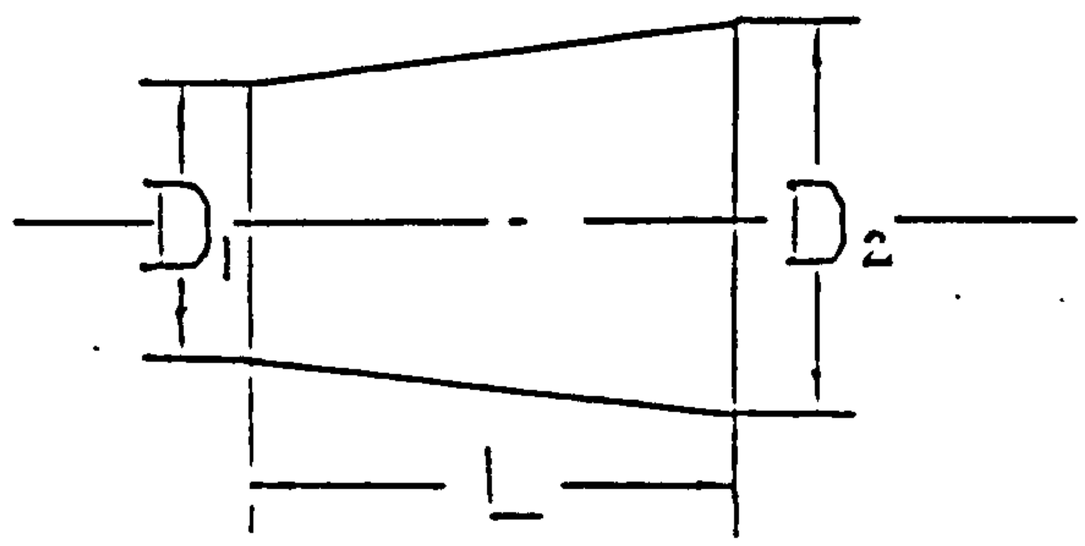

The divergent nozzle

Fig. 6.1 The nozzles used in the study

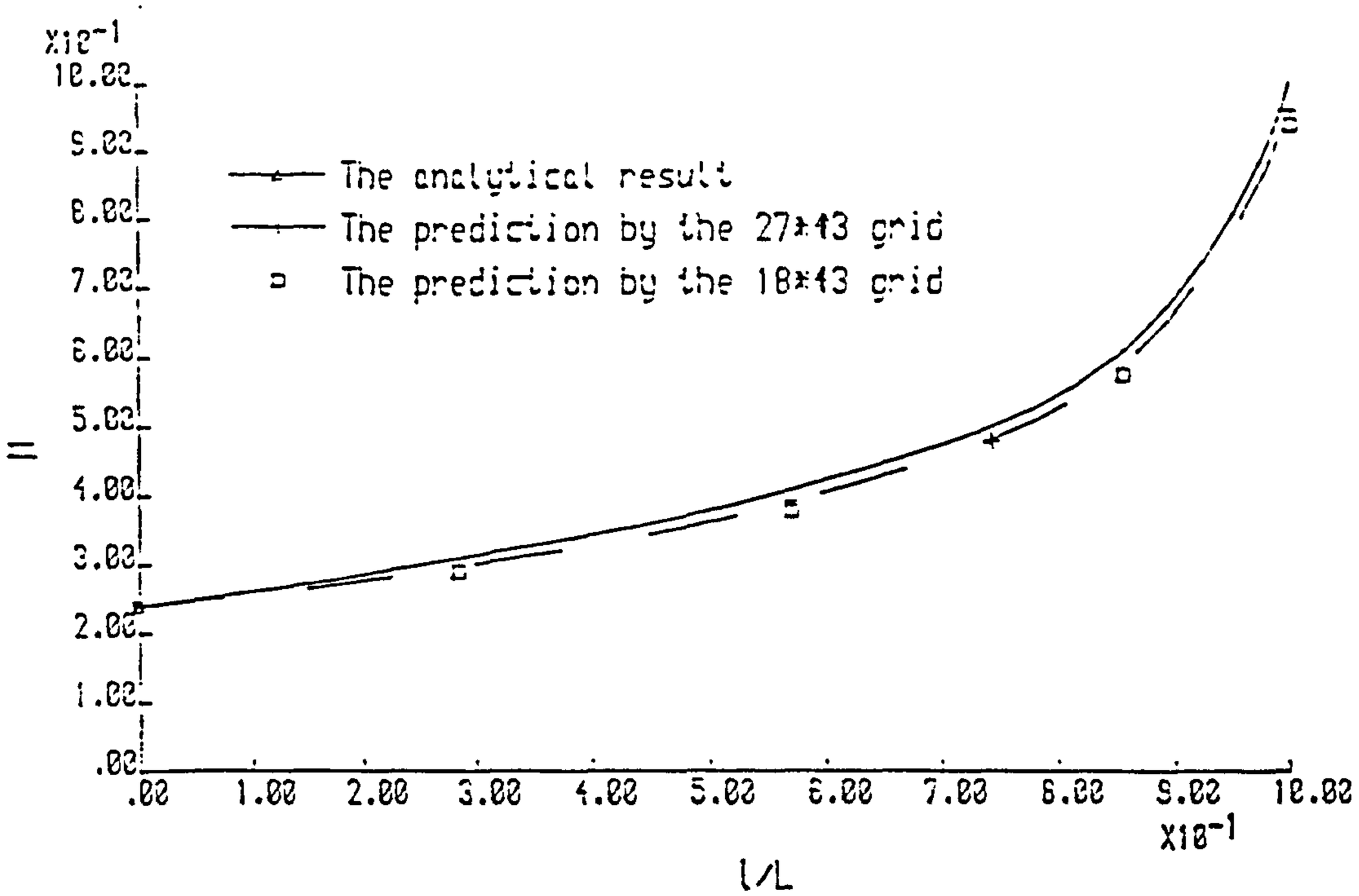

Fig. 6.2 Comparison between the predicted Mach number profile and the analytical result in the convergent nozzle.

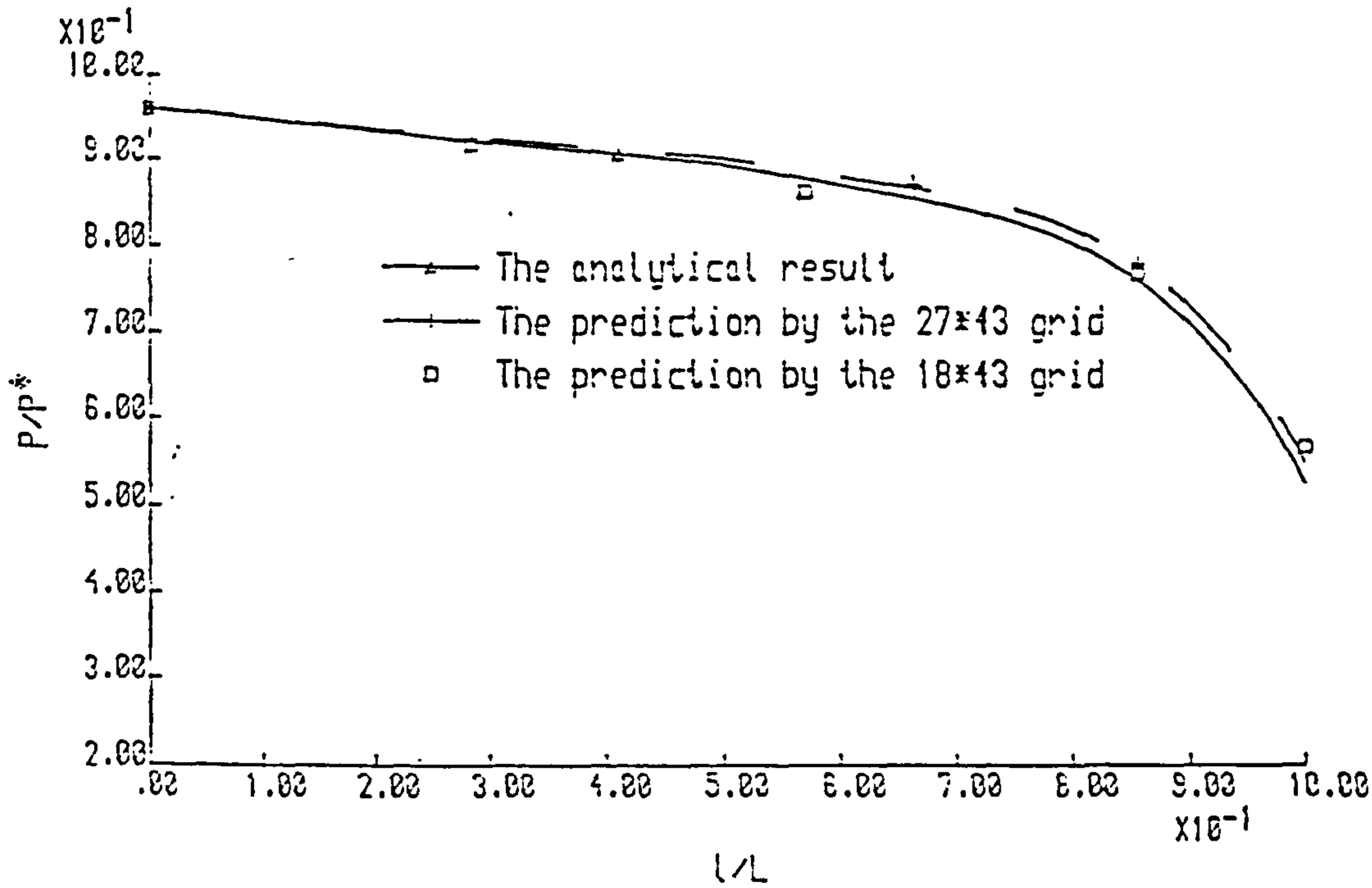

Fig. 6.3 Comparison between the predicted pressure profile and the analytical result in the convergent nozzle.

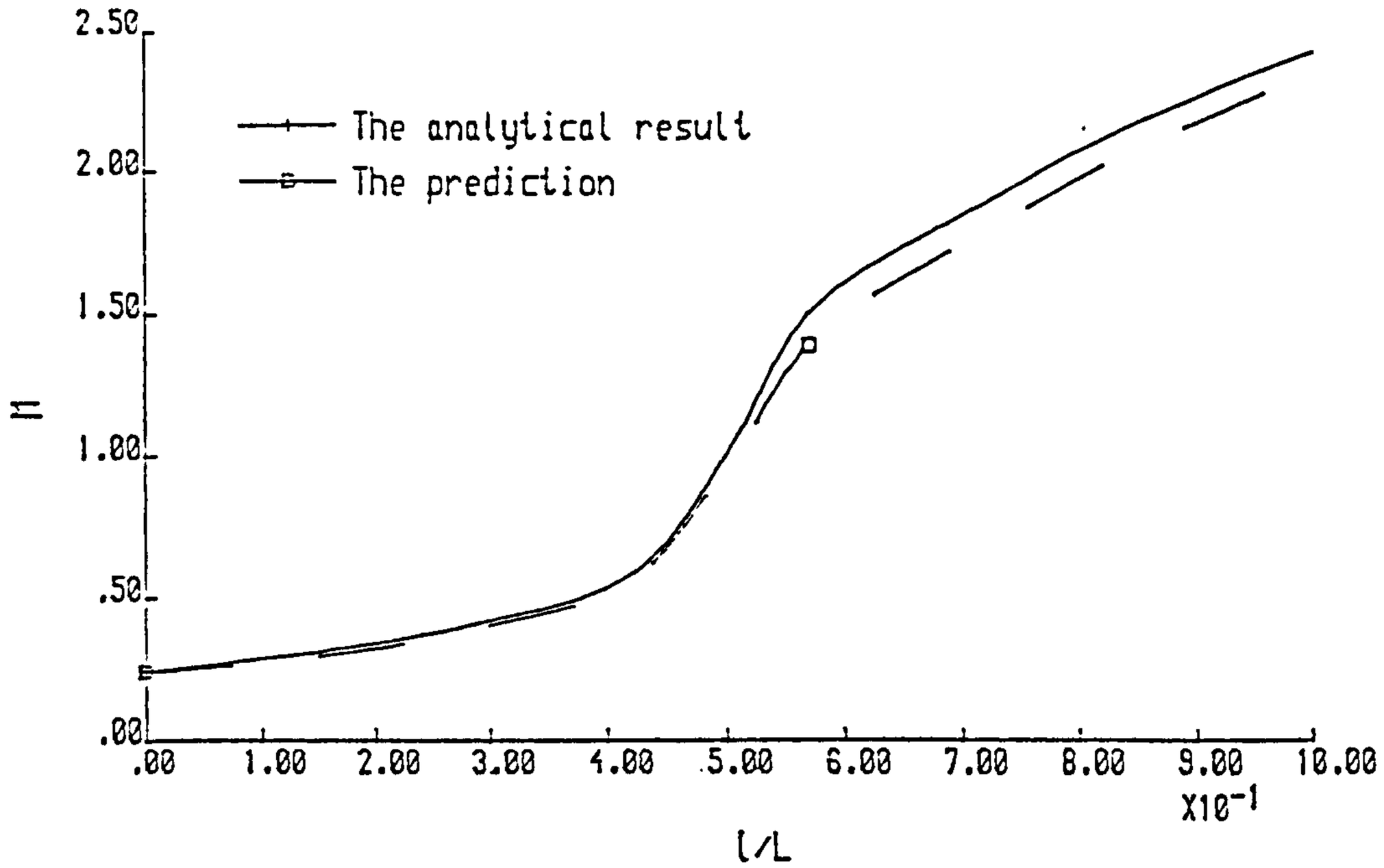

Fig. 6.4 Comparison between the predicted Mach number profile and the analytical solution in the convergent-divergent nozzle.

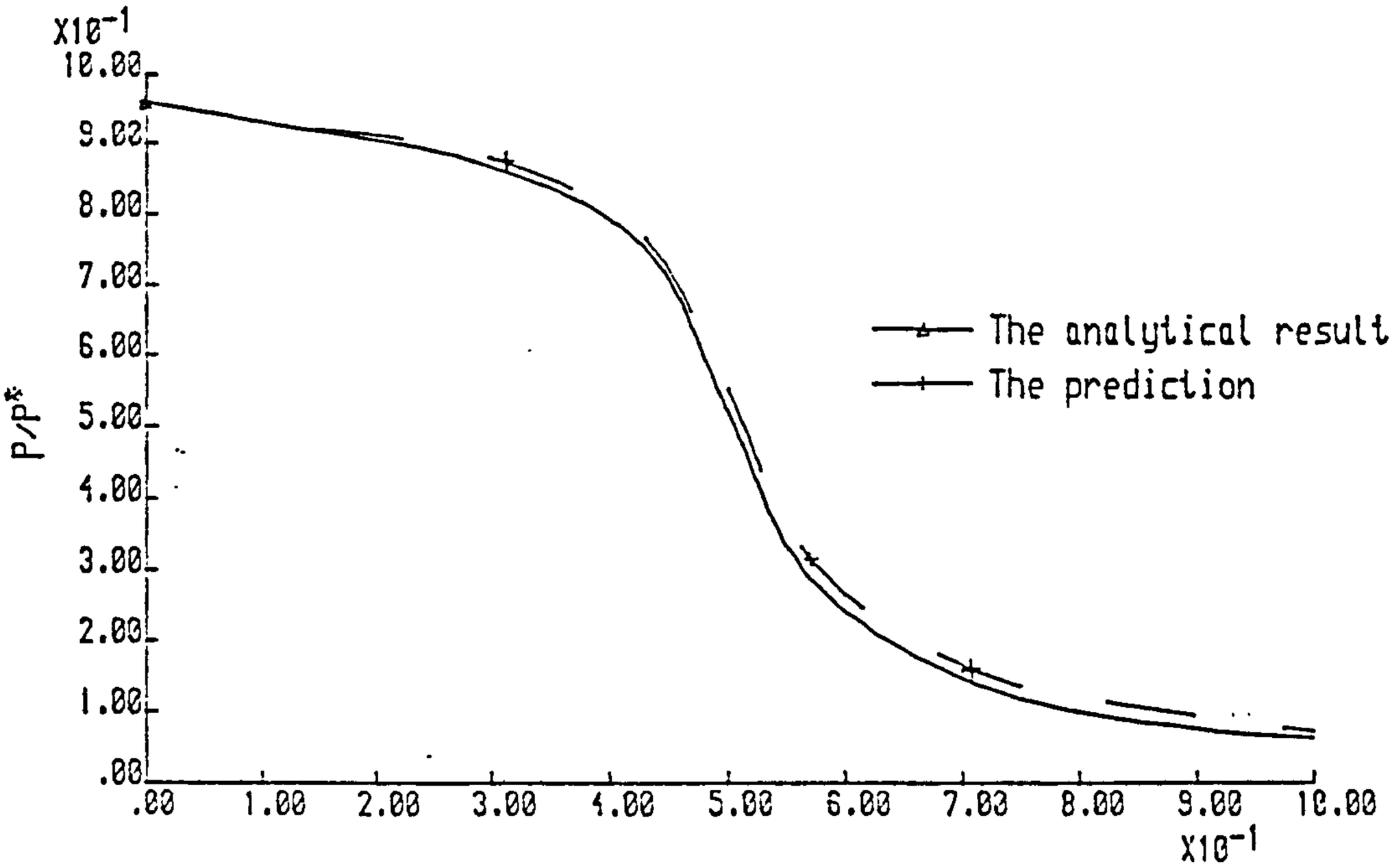

Fig. 6.5 Comparison between the predicted pressure profile and the analytical result in the convergent-divergent nozzle.

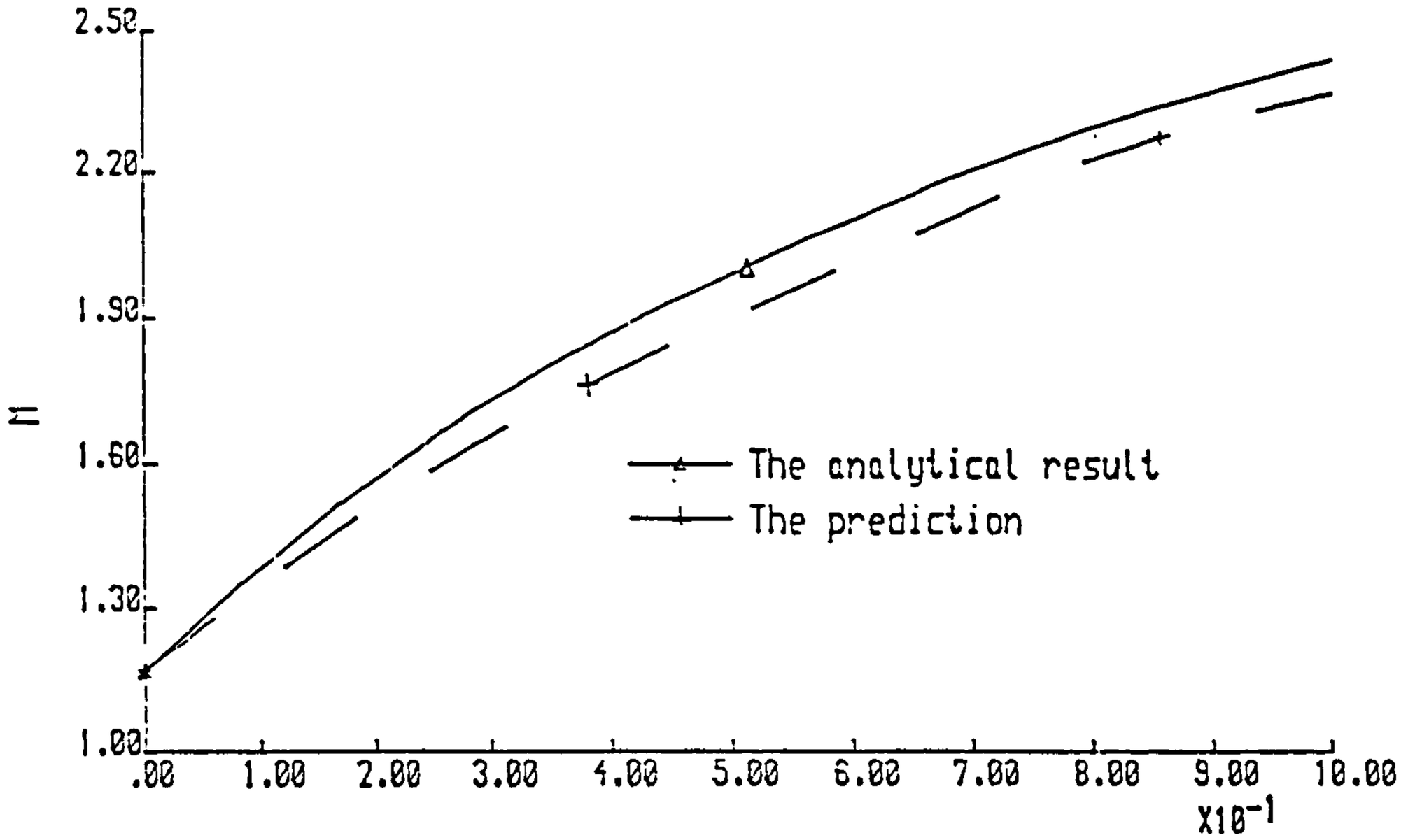

Fig. 6.6 Comparison beiween the predicted Mach number profile and the analytical result in the divergent nozzle.

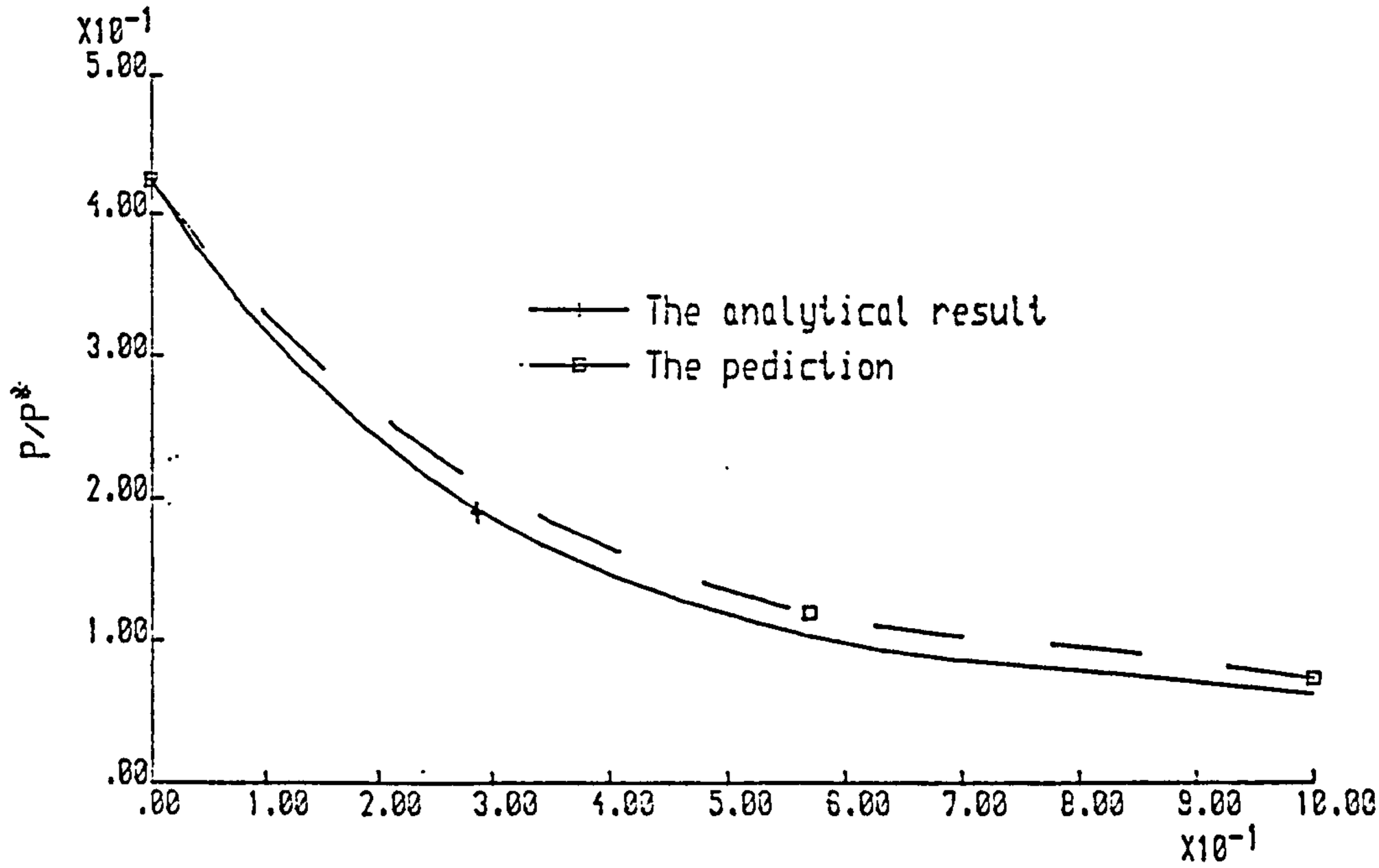

Fig. 6.7 Comparison beiween the predicted pressure profile and the analytical result in the divergent nozzle.

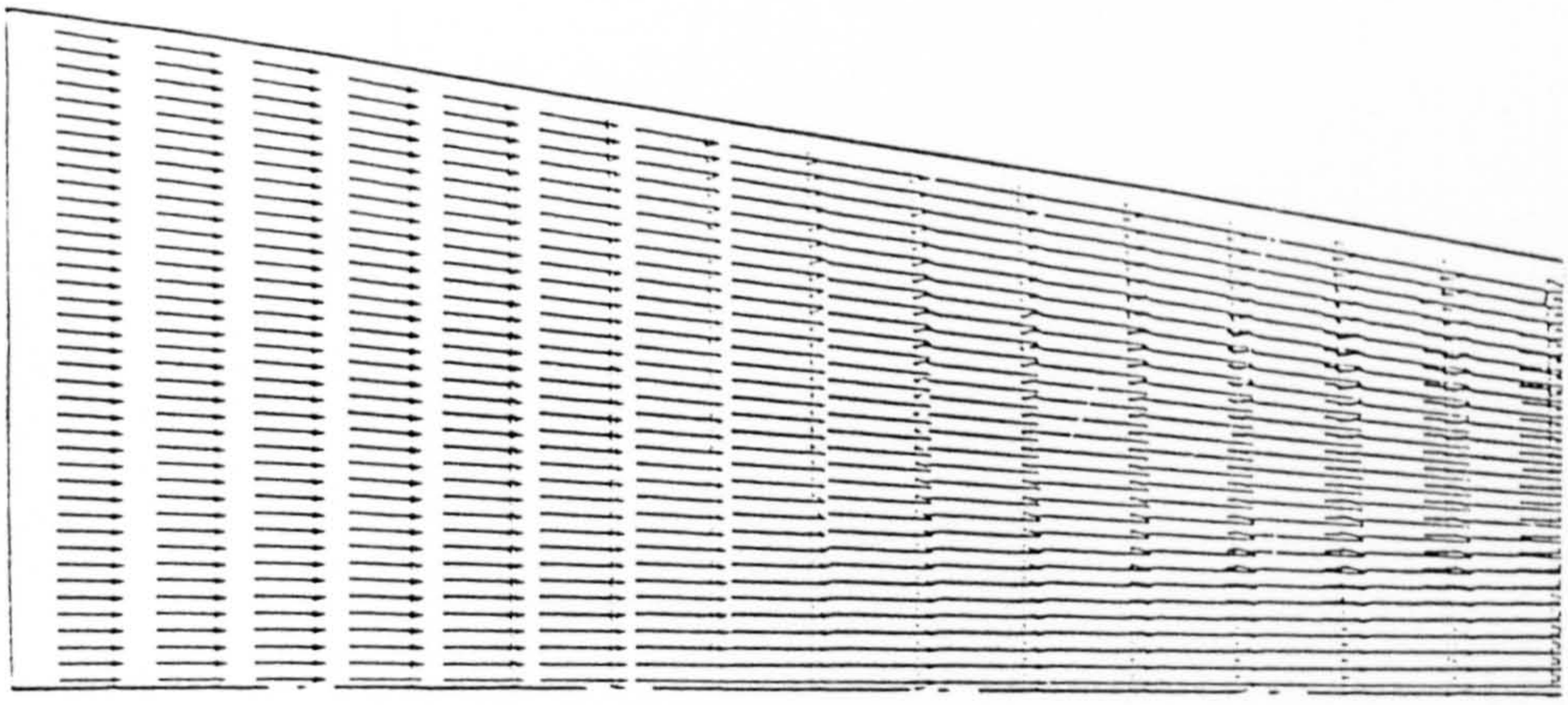

Fig. 6.8 The predicted velocity vectors in the convergent nozzle.

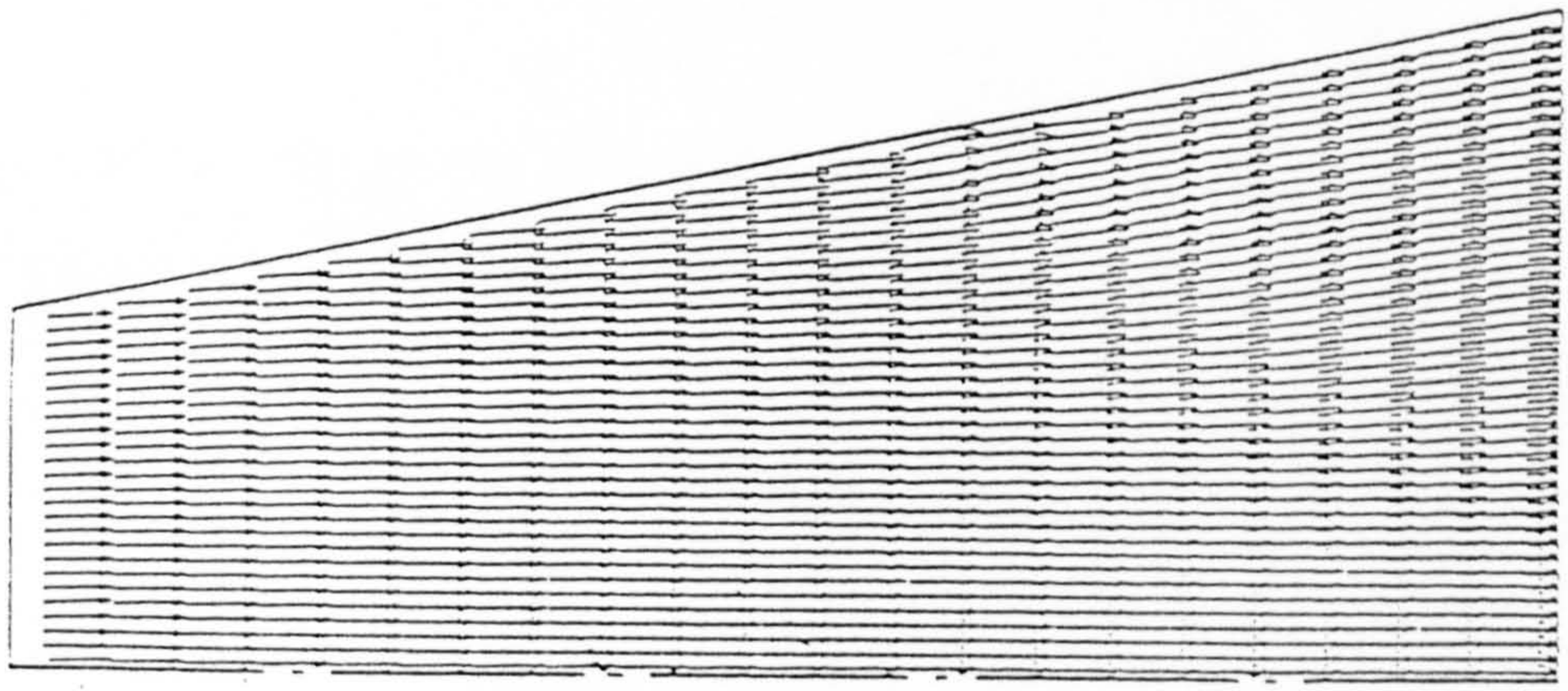

Fig. 6.9 The predicted velocity vectors in the divergent nozzle.

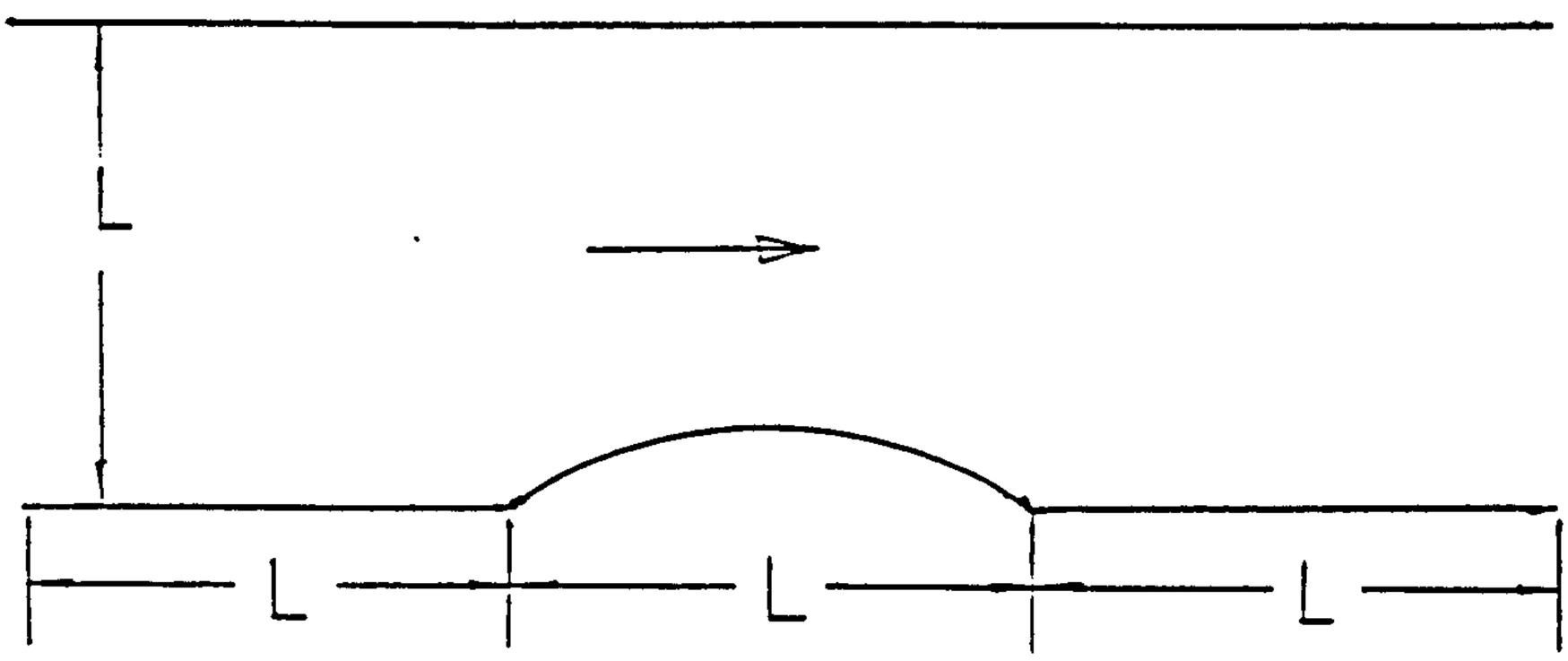

Fig. 6.10 The channel with a circular arc bump used in the study.

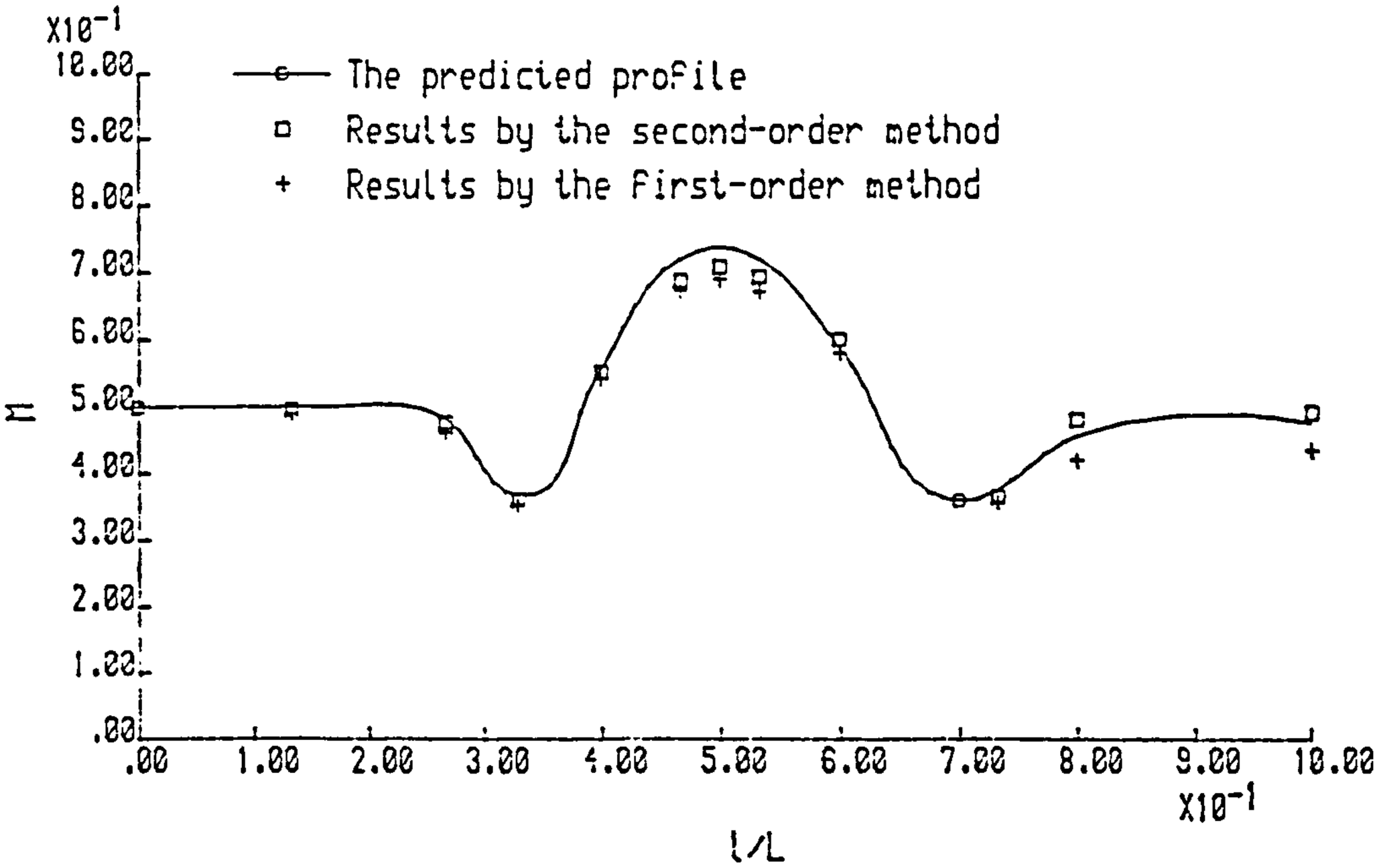

Fig. 6.11 Comparison between the predicted Mach number profile at the lower wall and the results obtained by the first and second-order Godunov methods for the subsonic flow.

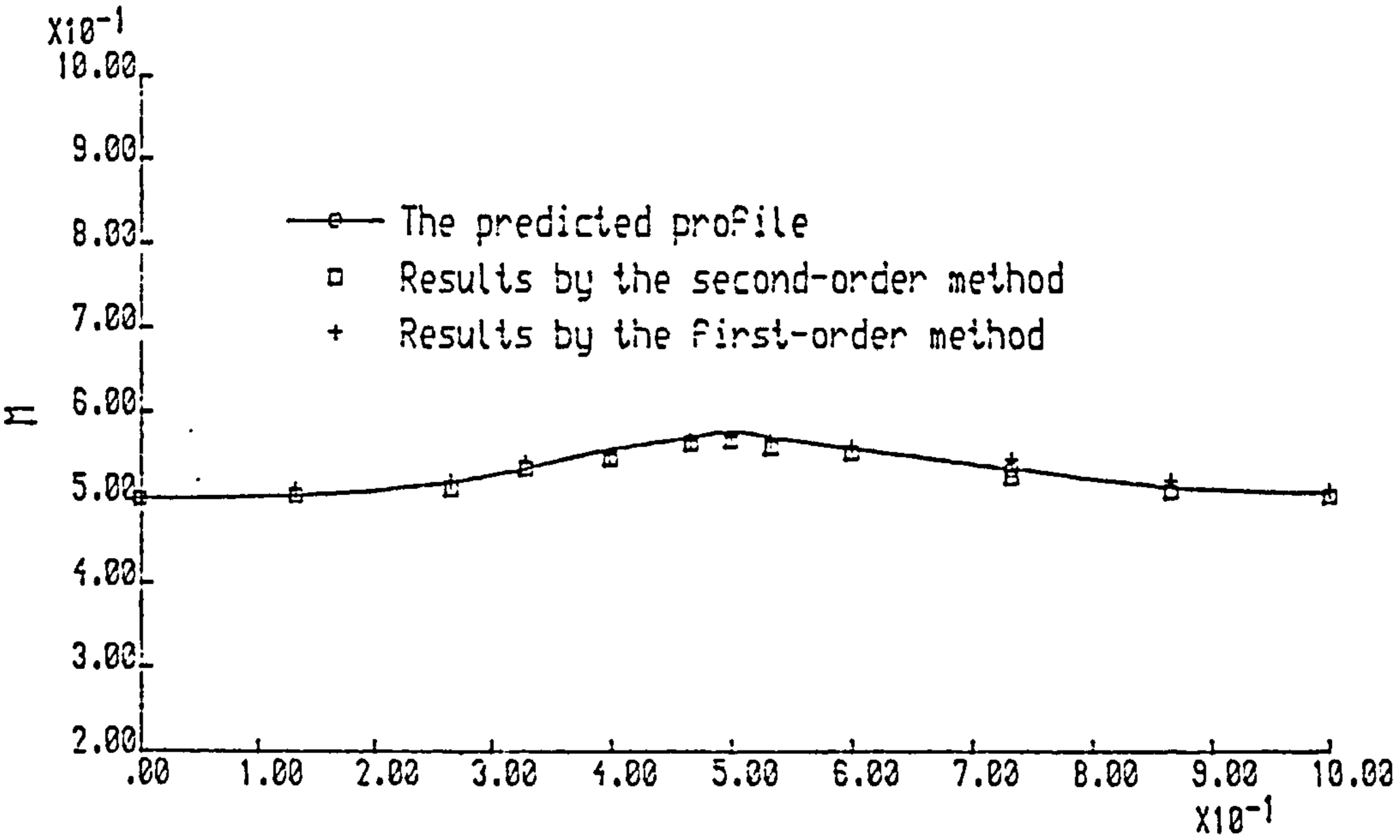

Fig. 6.12 Comparison between the predicted Mach number profile at the upper wall and the results obtained by the first and second-order Godunov methods for the subsonic flow.

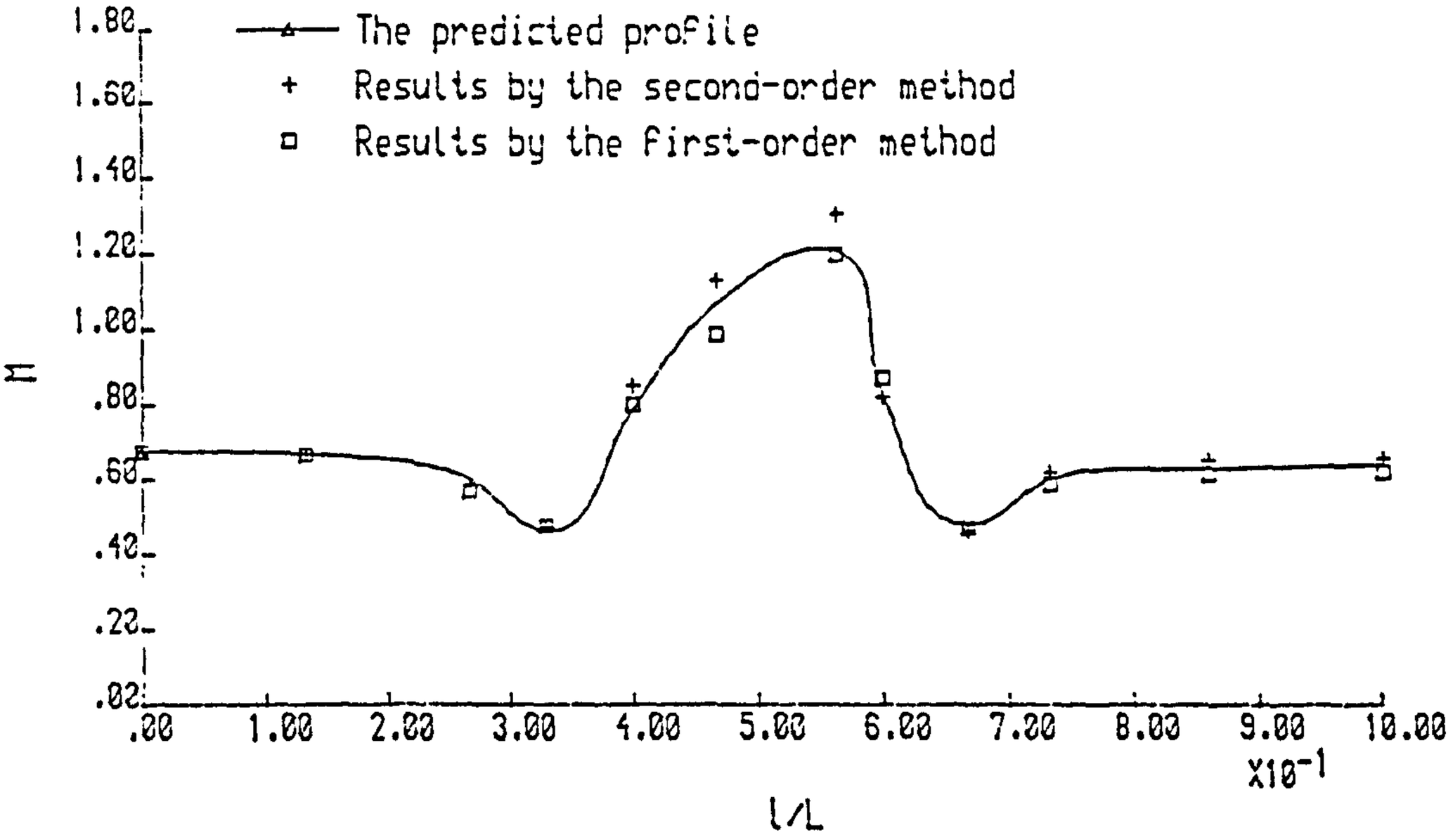

Fig. 6.13 Comparison between the predicted Mach number profile at the lower wall and the results obtained by the first and second-order Godunov methods for the transonic flow.

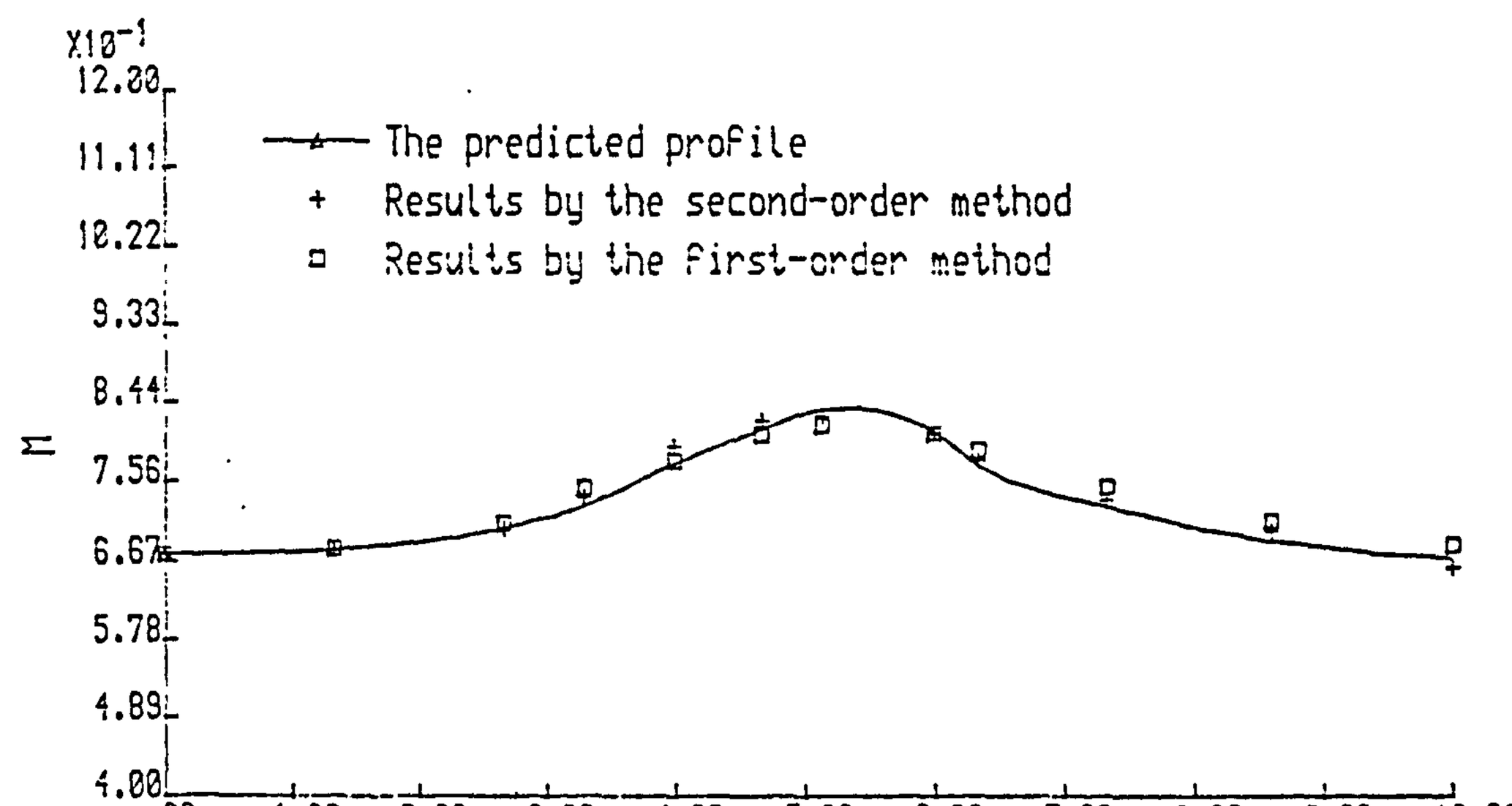

Fig. 6.14 Comparison between the predicted Mach number profile at the upper wall and the results obtained by the first and second-order Godunov methods for the transonic flow.

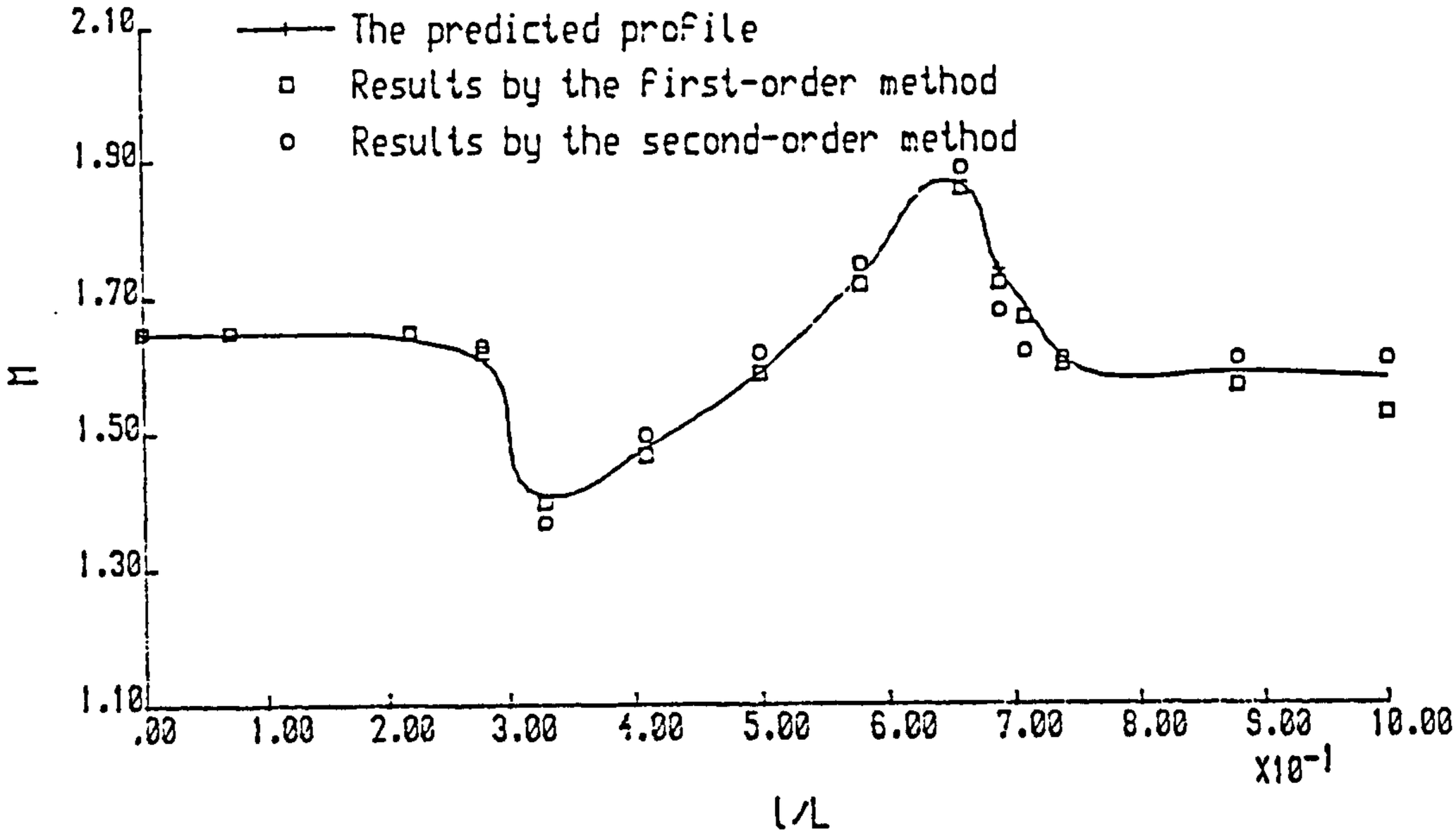

Fig. 6.15 Comparison between the predicted Mach number profile and the results obtained by the first and second-order Gudonov methods at the lower wall in the case of supersonic flow.

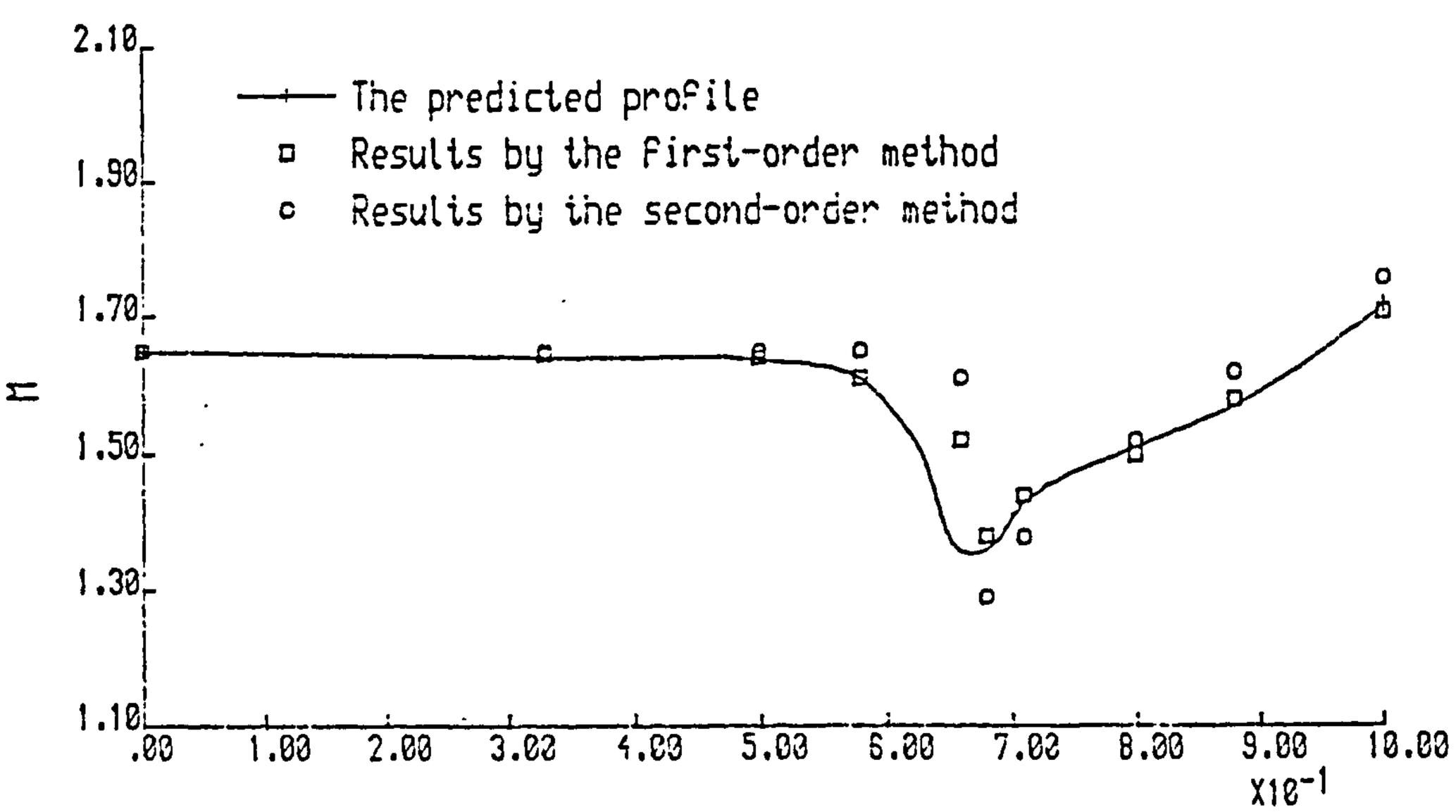

Fig. 6.16 Comparison between the predicted Mach number profile and the results obtained by the first and second-order Gudonov methods at the upper wall in the case of supersonic flow.

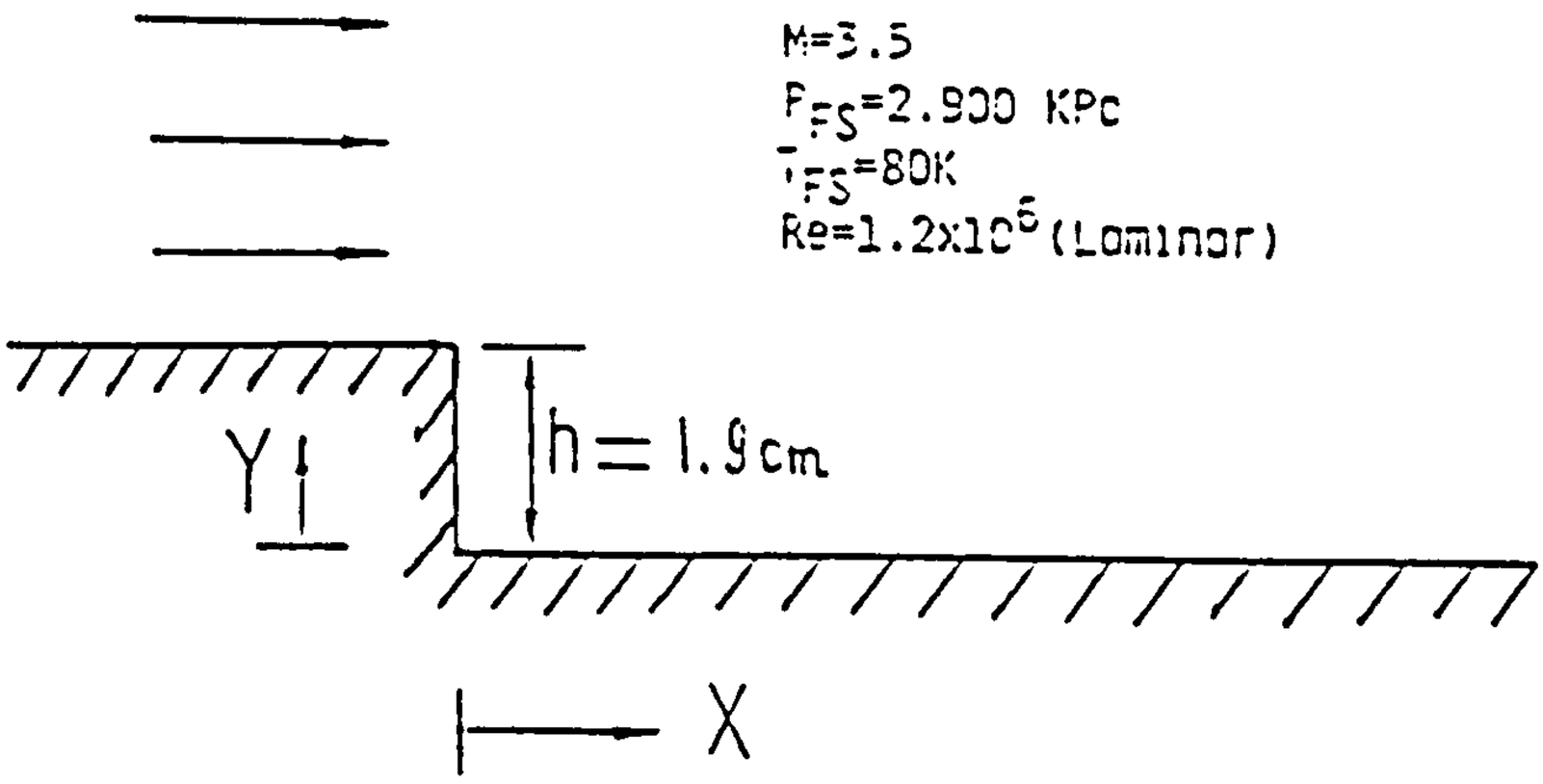

Fig. 6.17 Flow geometry.

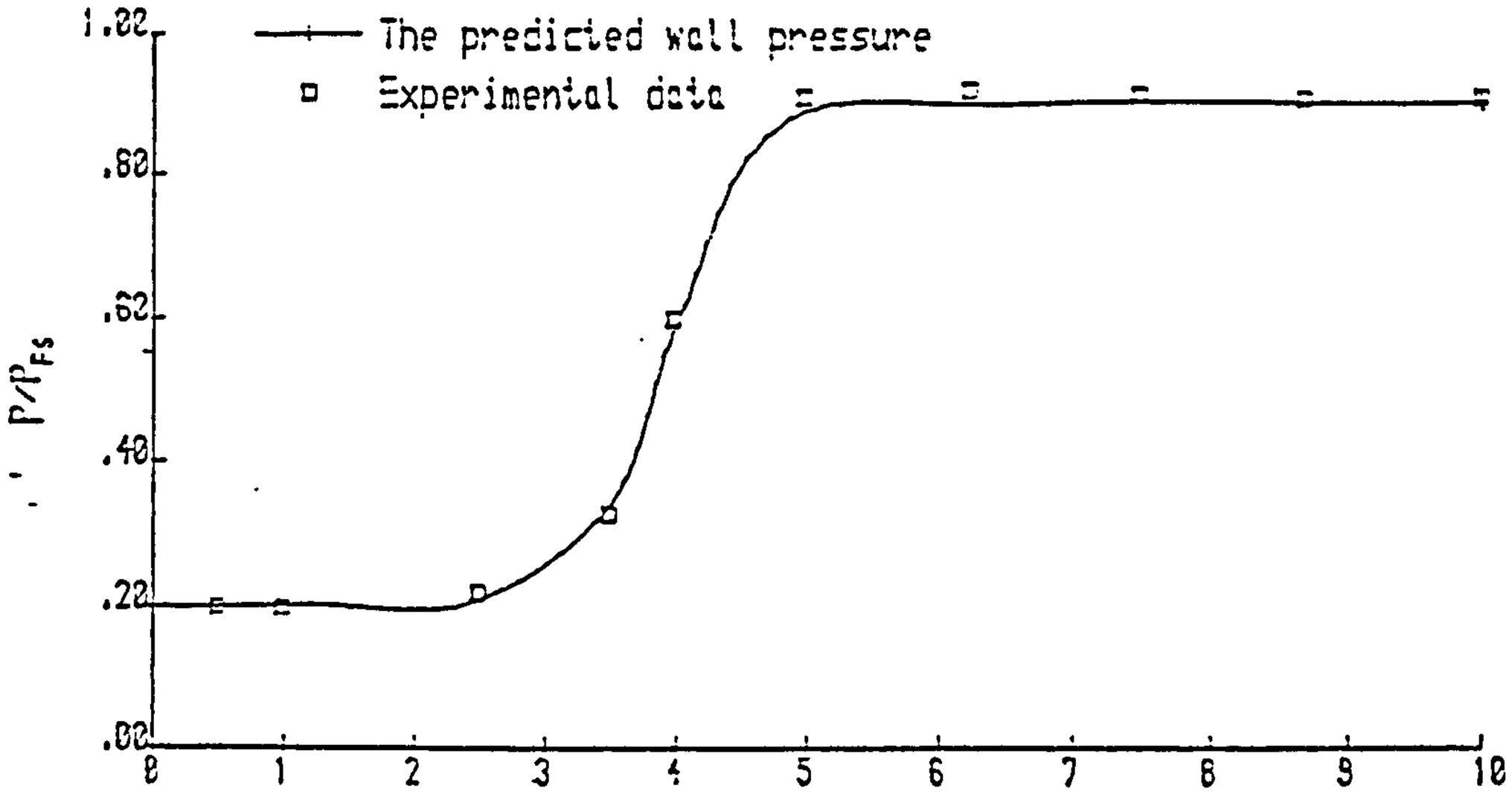

Fig. 6.18 Comparison between the predicted wall pressure distribution and experimental data for the supersonic laminar flow over a rearward-facing step.

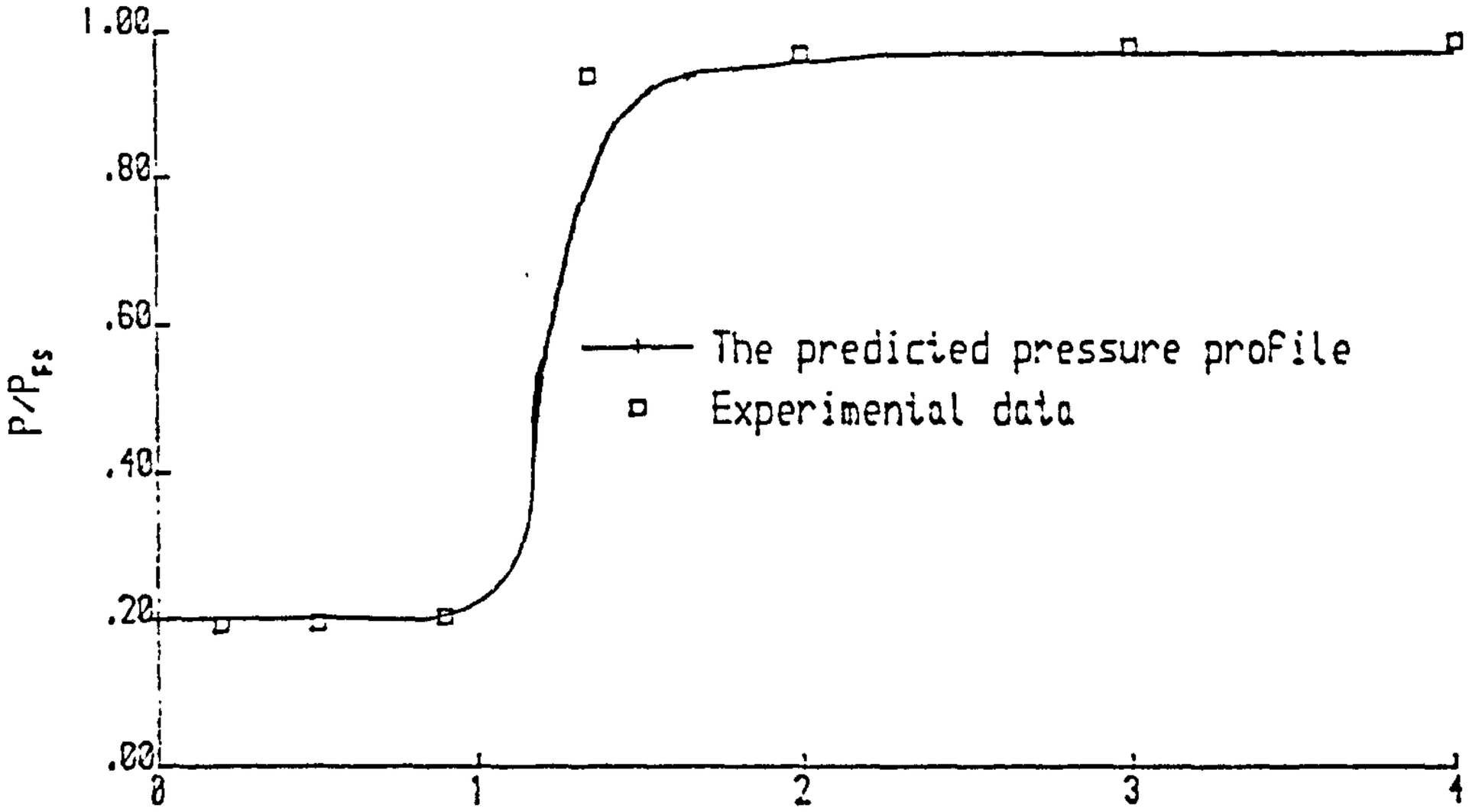

Fig. 6.19 Comparison between the predicted pressure profile and experimental data for the supersonic laminar flow behind a rearward-facing step at x/h=0.0537.

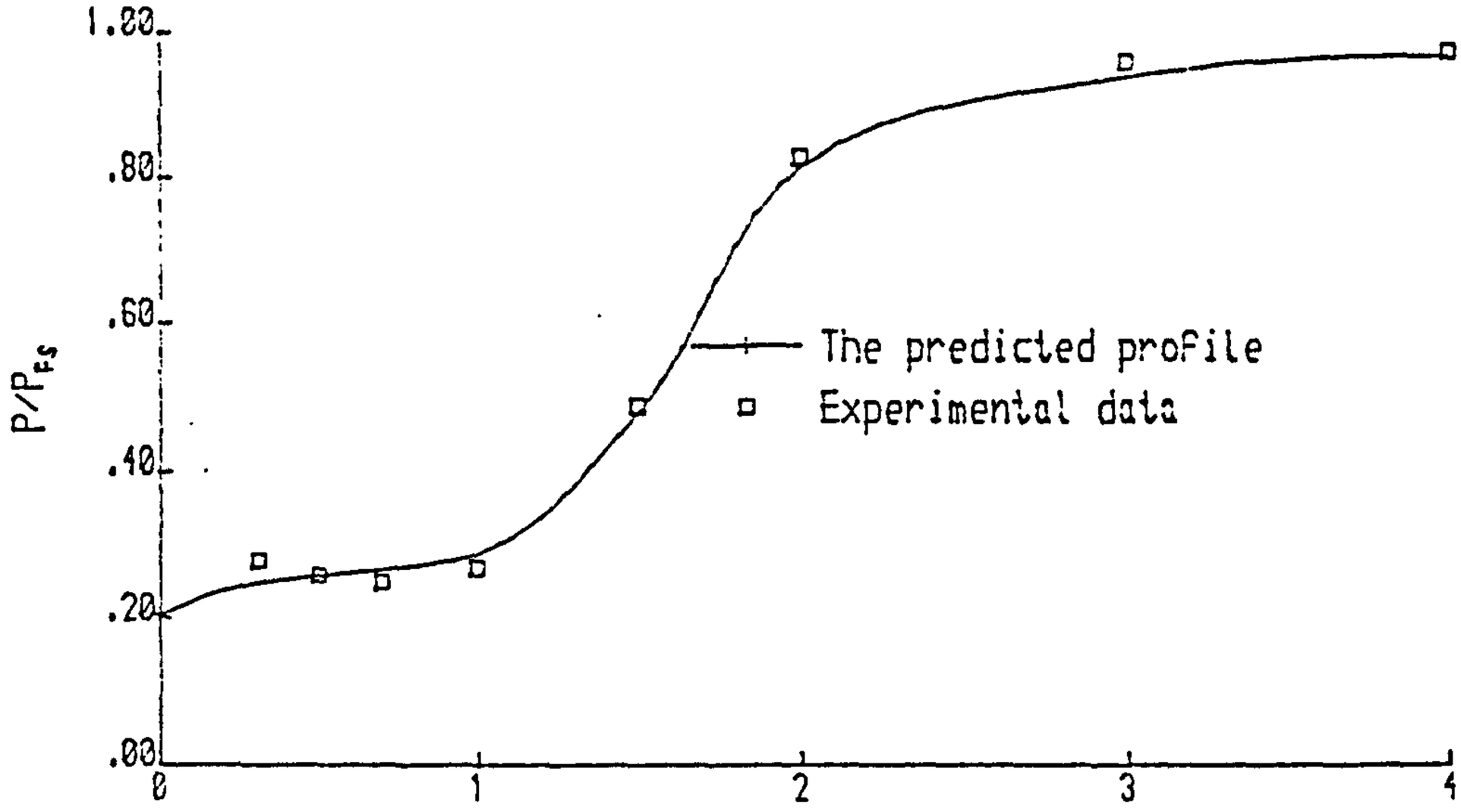

Fig. 6.20 Comparison between the predicted pressure profile and experimental data for the supersonic laminar flow behind a rearward-facing step at x/h=2.137.

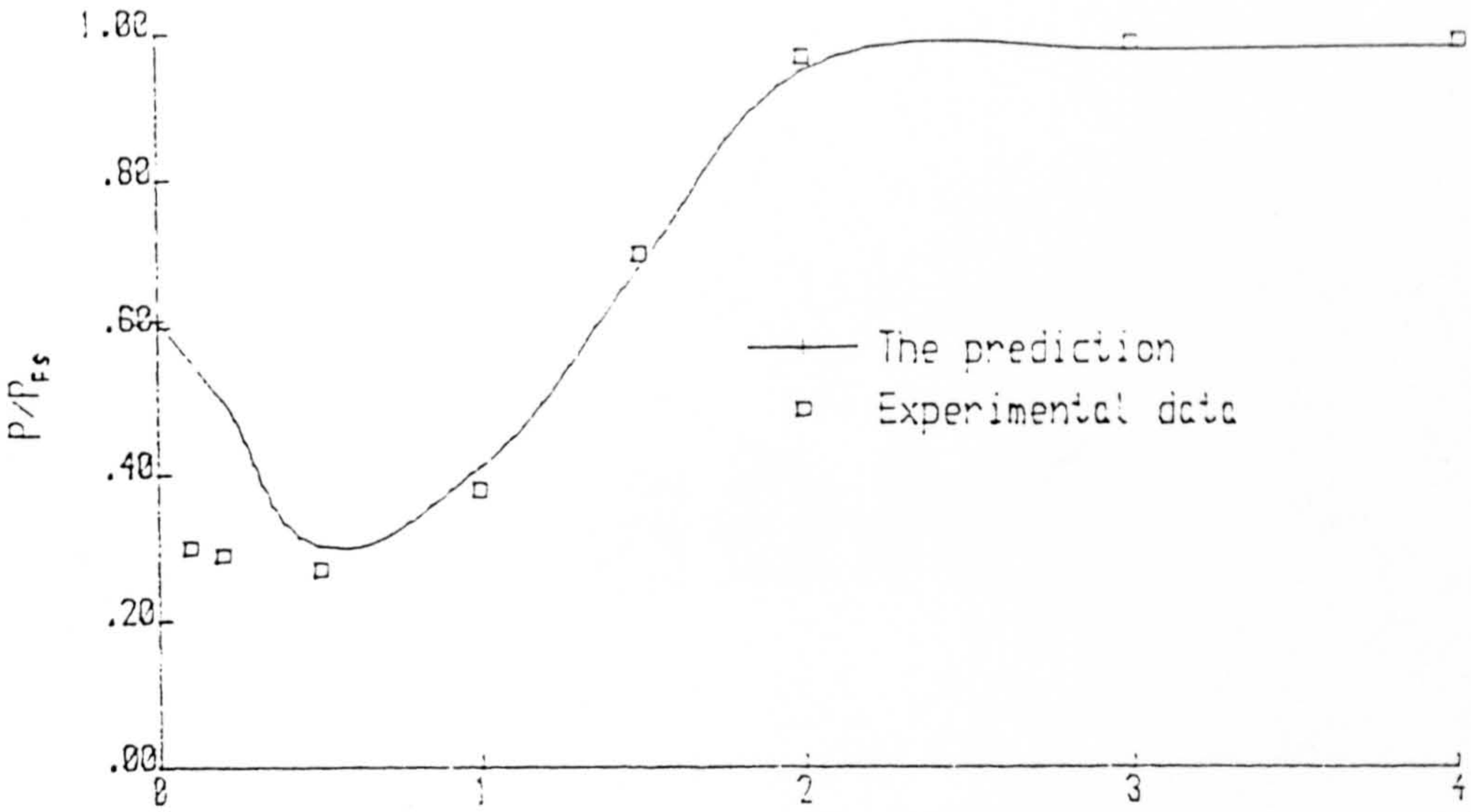

Fig. 6.21 Comparison between the predicted pressure profile and experimental data for the supersonic laminar flow behind a rearward-facing step at x/h=4.279.

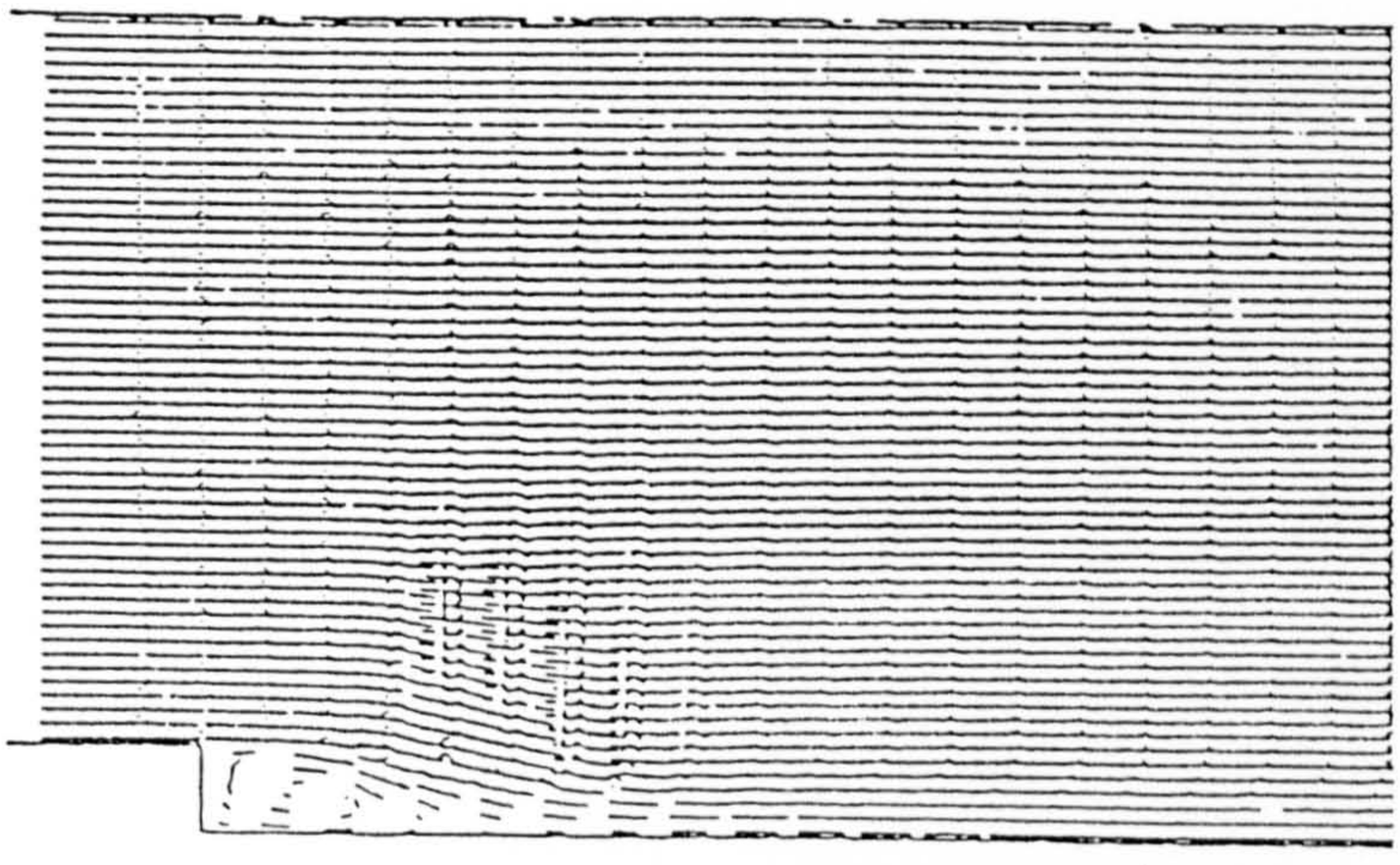

Fig. 6.22 The predicted velocity vectors for the supersonic laminar flow behind a rearward-facing step.

Chapter 7

CLOSURE

In this chapter, the concluding remarks are presented. The discussion will be divided into two parts. In the first part, a brief review of the whole thesis will be presented. This is followed by suggestions for further work in regard to the present study.

7.1 A Review of The Thesis

The main objectives of the present work are stated in chapter one.

1). The first objective is to develop a general elliptical prediction procedure which is valid for both incompressible flow and compressible flow at any Mach number. The prediction procedure is based on the SIMPLE algorithm and solves the steady-state form of the Navier-Stokes equations. In order to make the prediction procedure valid for both incompressible and compressible flows, pressure has to be chosen as a main dependent variable instead of density. This is in contrast

with the time-dependent (unsteady) methods which usually employ density as a main dependent variable and integrate the unsteady form of the Navier-Stokes equations to reach a steady state.

2). The second objective is to undertake a comparative study of the two-equation k-ϵ turbulence model and a Reynolds stress model in the case of strongly swirling flows in vortex throttles. It was anticipated that Reynolds stress models would give better performance than the two equation k-ϵ model in such a case.

The work reported in this thesis is summarized as follows to the extent to which these objectives have been attained.

7.1.1 Turbulence Models

In order to solve the time averaged Navier-Stokes equations, it is necessary to approximate the correlation terms representing the turbulent shear stresses by modelling assumptions. Several approaches have been discussed in the previous chapters. Among these the one-point closure approach has been widely used, and hence almost all the one-point closure turbulence models have been reviewed with particular emphases on the two-equation k-ϵ model and the Reynolds stress model.

The two-equation k-ϵ model, using the Boussinesq assumption, relates the turbulent shear stresses or the Reynolds stresses to the mean strain through the turbulent viscosity or eddy viscosity. This turbulence model has been widely used in engineering calculations. However, the two-equation k-ϵ model (and other two-equation turbulence models) have several limitations as pointed out in chapter

three. One of the practical limitations is the assumption of isotropic eddy viscosity. This affects its performance in the case of strongly swirling flows under consideration as anistropy then becomes important. In addition, some physical processes such as those due to streamline curvature, rotation, and buoyancy forces have to be modelled separately.

Reynolds stress models, however, do not have these limitations as the Boussinesq assumption is not employed and a transport equation is developed for each Reynolds stress. Moreover, the effects of streamline curvature, rotation, and buoyancy forces are believed to be accounted for automatically in Reynolds stress models. They are, therefore, in principle superior to the two-equation k-ϵ model. However, they have not been thoroughly tested for some complicated flows such as the very strongly swirling flows under study. In addition, they are more complicated and need enormous computer power.

Both the k-ϵ model and a Reynolds stress model have been applied to the strongly swirling flows in vortex throttles. The results obtained have confirmed that the Reynolds stress model gives overall better performance compared with the two-equation k-ϵ model. The k-ϵ model overpredicted the turbulent kinetic energy greatly compared with the Reynolds stress model. This could be the major reason (although there are some other reasons) why the k-ϵ model gives poor performance in such a case.

7.1.2 Numerical Aspects

The control volume method was used to discretize the governing non-linear partial differential equations. In order to avoid an unrealistic solution the staggered grid system was employed. The resultant finite difference equations were solved by a line-by-line iteration method and the variables along each line were obtained using the TDMA (Tri-Diagonal Matrix Algorithm). The pressure-velocity link was handled by employing the SIMPLE algorithm.

For compressible subsonic flow, some modifications have been made to the SIMPLE algorithm to calculate density. It has been found that one variable (usually static pressure or density) should be specified at the outlet boundary to ensure a realistic accurate solution.

When supersonic flow is of concern more modifications must be made to account for the hyperbolic nature of such flow. It has been stated that the evaluation of density at the control volume boundaries and the differencing of the pressure gradient are two important issues. It seems contradictory on one hand that downstream influences should be eliminated in the case of supersonic flow and on the other hand a central differencing scheme was still used for the pressure gradient. However, it should be pointed out that the so called downstream influences refer to some 'small disturbances', and it has been stated clearly that eliminating the downstream pressure influence is misleading, since it would result in some unrealistic conclusions. As a result of this, it may be fair to say that the prediction procedure simulates the hyperbolic nature of supersonic flow only partially as the downstream small disturbances cannot be eliminated completely.

Moreover, shocks were oversmeared by the prediction procedure as no special technique has been employed to handle them.

It has been argued that the pressure-correction equation should be modified for compressible flow as density changes in such a case. Nevertheless, the experiences gained by the present author has indicated that this is not necessary provided the density calculation is switched on after a reasonable pressure field has been established and proper under-relaxation factors are given. In fact, this means that density change lags one iteration behind which is equivalent to the treatment of the non-linearities of the momentum equations in the prediction procedure.

The established principle that no boundary conditions should be specified at the supersonic flow outlet is questionable. The treatment that all variables at the outlet boundary are interpolated may be valid in some cases. However, in some other cases such as the convergent and divergent nozzle flow under study at least one variable should be specified at the outlet boundary.

7.1.3 Validation of the Prediction Procedure

The prediction procedure was validiated by comparing the predictions with the known analytical and numerical results in two cases. The first study is the quasi-one dimensional inviscid subsonic, transonic and supersonic flows in the convergent, convergent and divergent, and divergent nozzles respectively. The comparison has been made between the known analytical results and the predictions. Good agreement has been achieved, especially for subsonic flow in the

convergent nozzle where the agreement is very good. The second validation test is the two dimensional subsonic, transonic and supersonic flow in a channel with a circular arc bump. This is a standard test problem. On the whole, the prediction procedure performed well but the shock was oversmeared as pointed out before. In addition, one factor that would affect the accuracy of the prediction procedure is that step grids were used to simulate different geometries, and it is believed that the use of body-fitted coordinates would improve the accuracy.

7.1.4 Applications to Other Cases

The prediction procedure has been also applied to other flow cases; the more severe and complicated supersonic laminar flow behind a backward-facing step which has embedded subsonic flow regions was calculated. The predicted pressure profiles were compared with the experimental data and good overall agreement was achieved. However, it is difficult to assess the performance of the prediction procedure in the turbulent case as additional problems related to the turbulence modelling may arise.

On the basis of the results reported in this thesis, the prediction procedure is, generally speaking, able to handle subsonic, transonic and supersonic flows. However, when flow with shocks is of concern the shock resolution is very poor as no special technique has been employed to handle shocks. Moreover, the hyperbolic nature of supersonic flow cannot be simulated exactly.

7.2 Suggestions for Future Work

The present study has not covered some areas both in depth and breadth. Further research could be usefully performed to improve the effectiveness of the prediction procedure and to deepen our understanding of some physical phenomena. Some examples are as follows:

The present numerical scheme simulates the hyperbolic nature of supersonic flow only partially. The linkage between each node and the neighboring nodes in the lateral direction have not been modified. In reality the variables at a certain location should be affected by the small disturbances only within certain 'influence zones' bounded by the characteristic curves. However, the characteristic angles vary throughout the flow field and are not known in advance. It is, therefore, very difficult but not impossible to construct the required grid to simulate this feature exactly.

The prediction procedure has not employed any special techniques to handle shocks, and hence shocks are oversmeared and the shock resolution is very poor. In order to solve supersonic shock flow successfully it is necessary to employ a more accurate shock-capturing numerical scheme to evaluate the steady-state Navier-Stokes equations.

Turbulence modelling is still a great challenge for incompressible flow, let alone compressible flow. Most turbulence models developed so far are only for incompressible flow and the literature on turbulence modell ing for the compressible case is much more scarce. There is considerable scope since a great deal of

research work in this area needs to be done so as to improve our understanding of the physical phenomena.

Systematic study should be undertaken to investigate the effects of computational boundary conditions on the whole solution procedure for compressible flow, in particular for supersonic flow. It has been stated that the established principle on the supersonic flow outlet boundary treatment is, in some cases, rather misleading. However, when there are no variables given at the outlet then what kind of boundary treatment should be used. The interpolation method may be valid in some cases but not always. Further study should be done on this aspect.

The flow field in scramjet combustor is very complicated due to highly turbulent reacting mixed supersonic/subsonic flow. It is of great value both for better understanding of mixed supersonic/subsonic reactive flow and engineering applications to be able to predict such complicated flow accurately. Further research work on reacting mixed supersonic/subsonic flow is of great importance to future long-range commerical aviation and outer-space exploration.

The vortex throttles used in the present study are very effective in producing a high pressure drop as a result of dissipating the high tangential velocity. However, in some applications it would be useful to exploit the centrifugal force and tangential velocity created within a vortex, without the penalty of the high overall pressure loss. This would require recovery of the vortex energy, as opposed to its dissipation as in the throttle. Turbulence usually extracts energy from the mean flow and dissipates it by viscous action, which is contrary to this objective. Nevertheless, turbulent kinetic energy is, in most cases, much less than the total

kinetic energy. For example, in our case, the turbulent kinetic energy predicted by the Reynolds stress model in the chamber is only about 3% of the total kinetic energy. Therefore, Significant energy recovery would be possible if losses due to the axial recirculation, the sudden expansion at the axial port , and friction losses within the port, could be minimised.

References

[1] Ballhaus, W. F., Jr., Computational Aerodynamics and Design. Eight International Conference on Numerical Methods in Fluid Dynamics Proceedings, Aachen, pp. 1-20, 1982.

[2] Roache, P. J., "Computational Fluid Dynamics". Hermosa, Albuquerque, 1972.

[3] Kutler, P., A Perspective of Theoretical and Applied Computational Fluid Dynamics. AIAA J., Vol. 23, No. 3, pp. 328-341, 1985.

[4] Nallasamy, M., Turbulence Models and Their Applications to the Prediction of Internal Flows: A Review. Computers & Fluids, Vol. 15, No. 2, pp. 151-194, 1987.

[5] Oran, E. S. and Boris, J. P., Detailed Modelling of Combustion System. Prog. Energy Combust. Sci., Vol. 7, pp. 1-72, 1981.

[6] Patankar, S. V. and Spalding, D. B., A Calculation Procedure for Heat, Mass and Momentum Transfer in Three-Dimensional Parabolic Flows. International J. of Heat and Mass Transfer, Vol. 15, pp. 1787-1805, 1972.

[7] Patankar, S. V., "Numerical Heat Transfer and Fluid Flow". Hemisphere, 1980.

[8] Launder, B. E. and Spalding, D. B., The Numerical Computation of Turbulent Flows. Comput. Meth. Appl. Mech. Engng., Vol. 3, pp. 269-289, 1974.

[9] Chorin, A. J., A Numerical Method for Solving Incompressible Viscous Flow Problems. J. Comp. Phys., Vol. 2, pp. 12-26, 1967.

[10] Harlow, F. H. and Welch, J. E., Numerical Calculation of Time-Dependent Viscous Incompressible Flow of Fluid with Free Surface. Phys. of Fluids, Vol. 8, No. 3, pp. 2182-2189, 1965.

[11] Donavan, L. F., A Numerical Solution of Unsteady Flow in Two-Dimensional Square Cavity. AIAA J., Vol. 8, No. 3, pp. 524-529, 1970.

[12] Lawal, A. and Mujumdar, A. S., Laminar Flow and Heat Transfer in Power-Law Fluids Flowing in Arbitrary Cross-Section Ducts. Numerical Heat Transfer, Vol. 8, pp. 217-244, 1985.

[13] Connell, S. D., Numerical Solution of the Equations of Viscous Flow. Ph.D Thesis, Nottingham University, 1983.

[14] Connell, S. D. and Stow, P., The Pressure Correction Method. Computer & Fluids, Vol. 14, No. 1, pp. 1-10, 1986.

[15] Patankar, S. V., Numerical Prediction of Three Dimensional Flows, in B. E. Launder (ed.), Studies in Convection: Theory, Measurment and Applications, Vol. 1, pp. 1-78, Academic, New York, 1975.

[16] Rubini, P. A., Flow Modelling in Pipe Bends. Ph.D Thesis, Sheffield University, 1987.

[17] Boysan, F. and Swithenbank, J., Numerical Prediction of Confined Vortex Flows. Sheffield Univ., Dept. of Chem. Eng. and Fuel Tech., Report No. HIC 370, 1980.

[18] Hjertager, B. H. and Magnussen, B. F., Computation of Some Three Dimensional Laminar Incompressible Internal Flows. Proc. 1976 Heat Transfer and Fluid Mechanics Institute, Stanford Univ. Press, pp 436-451.

[19] Patankar, S. V., A Calcualtion Procedure for Two-Dimensional Elliptic Situations. Numerical Heat Transfer, Vol. 4, pp. 409-425, 1981.

[20] Raithby, G. D. and Schneider, G. E., Numerical Solution of Problems in Incompressible Fluid Flow: Treatment of the Velocity - Pressure Coupling. Numerical Heat Transfer, Vol. 2, pp. 417-440, 1979.

[21] VanDoormaal, J. P. and Raithby, G. D., Enhancements of the SIMPLE Method for Predicting Incompressible Fluid Flows. Numerical Heat Transfer, Vol. 7, pp. 147-163, 1984.

[22] Latimer, B. R. and Pollard, A., Comparison of Pressure-Velocity Coupling Solution Algorithms. Numerical Heat Transfer, Vol. 8, pp. 635-652, 1985.

[23] White, M. E., Drummond, J. P. and Kumar, A., Evolution and Status of CFD Techniques for Scramjet Applications. AIAA-86-0160, January, 1986.

[24] MacCormack, R. W., Current Status of Numerical Solutions of the Navier-Stokes Equations. AIAA-85-0035, January, 1985.

[25] Anderson, D. A., Tannehill, J. C. and Pletcher, R. H., "Computational Fluid Mechanics and Heat Transfer". Hemiphere, 1984.

[26] MacCormack, R. W., The Effect of Viscosity in Hypervelocity Impact Cratering. AIAA Paper 69-354, April, 1969.

[27] Baldwin, B. S. and MacCormack, R. W., Numerical Solution of the Interaction of a Strong Shock Wave with a Hypersonic Turbulent boundary Layer. AIAA Paper 74-558, 1974.

[28] Shang, J. S. and Hankery Jr, W. L., Numericla Solution for Supersonic Turbulent Flow Over a Compression Ramp. AIAA J., Vol. 13, No. 10, pp. 1368-1374, 1975.

[29] Knight, D. D., Numerical Simulation of High Speed Inlets Using the Navier-Stokes Equations. AIAA J., Vol. 15, No. 11, 1977.

[30] Drummond, J. P., Numerical Study of a Ramjet Dump Combustor Flowfield. AIAA J., Vol. 23, pp. 604-611, 1985.

[31] Uenishi, K. and Roger, R. C., Three Dimensional Computation of Mixing of Transverse Injector in a Ducted Supersonic Airstream. AIAA-86-1423, June, 1986.

[32] Uenishi, K., Roger, R. C. and Northam, G. B., Three-Dimensional Numerical Predictions of the Flow Behind a Rearward-Facing Step in a Supersonic Combustor. AIAA-87-1962, June, 1987.

[33] Dash, S. M. and Thorpe, R. D., Shock-Capturing Model for One- and Two-Phase Supersonic Exhaust Flow. AIAA J., Vol. 19, No. 7, pp. 842-851, 1981.

[34] Briley, W. R. and McDonald, H., Solution to the Multi-Dimensional Compressible Navier-Stokes Equations by a Generalized Implicit Method. J. of Comp. Phys., Vol. 24, pp. 372-379, 1977.

[35] Beam, R. and Warming, R. F., An Implicit Factored Scheme for the Compressible Navier-Stokes Equations. AIAA J., Vol. 16, pp. 393-402, 1978.

[36] Visbal, M., Numerical Simulation of Shock/Turbulent Boundary Layer Interaction over Two-Dimensional Compression Corners. Ph.D Thesis, Rugters University, 1983.

[37] Visbal, M. and Knight, D. D., The Baldwin-Lomax Turbulence-Model for Two-Dimensional Shock Wave/Boundary-Layer Interactions. AIAA J., Vol. 22, No. 7, 1984.

[38] Pulliam, T. H. and Steger, J. L., Implicit Finite-Difference Simulation Three-Dimensional Compressible Flow. AIAA J., Vol. 18, pp159-167, 1980.

[39] Baldwin, B. S. and Lomax, H., Thin Layer Approximation and Algebraic Model for Separated Turbulent Flows. AIAA Paper No. 78-257, 1978.

[40] Pulliam, T. H. and Steger J. L., Recent Improvements in Efficiency, Accuracy and Convergence of an Implicit Approximate Factorization Scheme. AIAA Paper No. 85-0360, 1985.

[41] Shamroth, S. J., McDonald , H. and Briley, W. R., Prediction of Cascade Flow Fields Using the Averaged Navier-Stokes Equations. J. of Engineering for Gas Turbine and Power, Vol. 106, pp. 383-390, 1984.

[42] Weinberg, B. C., Yang, R. J., McDonald, H. and Shamroth, S. J., Calculation of Two and Three Dimensional Transonic Cascade Flow Fields Using the Navier-Stokes Equations. J. of Engineering for Gas Turbine and Power, Vol. 108, pp. 93-102, 1986.

[43] MacCormack, R. W., A Numerical Method for Solving the Equations of Compressible Viscous Flow. AIAA J., Vol. 20, No. 9, pp. 1275-1281, 1982.

[44] MacCormack, R. W., An Efficient Numerical Method for Solving the Time-Dependent Compressible Navier-Stokes Equations at High Reynolds Number. Computing in Applied Mechanics, Applied Mechnical Div., Vol. 18, the American Society of Mechnical Engineers, 1976.

[45] White, M. E. and Anderson, J. D., Application of MacCormack's Implicit Method to Quasi-One-Dimensional Nozzle Flows. AIAA Paper 82-0992, 1982.

[46] Kneile, K. R. and MacCormack, R. W., Implicit Solution of the Three-Dimensional Compressible Navier-Stokes Equations Internal Flows. Lecture Notes in Physics, Vol. 218, Springer-Verlag, pp. 302-307, 1985.

[47] Lawrence, S. L., Tannehill, J. C. and Chausse, D. S., Application of Implicit MacCormack Scheme to the Parabolized Navier-Stokes Equations. AIAA J., Vol. 22, pp. 1755-1763, 1984.

[48] Knight, D. D., A Hybrid Explicit-Implicit Numerical Algorithm for the Three-Dimensional Compressible Navier-Stokes Equations. AIAA-83-0223, January, 1983.

[49] Knight, D. D., Improved Calculation of High Speed Inlet Flows: Part 1, Numerical Algorithm. AIAA J., Vol. 19, pp. 34-41, 1981.

[50] Knight, D. D., Improved Calculation of High Speed Inlet Flows: Part 2, Results. AIAA J., Vol. 19, pp. 172-179, 1981.

[51] Knight, D. D., Calculation of High Speed Inlet Using the Navier-Stokes Equations. J. Aircraft, Vol. 18, pp. 748-754, 1981.

[52] Lax, P. D., Weak Solutions of Nonlinear Hyperbolic Equations and Their Numerical Computation. Commun. Pure Appl. Math. 7: 159-193, 1954.

[53] Moretti, G., Three-Dimensional, Supersonic, Steady Flows with Any Number of Embedded Shocks. AIAA Paper 74-10, 1974.

[54] Marconi, F. and Salas, M., Computation of Three-Dimensional Flows about Aircraft Configurations. Computer & Fluids, Vol. 1, pp. 185-195, 1973.

[55] Salas, M., Shock Fitting Method for Complicated Two-Dimensional Supersonic Flows. AIAA J., Vol. 14, No. 5, pp. 583-588, 1976.

[56] de Neef, T., Moretti, G., Shock Fitting for Everybody. Computer & Fluids, Vol. 8, pp. 327-334, 1980.

[57] Moretti, G., Computation of Flows with Shocks. Ann. Rev. Fluid Mech., Vol. 19, pp. 313-337, 1987.

[58] Jespersew, D. C., Design and Implementation of a Multigrid Code for the Euler Equations. Applied Math. and Comp, Vol. 13, pp. 357-374, 1983.

[59] Atkins, H. L. and Hassan, H. A., Transonic Flow Calculations Using the Euler Equations. AIAA J., Vol. 23, pp. 842-847, 1983.

[60] Johnson, G. M., Relaxation Solution of the Full Euler Equations. Lecture Notes in Physics, Vol. 17, pp. 273-279, Springer-Verlag, 1982.

[61] Drummond, J. P., Rogers, R. C. and Evans, J. S., Combustor Modelling for Scramjet Engines. AGARD-CP-275, Oct. 1979.

[62] Issa, R. I. and Lockwood, F. C., On the Prediction of Two-Dimensional Supersonic Viscous Interactions Near Walls. AIAA J., Vol. 15, No. 2, pp. 182-188, 1977.

[63] Hah, C., Modelling of Turbulent Flow Fields Through a Cascade of Airfoils at Stall Conditions. AIAA J., Vol. 23, pp. 1411-1417, 1985.

[64] Karki, K. C., A Calculation Procedure for Viscous Flows at All Speeds in Complex Geometries. Ph.D Thesis, The University of Minnesota, June, 1986.

[65] Reynolds, O., Phil. Trans. A 186, 123, 1895.

[66] Vandromme, D., Turbulence Modeling in Variable-Density Flows. Ph.D Thesis, University of Brussel, 1980.

[67] Chen, J. Y., Second-order Modeling of Variable Density Turbulent Flows with Favre Averaging and a Consistent Form for Pressure Fluctuation Correlations. Sandia Report, Sand 86-8856, 1986.

[68] Jones, W. P. and Whitelaw, J. H., Calculation Methods for Reacting Turbulent Flows: A Review. Combustion and Flame, Vol. 48, pp. 1-26, 1982.

[69] Boussinesq, J., Essai Sur La Theorie Des Eaux Courantes. Mem. Presentes Acad. Sci., Vol. 23, Paris, p. 46, 1877.

[70] Reynolds, W. C., Computation of Turbulent Flows. Ann. Rev. Fluid Mech., Vol. 8, pp. 183-208, 1976.

[71] Mellor, G. L. and Herring, H. J., A Survey of the Mean Turbulent Field Closure Models. AIAA J., Vol. 11, pp. 590-599, 1973.

[72] Rodi, W., Examples of Turbulence Models for Incompressible Flows. AIAA J., Vol. 20, pp. 872-879, 1982.

[73] Spalding, D. B., Turbulence Models. A Lecture Course, Imperial College of Science and Technology, 1982.

[74] Launder, B. E. and Spalding, D. B., The Numerical Computation of Turbulent Flows. Comput. Meth. Appl. Mech. Eng., Vol. 3, pp. 269-289, 1974.

[75] Bradshaw, P., The Understanding and Prediction of Turbulent Flow. Aeronaut. J., Vol. 76, pp. 403-417, 1972.

[76] Launder, B. E. and Spalding, D. B., "Mathematical Models of Turbulence". Academic Press, London, 1972.

[77] Bradshaw, P. and Cebeci, T., "Engineering Calculation Methods". Academic Press, London, 1978.

[78] Lumley, J. L., Computational Modelling of Turbulent Flows. Adv. Appl. Meth., Vol. 18, pp. 123-176, 1978.

[79] Lumley, J. L., Turbulence Modelling. J. Appl. Meth., Vol. 50, pp. 1097-1103, 1983.

[80] Launder, B. E., Stress Transport Closure - into the Third Generation. Symp. Turbulent Shear Flows, Vol. 3, pp. 259-266, 1982.

[81] Lekshininarayana, B., Turbulence Modelling for Complex Flows. AIAA-85-1652, 1985.

[82] Patel, V. C., Rodi, W. and Scheuerer, G., Turbulence Models for Near Wall and Low Reynolds Flows: A Review. AIAA J., Vol. 23, pp. 1308-1319, 1985.

[83] Deardorff, J. W., A Numerical Study of Three-Dimensional Turbulent Channel Flow at Large Reynolds Number. J. Fluid Mech., Vol. 41, pp. 452-480, 1970.

[84] Tennekes, H. and Lumley, J. L., "A First Course in Turbulence". M.I.T. Press, 1972.

[85] Daly, B. J. and Harlow, F. H., Transport Equations in Turbulence. Phys. Fluids, Vol. 13, pp. 2634-2649, 1970.

[86] Jones, W. P. and Launder, B. E., The Calculation of Low-Reynolds-Number Phenomena With a Two-Equation Model of Turbulence. Int. J. Heat Mass Transfer, Vol. 16, pp. 1119-1130, 1972.

[87] Launder, B. E., Reece, G. J. and Rodi, W., Progress in the Development of a Reynolds-Stress Turbulence Closure. J. Fluid Mech., Vol. 68, pp. 537-566, 1975.

[88] Hanjalic, K. and Launder, B. E., A Reynolds Stress Model of Turbulence and Its Application to the Thin Shear Flows. J. Fluid Mech., Vol. 52, p. 609, 1972.

[89] Rotta, J. C., Statistische Theorie Nichthomog Ener Turbulenz. Z. Phys., Vol. 129, p. 547, 1951.

[90] Rodi, W., The Prediction of Free Boundary Layers by Use of a Two-Equation Model of Turbulence. Ph.D Thesis, University of London, 1972.

[91] Rodi, W., A New Algebraic Relation for Calculating the Reynolds Stresses. ZAMM, Vol. 56, T219-T221, 1976.

[92] Donaldson, C. dup., Calculation of Turbulent Shear Flows for Atmospheric and Vortex Motions. AIAA J., Vol. 10, pp 4-12, 1972.

[93] Schumann, U., Realizability of Reynolds Stress Turbulence Models. Phys. Fluids, Vol. 20, pp. 721-725, 1977.

[94] Hanjalic, H., Launder, B. E. and Schistel, R., Multiple-Time-Scale Concepts in Turbulent Transport Modeling. Proc. Turbulent Shear Flows, Vol. 2, pp. 10.31-10.36, 1979.

[95] Lilley, D. G., Prediction of Inert Turbulent Swirl Flows. AIAA J., Vol. 11, p. 955, 1971.

[96] Gupta, A. K., Lilley, D. G. and Syred, N.,"Swirl Flows". Abacus Press, Kent, 1984.

[97] Johnson, R. W., Ph.D Thesis, Dept. of Mech. Engin., UMIST, 1984.

[98] Chieng. C. C. and Launder, B. E., On the Calculation of Turbulent Heat Transfer Downstream from an Abrupt Pipe Expansion. Num. Heat Trans., Vol. 3 p. 189, 1980.

[99] Boysan, F., Ayers, W. H. and Swithenbank, J., A Fundamental Mathematical Modelling Approach to Cyclone Design, Trans. Instn. Chem. Engrs., Vol. 60, pp. 223-230, 1982.

[100] Gupta, A. K. and Lilley, D. G., "Flowfield Modelling and Diagnostics. Abacus Press, Kent, 1985.

[101] Fejer, A., Lavan, Z. and Wolf, Jr., L., Study of Swirling Fluid Flows. ARL-68-0173, Aerospace Research Laboratories, USAF, Wright-Patterson AFB, Ohio, Oct., 1968.

[102] Allan, R. A., Ph.D Thesis, Dept of Chem. Eng. and Fuel Tech., Sheffield Univ., England, 1970.

[103] Syred, N., Beer, J. M. and Chigier, N. A., Proc. of Salford Symp. on Internal Flows, Inst. of Mech. Eng., London, 1971.

[104] Eidelman, S., Collela, P. and Shreeve, R. P., Application of the Godunov Method and Its Second-Order Extension to Cascade Flow Modelling, AIAA J., Vol. 22, pp. 1609-1615, 1984.

[105] Rizzi, A. and Viviand, H., Eds., Numerical Methods for the Computation of Inviscid Transonic Flows with Shock Waves, Notes on Numerical Fluid Mechanics, Vol. 3, Vieweg, 1981.

[106] Liepmann, H. W. and Roshko, A., "Elements of Gasdynamics," John Wiley & Sons, Inc., New York, 1957.

[107] Rudy, D. H. and Strikwerda, J. C., Boundary Conditions for Subsonic Compressible Navier-Stokes Calculations. Computer and Fluids, Vol. 9, pp. 327-338, 1981.

[108] Crocco, L., A Suggestion for the Numerical Solution of the Steday Navier-Stokes Equations. AIAA J., Vol. 3, pp. 1824-1832, 1965.

[109] Benison, G. I. and Rubin, E. L., A Difference Method for the Solution of the Unsteady Quasi-One Dimensional Viscous Flow in a Divergent Duct. PIBAL Report, No. 69-9, Polytechnic Institute of Brooklyn, New York.

[110] Kurzrock, J. W., Exact Numerical Solution of the Time-Dependent Compressible Navier-Stokes Equations. Ph.D Thesis, Cornell University, Ithaca, New York, 1966.